Controlling apoptosis with computationally designed inhibitors targeting pro-survival and pro-apoptosis BCL2 family members

Stephanie Berger

A dissertation

submitted in partial fulfillment of the

requirements for the degree of

Doctor of Philosophy

University of Washington

2017

Reading Committee:

David Baker, Chair

Patrick Stayton

David Hockenbery

Program Authorized to Offer Degree:

Bioengineering

University of Washington

Abstract

Controlling apoptosis with computationally designed inhibitors targeting pro-survival and pro-apoptosis BCL2 family members

Stephanie Berger

Chair of Supervisory Committee:

Professor David Baker

Biochemistry

BCL2 family proteins regulate apoptosis and thus play a critical role in tissue homeostasis and development in healthy cells. A number of pathologies exploit the BCL2 family to promote artificially prolonged life or premature death. The doctoral research presented here has employed computational protein design and *in vitro* evolution to create inhibitors with high affinity and specificity for each of the eight globular pro-survival and pro-apoptotic BCL2 homologs, including the first-ever specific inhibitors for Bcl-w, Bcl-B, Bak and Bax. Inhibitors targeting pro-survival BCL2 proteins have been used to determine the unique BCL2 profiles of a variety of cancers, elucidating which homologs are most critical for survival and therefore identifying prime therapeutic targets. Inhibitors targeting pro-apoptotic BCL2 proteins are used in continuing work to improve gene editing efficiency in notoriously delicate hematopoietic stem cells and more broadly as a selection tool for other human cell engineering applications. This suite of high affinity protein inhibitors can furthermore be used to study apoptosis in normal and pathological biology, with advantages of spatiotemporal control and specific inhibition at the protein level compared to gene knock-out or knock-down approaches. More generally, this work shows that designed inhibitors can be generated for each member of a protein family with high structural similarity to probe the importance of specific protein-protein interactions in complex biological processes.

Acknowledgements

The past five years in the Baker Lab and UW Bioengineering graduate program have been the most demanding and the most fulfilling of my life. My positive graduate school experience is in no small part due to the many talented scientists with whom I've had the pleasure of working. Thanks to Pat Stayton for taking me on as a first-year graduate student and for years of continued advice, and thanks to Stayton Lab mentors Matt Manganiello, Brittany Lundy, Geoffrey Berguig, and Tony Convertine. Huge thanks to Erik Procko, my primary mentor in the Baker Lab, for many hours of patient guidance and thorough instruction. Thanks to David La, Daniel Adriano-Silva, Possu Huang, Yifan Song and Lei Shi for much help with Rosetta and computer work generally, especially Daniel for developing software that was used in this work. Thanks to many including Eva Strauch, Cassie Bryan, Ta-Yi Yu, Yakov Kipnis, Inna Goreschnik and Christy Tinberg for help with FACS, next gen sequencing, data analysis and other wet-lab-related items. A special thank you to Lauren Carter, Stephen Rettie and the rest of the Protein Production Group for providing many grams of pure protein and saving me days of work; Darwin Alonso and Patrick Vecchiato for technical support and maintenance of the computing resources on which much of this work depended; and current and former lab managers Michael Murphy, Rashmi Ravichandran and Jasmine Gallaher who keep the lab running. Finally, a huge thank you to David Baker for providing the opportunity to work on super interesting, cutting-edge scientific research, providing consistent guidance and encouragement, and fostering an all-around excellent work environment.

Thank you to all our fantastic collaborators for excellent work and invaluable insight: Erinna Lee and Doug Fairlie, ONJCRI in Melbourne, Australia; Daciana Margineantu and David Hockenbery, FHCRC; Betty Shen and Barry Stoddard, FHCRC; Alex Zelter and Trisha Davis, UW Biochemistry.

Thanks to the members of my Supervisory Committee including David and Pat, David Hockenbery, Dan Ratner and Chris Kemp for their time and guidance.

Thanks especially to my husband Cody, the rest of my family, and friends for their constant support and the many beers purchased when experiments succeeded fantastically or failed miserably.

Table of Contents

Preface

Programmed cell death is a tightly controlled process, involving both pro-survival and pro-apoptotic proteins that regulate permeability of the outer mitochondrial membrane. As cells enter apoptosis, mitochondrial membrane permeability increases, releasing mitochondrial factors such as cytochrome *c* that initiate destructive protease cascades in the cytosol. The key regulators of mitochondrial outer membrane permeability are B cell lymphoma-2 (BCL2) family proteins which are categorized functionally by their effect on cell fate, and structurally by the presence of BCL2 homology (BH) motifs. Pro-apoptotic effector proteins Bak and Bax have three of four distinct BH domains and homo-oligomerize upon activation to form pores in the mitochondrial outer membrane, committing the cell to apoptosis. Pro-survival homologs (six in humans: Bcl-2, Bcl-xL, Bcl-w, Mcl-1, Bfl-1 and Bcl-B) are structurally similar to Bak and Bax, having all four BH domains, but functionally opposite; they inhibit apoptosis by binding Bak and Bax, as well as sequestering pro-apoptotic BH3-only proteins (BOPs). BOPs can activate effectors directly through transient binding interactions (Dai et al., 2011; Kim et al., 2009; Walensky et al., 2006) or indirectly by binding pro-survival proteins and out-competing bound effectors (Ku et al., 2010a; Willis et al., 2007) or other direct activator BOPs (Kuwana et al., 2005; Letai et al., 2002; Figure 1). Interactions between BCL2 members are mediated by an amphipathic, helical BH3 motif that recognizes a conserved hydrophobic cleft present in the effectors and pro-survival proteins. The balanced network of interactions between pro-apoptotic and pro-survival members can be tipped toward cell death by cellular stress signals that induce transcription (Essafi et al., 2005; Nakano and Vousden, 2001) or post-translational modification of BOPs (Desagher et al., 2001; Fricker et al., 2010; reviewed in Shamas-Din et al., 2011).

Since the discovery of the first BCL2 gene in 1986 (pro-survival member and family namesake Bcl-2; Tsujimoto and Croce, 1986), great strides have been made in understanding the molecular and structural biology of BCL2 intra-family protein-protein interactions and their effect on cell fate. However, many questions remain about the physiological roles of each homolog in normal and abnormal biology. Due to their structural similarity, homologs often have overlapping binding interaction profiles. Inhibitors with high affinity and specificity for each homolog can provide a much-needed toolset to intricately probe BCL2 biology, especially in contexts such as development where gene knock-out and knock-down models are difficult or impossible to attain. Further, the ability to control apoptosis with very specific protein inhibitors enables the manipulation of apoptosis for our benefit, for example inducing apoptosis in cancer cells or temporarily stalling apoptosis in cells genetically modified for

therapy. The following chapters describe the design, characterization and application of protein inhibitors with high specificity and affinity for each of eight BCL2 family proteins.

Chapter 1: Pro-survival BCL2 inhibitors

Introduction

Pro-survival and pro-apoptotic members of the BCL2 family mediate the critical cellular process of apoptosis. Pathology arises when apoptosis is dysregulated. Overexpression of one or more pro-survival homologs enables cancers to resist apoptosis, and different cancers have different profiles of pro-survival protein overexpression (Kelly and Strasser, 2011; Placzek et al., 2010). This chapter focuses on the design of inhibitors targeting six human pro-survival BCL2 proteins and their application in delineating the distinct role of each homolog in different cancers.

Small molecule and peptide therapeutics mimic BOPs by binding pro-survival proteins, inducing apoptosis by disrupting inhibition of Bak and Bax and limiting sequestration of BOPs. However, BH3-mimetics that non-specifically target multiple BCL2 proteins can cause harmful side effects by unnecessarily suppressing normal biological functions. For example, the small molecule ABT-737 (and related ABT-263) targeting Bcl-2, Bcl-xL and Bcl-w exhibits dose-limiting thrombocytopenia in treating Bcl-2-dependent chronic lymphocytic leukemia due to excessive inhibition of Bcl-xL, which has a role in platelet development (Mason et al., 2007; Roberts et al., 2012). Delineation of the roles of pro-survival homologs in a given cancer, termed BCL2 profiling, aims to reveal which homolog or homologs a tailored treatment should target to maximize anti-cancer activity and minimize toxicity. BCL2 profiling using natural BOPs, BH3-mimicking peptides or small molecules is complicated by their low specificity (Certo et al., 2006; Chen et al., 2005; DeBartolo et al., 2012; London et al., 2012). Designed peptides and small molecules have achieved high affinity and excellent specificity for Bcl-2 (Leverson et al., 2013), Bcl-xL (Leverson et al., 2015a), Mcl-1 (Foight et al., 2014; Leverson et al., 2015b), and Bfl-1 (Dutta et al., 2013), and highly specific small molecule inhibitors of Bcl-2 and Bcl-xL (ABT-199 and A-1155463) have defined the dependency of ABT-263-sensitive cancer cell lines on Bcl-2, Bcl-xL or both (Leverson et al., 2015a). However, there are currently no highly specific inhibitors for Bcl-w and Bcl-B, and hence general mechanistic aspects of apoptotic regulation remain unclear.

This chapter describes the computational design and experimental characterization of specific, high affinity protein inhibitors for all six pro-survival BCL2 homologs (Figure 1—figure supplement 1). The inhibitors exhibit high specificity in engineered cell lines, and in defined combinations they induce apoptosis in representative cancer cell lines. This comprehensive set of molecular probes should be useful to elucidate the molecular mechanisms of

mitochondrial apoptosis, determine BCL2 profiles of individual cancers, and provide a superior guide for tailored therapies.

Results

Computational design of BCL2 binding proteins

We recently described a *de novo* designed protein inhibitor of BHRF1, an Epstein-Barr viral BCL2 homolog. The three helix bundle protein, called BINDI, is complementary to the canonical BH3-binding groove of BHRF1. BINDI consists of a central BH3-like motif and two additional helices that both stabilize the BH3-motif and provide extra contacts for high affinity and specific binding (PDB 4OYD; Procko et al., 2014). Pro-survival homologs share similar sequences (40-60% similarity between any two) and structures (approximately 3 Å RMSD), including the conserved hydrophobic cleft; thus, we hypothesized that BINDI's complementary interface would provide an excellent scaffold upon which to re-engineer specific binding to each of the six human pro-survival homologs (Figure 2).

The BINDI scaffold was docked into the hydrophobic binding cavities of crystal structures of the six pro-survival homologs bound to various ligands (Table 1). If the target structure included a bound BH3 motif, this was used to structurally align the BH3-equivalent residues of BINDI in the binding groove. If the target structure was bound to an unnatural ligand, such as a small molecule or α/β-foldamer, the model of the pro-survival homolog was first aligned to an alternative structure bound to a helical BH3 motif, which then served as a guide for structural alignment of BINDI. One docked model was generated for each crystal structure. Key interfacial residues were transferred to the BINDI scaffold (Correia et al., 2010), borrowing side chains from each crystal structure's bound peptide ligand, and informed by peptide SPOT array data (DeBartolo et al., 2012) and the sequences of selective BOPs and BH3-mimetic peptides (Chen et al., 2005; Dutta et al., 2010; Table 1).

Following docking and side chain grafting, ROSETTA Monte Carlo sequence design calculations were carried out on BINDI residue positions within 8 Å of the target interface to minimize the energy of the bound complex (Leaver-Fay et al., 2011). Grafted residues and protein backbone conformations were kept fixed. Side chain rotamers of the target BCL2 homolog were allowed to sample alternative conformations compatible with the redesigned interface. In a second round of design calculations, the designable interface was expanded to include BINDI residues within 12 Å of the target, followed by rigid-body minimization. Five to 10 designs were generated

for each initial docked configuration, and those with the most favorable binding energy, smallest number of buried polar atoms, and greatest shape complementarity to the target's surface were selected.

Genes encoding the selected designs were synthesized, and nearly all the proteins were expressed and soluble in *E. coli* (summary in Table 1; sequences in Table 2). The purified proteins were screened with single-concentration biolayer interferometry (BLI; Figure 2—figure supplement 1F) to qualitatively assess affinity and specificity for the target BCL2 protein. Affinities of the most specific designs were quantitatively determined using multiple-concentration BLI (Figure 2—figure supplement 1G). 2-CDP06 (for Bcl-2-targeting Computationally Designed Protein), X-CDP07 (Bcl-xL), M-CDP04 (Mcl-1), and F-CDP01 (Bfl-1) bound their intended targets with highest affinity, while the affinity of B-CDP01 to its intended target Bcl-B was second only to Mcl-1 (Figures 2 and Figure 2—figure supplement 1H).

Initial Bcl-w-targeting designs, however, did not bind Bcl-w or any other BCL2 protein, likely because the designs were based on the crystal structure of Bcl-w bound to a ligand that is not BH3-like (PDB 4K5A), unlike successful designs that were based on BH3-liganded structures (Table 1). Therefore, we generated helix-bound Bcl-w models by threading the Bcl-w sequence onto high-resolution structures of other homologs bound to BH3 peptides and sampled alternative superpositions of the BINDI scaffold onto the modeled BH3 peptide (Figure 2—figure supplement 1C). Each docked conformation was then designed as described above, and 36 sequences passing design filters were pooled and expressed on the yeast cell surface as fusions with Aga2p. The yeast library was sorted by fluorescence-activated cell sorting (FACS) for binding to biotinylated Bcl-w in the presence of the other BCL2 pro-survival homologs as unlabeled competitors; this enriched designs with high affinity and specificity for Bcl-w. Enriched designs were expressed in *E. coli* and screened by BLI. Design W-CDP03 was the most specific, binding Bcl-w with nanomolar affinity and moderate specificity (Figures 2C and Figure 2—figure supplement 1H). Notably, the location of the BH3-like motif in W-CDP03 is shifted by one α-helical turn relative to BINDI, perhaps to better accommodate the Bcl-w surface (Figure 2—figure supplement 1D and E).

The αMCL1•Mcl-1 crystal structure is very similar to the design model

The computational design calculations succeeded in generating proteins that bound to each of the six human BCL2 homologs with nanomolar affinity and at least partial specificity. One design, M-CDP04 (subsequently called αMCL1, or anti-Mcl-1), was highly specific for Mcl-1 and bound with picomolar affinity.

Cross-linking studies of αMCL1 with Mcl-1 were consistent with the designed binding interactions, supporting the structural model at low resolution (Figure 3—figure supplement 1, Table 4).

The crystal structure of the αMCL1•Mcl-1 complex at 2.75 Å resolution reveals how high affinity and specificity were achieved (Figure 3, Table 3). When Mcl-1 in the design model is superimposed on Mcl-1 in the crystal structure, αMCL1 crystal and design models closely align, highlighting the accuracy of our design calculations (2.1 Å average RMSD among the six separate complexes observed in the asymmetric unit; the N-terminal end of αMCL1 in the crystal structure lying slightly closer to Mcl-1 than in the design).

Native BH3 motifs interact with pro-survival homologs via defined hotspot residues on five consecutive turns of the BH3 helix, denoted h0 through h4 (Figure 4A). The BH3-mimetic helix 2 of αMCL1 has three additional helix turns beyond h0 and h4 that have side chains close enough to interact with Mcl-1. These extra contacts, combined with those made by the peripheral helices, expand the classic BH3 interface by 534 $Å^2$ (Figure 3B). While many residues in the αMCL1 BH3-mimetic helix were borrowed from pan-specific Bim (Table 1), designed residues at the expanded interface provide tailored complementarity with Mcl-1 for improved affinity and specificity (Figure 3C-F).

Affinity and specificity maturation

To improve the affinity and specificity of the designed inhibitors targeting other BCL2 homologs, the genes for 2-CDP06, X-CDP07, W-CDP03, F-CDP01 and B-CDP01 were diversified by site-directed saturation mutagenesis (SSM). Each codon was mutagenized to NNK (N is A, G, C or T; K is G or T) by overlap PCR (Procko et al., 2013), producing a library comprising all possible single amino acid substitutions. Each library was screened by yeast display for specific binding to labeled target homolog in the presence of unlabeled competitors (sort conditions in Table 5). DNA from the naïve and post-sort libraries was extracted and deep sequenced.

The enrichment or depletion of each sequence variant in the selected versus unselected pools is a measure of the variant's fitness with respect to affinity and/or specificity toward the target homolog (Figure 5—figure supplement 1A). Enriching mutations were found on the central BH3-mimicking helix and at positions on the peripheral helices that contact the target. To assess the accuracy of the computational design in identifying optimal amino acids at the interface, we calculated the deviation of each designed residue's enrichment ratio from the maximum enrichment ratio at that position. For all CDPs, nearly all designed residues have enrichment ratios very

close to the maximum (Figure 5A, Figure 5—figure supplement 1B), on average deviating by 2.0 (2-fold worse enrichment) while the average deviation per position is 7.8 (Figure 5B).

To experimentally evaluate the contribution of computational design, we carried out control evolution experiments starting from a single, partially-specific Mcl-1-targeting design aiming for specificity toward each of the other pro-survival BCL2 proteins. An SSM library based on M-CDP02 was sorted as described above. Mutations that enhance the affinity of M-CDP02 for BCL2 members other than Mcl-1 include prolines in the first and third helical segments, substitutions of apolar to polar amino acids in the hydrophobic core, and premature stop codons in the third helix. These mutations likely cause unfolding of the helix bundle and expose the Bim-BH3-like motif in the second helix, thus converting a protein that binds Mcl-1 with high affinity and partial specificity to a pan-specific high-affinity binder similar to the Bim-BH3 motif (Figure 5—figure supplement 1C). In contrast, none of these destabilizing mutations were enriched during the evolution of the individual computational designs explicitly targeting each BCL2 homolog. Thus, using our experimental approach, computational design is necessary to provide partially-specific starting points for evolution which are superior to a non-specific construct.

For X-CDP07, W-CDP03, F-CDP01 and B-CDP01, combinatorial libraries were constructed containing the mutations that produced the greatest increase in specificity (highlighted in Figure 5—figure supplement 1A; Table 6), and sorted by FACS for multiple rounds under increasingly stringent conditions (Table 5). Each library converged on a small number of enriched combinatorial mutants (ECMs), which were screened by BLI. We anticipated that few mutations within the moderately-specific 2-CDP06 design would be necessary to achieve high specificity for Bcl-2. Thus, in lieu of generating a combinatorial library, single amino acid mutants were screened with BLI, and three mutations improving both specificity and affinity were combined in αBCL2 (Figure 2G, Table 6).

While X-ECM04 and W-ECM01 (hereafter called αBCLXL and αBCLW) have high affinity and excellent specificity (Figure 2H-I), F-ECM04 and B-ECM01 exhibited less than 100-fold specificity for their targets. These sequences were therefore diversified by error-prone PCR, evolved and screened as previously (Table 5). Three additional specificity-enhancing mutations were identified per construct and combined in the final variants αBFL1 and αBCLB (Figure 2J-K, Table 6). Overall, the optimized designs exhibit slight to moderate decreases in stability compared to their predecessors based on chemical denaturation, but unfolding remains cooperative (Figure 2—figure supplement 1I), suggesting a well-packed core.

We carried out computational docking experiments on partially specific CDPs and optimized variants to determine the robustness of our computational protocol (Figure 5—figure supplements 2 and 3). Each CDP and optimized inhibitor was docked into the canonical binding groove of each BCL2 homolog, and thousands of docked configurations were sampled both locally (low RMSD to input configuration) and globally (entire protein surface). Overall, both the partially-specific CDPs and optimized, specific inhibitors exhibit more favorable absolute binding energy (local minimum ddG) and relative binding energy (local minimum versus global minimum ddG) when docked to on-target homologs compared to off-target homologs. These calculations resemble trends in the experimental binding data, but they do not discriminate between the highly specific, optimized inhibitors and partially specific precursors. Thus, while adding computational docking or multi-state design against off-target homologs to our design protocol may improve the initial success rate of achieving high affinity and at least partially specific binding, the resolution of these calculations limits discrimination between variants with low versus high specificity.

Determinants of specificity

The crystal structure of the αBCL2•Bcl-2 complex at 2.1 Å resolution together with the αMCL1•Mcl-1 complex described above illuminate the structural basis for affinity and specificity achieved by both computational design and evolution. The sequence variability of the designed proteins complements that of the BCL2 proteins across the interface, indicating that the designed proteins gain specificity by taking advantage of regions where BCL2 homologs differ (Figure 4B-C). Mutations that enhanced specificity localize to three regions: the interface periphery, the hydrophobic core, and the BH3-like region.

Many mutations at the interface periphery change surface electrostatic potential to improve charge complementarity with the target or oppose interactions with off-target BCL2 proteins. For example, designed negatively charged residue E111 of αMCL1 complements a positively charged region of Mcl-1 and opposes negatively charged analogous regions of Bcl-2, Bcl-xL and Bfl-1. αBCL2, αBCLXL and αBFL1 each have designed (αBCL2) or evolved (αBCLXL, αBFL1) positively charged side chains at position 111, which likewise complement on-target binding and oppose binding to Mcl-1 (αMCL1•Mcl-1 and αBCL2•Bcl-2 crystal structures shown in Figure 6A; Bcl-xL and Bfl-1 comparison using structural alignment of existing models). Additional examples of designed and evolved electrostatic complementarity are illustrated in Figure 6B-D.

Conservative mutations in the hydrophobic core may improve core packing or alter the backbone conformation for enhanced complementarity to the target surface. For example, the binding mode of αBCL2 in the hydrophobic cleft of Bcl-2 differs significantly between the crystal structure and backbone-constrained design model; after Bcl-2 alignment, Cα backbones of the αBCL2 crystal and design models deviate by 4.0 Å RMSD (average amongst the two complexes observed in the asymmetric unit; Figure 6—figure supplement 1A-C). The SSM-guided mutation of 2-CDP06 core residue G107R is likely responsible, requiring the first and third helices of αBCL2 to shift relative to the BH3-mimetic helix and positioning the third helix much further from Bcl-2 than the αMCL1•Mcl-1 binding mode (Figure 6A). The αBCL2 binding mode enables electrostatic interactions between αBCL2 R107 and Bcl-2 residues D111 and E114.

Mutations within the hydrophobic center of the interface, formed by the BH3-like region of the designs, were generally conservative, but occasionally included substitutions of hydrophobic to polar residues. In particular, the position analogous to a conserved isoleucine within natural BH3 motifs (h3 in Figure 4A) is mutated to a polar residue in αBCL2 (N57), αBCLXL (H57), αBCLW (E61) and αBFL1 (H57). Mutation of this residue was not allowed during the design of αMCL1 or the design and evolution of αBCLB, which therefore both preserve the isoleucine hotspot. The αBCL2•Bcl-2 crystal structure reveals that Bcl-2 residue D111 makes a hydrogen bond with αBCL2 N57, satisfying a polar atom that is likely buried in the interface when binding other homologs (Figure 6C). Specificity appears to be achieved in part by introducing a small number of mutations that universally reduce binding affinity but improve specificity at the interface center, like αBCL2 N57 which can be uniquely tolerated by Bcl-2 but likely reduces binding to other homologs, coupled with many specific, affinity-enhancing mutations at the interface periphery.

Engineered BH3-mimetic peptides span residues analogous to the BH3-like core interface of the designed inhibitors. The specificity of small peptides thus depends on mutations within this limited region. Like αMCL1, αBCL2 expands the classic BH3 interface by 452 $Å^2$ (Figure 6—figure supplement 1D). While the designed proteins share some specificity-enhancing residues with designed peptides (Dutta et al., 2010; 2013), they also conserve non-specific residues at these positions; for example, aspartate at position h2+1 of the MB1 peptide is thought to confer specificity to Mcl-1, but αMCL1 retains arginine as in pan-specific BOP Bim (Figure 4D). Further, several positions that contribute to the specificity of designed peptides and some BOPs are restricted in the

designed proteins to conserved hydrophobic residues as they fall within the helix bundle's core (h1+2, h2+2, and h3+3; Figure 4A). Our design strategy achieves specificity by employing a lower-affinity central interface and designing additional interactions over the expanded target-inhibitor interface.

Validation of binding specificity and mechanism in engineered cell lines

We investigated the BCL2 binding profiles and mechanism of action of the optimized inhibitors in mammalian cells, employing a suite of engineered mouse embryonic fibroblasts (MEFs). We tested whether our inhibitors could selectively induce a hallmark of apoptosis by monitoring cytochrome *c* release from mitochondria into the cytosol of MEFs with engineered dependence on a single pro-survival BCL2 homolog. Strikingly, permeabilized MEFs treated with each designed inhibitor induced cytochrome *c* release only in the cell line dependent on the corresponding target BCL2 protein. No cytochrome *c* release was observed in $Bak^{-/-}Bax^{-/-}$ cells, confirming that mitochondrial outer membrane permeability following inhibitor treatment occurs specifically via the BCL2-regulated intrinsic pathway, as expected (Figure 7A).

To further validate binding specificity we examined the effect of a subset of inhibitors (αMCL1 and αBFL1) on long-term (i.e. seven day) colony survival in MEFs engineered to inducibly express each inhibitor. Consistent with binding profiles and cytochrome *c* release data, large effects were only seen with αMCL1 in the Mcl-1-dependent line, causing a 90 ± 11 % decrease in survival, and with αBFL1 in the Bfl-1-dependent line, causing a 85 ± 6 % decrease in survival (Figure 7—figure supplement 1A). Minimal effects on cell survival were observed in lines expressing non-cognate pro-survival proteins. These data validate the specificity of the designed proteins and their capacity to functionally engage BCL2 family members in a cellular milieu.

While engineered MEFs provided an excellent model system to study our designed proteins, we sought further mechanistic validation in a context relevant to their primary application: probing BCL2 family interactions and generating functional BCL2 dependency profiles in cancer. A representative cancer cell line (HeLa) was engineered to overexpress Mcl-1, Bcl-2 or Bcl-xL, and we assayed the activity of the designed inhibitors in each setting (Figure 7B). Previous studies revealed that HeLa cells are resistant to expression of Noxa (which targets Mcl-1 and Bfl-1) and ABT-737 (Bcl-2 and Bcl-xL) independently, but are potently killed with the combination of Noxa with ABT-737 (van Delft et al., 2006). Likewise, single designed inhibitors had little effect on survival. The combination of αMCL1 with αBCL2 caused more substantial cell death (28 ± 5 % survival) than αMCL1 with

αBCLXL (53 ± 6 %) and even more so than αBCL2 with αBCLXL (70 ± 5 %). These data, and similar results in Mcl-1-overexpressing (Mcl-1+) HeLa cells, suggest that Mcl-1 plays a more crucial role in wild-type HeLa survival than Bcl-2 or Bcl-xL, and Bcl-2 is a more important secondary target than Bcl-xL.

Compared to wild-type and Mcl-1+ HeLa cells, Bcl-xL-overexpressing (Bcl-xL+) cells are more resistant to the combination of αMCL1 with αBCL2, and likewise, Bcl-2-overexpressing (Bcl-2+) cells are more resistant to the combination of αMCL1 with αBCLXL. Thus, increased expression of a given BCL2 protein can compensate for the inhibition of others. The triple combination of αMCL1, αBCL2, and αBCLXL had greater efficacy than double combinations, indicating a contribution of each pro-survival protein to basal survival. Bcl-xL+ cells were generally more resistant than all other cell lines; the inability to completely inhibit Bcl-xL's survival function in Bcl-xL+ cells suggests that in this context, Bcl-xL may interact with proteins that are not displaced efficiently by αBCLXL.

To investigate potential mechanisms underlying these results, we assessed the binding profile of a representative BOP, Bim, to pro-survival homologs with co-immunoprecipitation (co-IP) experiments in wild-type and over-expressing cell lines, with and without added αMCL1 (Figure 7—figure supplement 1C). In wild-type HeLa cells, Bim associated primarily with Mcl-1. Introduction of αMCL1 resulted in displacement of Bim from Mcl-1, with modest compensatory sequestration of Bim by Bcl-2. In Bcl-2+ cells, Bim is redistributed and preferentially binds Bcl-2 rather than Mcl-1, likely due to the stoichiometric excess of Bcl-2, and αMCL1 has no effect**.** The cell-killing activity of αMCL1 with αBCL2 in wild-type, Mcl-1+ and Bcl-2+ cells is consistent with these data; inhibition of both Mcl-1 and Bcl-2 in these settings likely overwhelms BOP sequestration, and a higher proportion of Bim and other activator BOPs may be free to interact with Bak and Bax, inducing apoptosis.

Designed inhibitors elucidate the dependence of human cancer cell lines on pro-survival BCL2 homologs

Next, we set out to define functional BCL2 dependency profiles of other cancer cell lines using a larger set of our designed inhibitors. Apoptotic resistance in melanoma is thought to act via Bfl-1 ((Hind et al., 2015), and likewise in glioblastoma via Bcl-2 (Weller et al., 1995) and Bcl-xL (Nagane et al., 2000). Further, oncogenic EGFR mutations in glioblastoma are associated with apoptotic resistance via increased Bcl-xL expression (Latha et al., 2012). Therefore, melanoma and EGFR-modified glioblastoma cell lines provide diverse contexts to test the BCL2-profiling capacity of the designed proteins.

In all cell lines, single inhibitors again were unable to induce apoptosis. While SK-MEL-5 were overall more resistant to apoptosis, LOX-IMVI melanoma cells were sensitive to double combinations that included αMCL1 and triple combinations (Figure 8A). αBFL1 with αBCL2 or αBCLXL had less effect, indicating that Mcl-1 plays a more critical role in survival than Bfl-1 in LOX-IMVI, in contrast to mRNA profiling suggesting the opposite (Hind et al., 2015). All glioblastoma cell lines showed similar trends in response to all combinations, while EGFR variants were in some instances more resistant than parental (Figure 8B). Sensitivity to many different double combinations suggests that in these contexts, pro-survival homologs may resist apoptosis via "mode 1" interactions with the pan- or partially-specific BOPs (Llambi et al., 2011).

To more fully assess the capacity of the designed inhibitors to determine BCL2 profiles, we tested them alongside existing, selective BH3-mimetics in a larger number of cell lines from one type of cancer. In previous studies, colon cancers showed variable response to small-molecule-mediated Bcl-xL inhibition, and RNAi experiments identified Mcl-1 as a resistance factor (Zhang et al., 2015). To determine whether Mcl-1 antagonism could render colon cancers sensitive to Bcl-xL neutralization and assess the influence of other pro-survival homologs on survival, we modified a panel of seven colon cancer lines to inducibly express either αMCL1 or αBFL1, and treated them with small molecules to selectively inhibit Bcl-2 (ABT-199), Bcl-xL (A-1331852), or Bcl-2 and Bcl-xL simultaneously (ABT-263).

Inhibiting a single pro-survival homolog had little effect on short-term survival; only SW48 cells showed greater than a 50% decrease in viability after treatment with A-1331852, consistent with a previous study showing SW48 is sensitive to Bcl-xL inhibition (Zhang et al., 2015; Figure 9A). Combined inhibition of both Mcl-1 and Bcl-xL caused nearly complete cell death after 24 hours in all colon cancers except HCT-116; further analyses showed that αMCL1-mediated Mcl-1 inhibition strongly sensitizes most colon cancers to A-1331852 (and to a lesser extent ABT-263), with a 4.6-fold or greater decrease in EC_{50} values observed in all cell lines except HCT-116 (Figure 9—figure supplement 1A-B). All other combinations had much smaller effects. Thus, in contrast to gliobastoma where pro-survival proteins appeared largely redundant, inhibition of two pro-survival proteins was required and sufficient for cell killing. These results suggest that in context of colon cancer, pro-survival proteins may resist apoptosis primarily via "mode 2" inhibition of the direct effector Bak, which interacts preferentially with Mcl-1 and Bcl-xL (Llambi et al., 2011). As αMCL1 targets Mcl-1 in a manner more akin to a drug (i.e. antagonism) compared to

RNAi, our data provide further evidence that treatment strategies involving Mcl-1 and Bcl-xL inhibition could be effective in these malignancies.

In long-term survival assays, αMCL1 had negligible effect, but remarkably, αBFL1 caused a significant (63 ± 4%) decrease in RKO cell survival (Figure 9B). Thus, long-term assays detect sensitivities that short-term assays miss, on a timescale that may provide a more informative preview of therapy. Overall, these data show the utility and sensitivity of our inhibitors in establishing the critical survival factors in colon cancer.

Discussion

This work offers the first complete set of specific inhibitors for each of the six pro-survival BCL2 proteins, including the first reported specific inhibitors for Bcl-w and Bcl-B. Our designed inhibitors exhibit greater specificity and in many cases higher affinity than small molecule alternatives, and have advantages unique to their protein composition. For example, the designed proteins can be easily modified for added functionality, such as adding a mitochondrial targeting sequence, or fusing an E3 ligase to each design to catalyze degradation of their target BCL2 proteins. The designed protein inhibitors can be genetically encoded, enabling spatial and temporal control of expression, and have distinct advantages over broadly eliminating the target BCL2 protein using CRISPR- or RNAi-mediated knockdown or knockout. The designs can be used to probe mechanism; we show that specific inhibitors cause the redistribution of a representative BOP, Bim, and the approach can be used to probe other BOPs and compare "mode 1" versus "mode 2" inhibition of apoptosis (Llambi et al., 2011). Some BCL2 proteins translocate from the cytosol to the mitochondrial membrane in response to apoptotic stimuli, and the effect of inhibition in these different compartments can be probed by localizing the designed inhibitors with the appropriate targeting sequences and inducing expression before and after apoptotic stimuli. The designed proteins can also be used to distinguish interactions at sites other than the BH3-binding groove; for example, Bcl-xL is thought to interact with p53 at a site opposite the BH3-binding groove (Petros et al., 2004), and Bcl-2 is reported to interact with the IP3 receptor in the endoplasmic reticulum via Bcl-2's BH4-domain (Rong et al., 2009). These studies are simply impossible with CRISPR or RNAi strategies.

Our computational design calculations using the stable *de novo* designed protein BINDI as a starting point enabled us to achieve, in the cases of Mcl-1 and Bcl-2, high specificity and affinity immediately following design, and in the cases of Bcl-xL, Bcl-w, Bfl-1 and Bcl-B, superior starting points for optimization compared to a single, pan-specific construct. Our success in designing not one but six specific inhibitors demonstrates the generality of the

design method. We are not aware of any precedent among designed proteins or indeed in nature for two sets of six closely related proteins in which each protein in one set has the extremely high specificity (100-100,000 fold) for a unique member of the other set that we have been able to achieve.

As confirmed by biochemical analyses and X-ray crystal structures, the designed proteins engage the BH3-binding grooves of their specific target pro-survival BCL2 family members. The designs were used to determine the BCL2-dependence of different cancers, providing a more direct guide for therapy than knockdown/knockout strategies or mRNA analysis by mimicking the mechanism of action of BCL2-targeting small molecule drugs. While mRNA profiling suggests that Bfl-1 confers apoptotic resistance in SK-MEL-5 and LOX-IMVI melanomas (Hind et al., 2015), our combinatorial antagonism of pro-survival homologs indicates that Mcl-1 plays a more critical role and further discriminates between sensitive LOX-IMVI and resistant SK-MEL-5. We also provide further evidence that many colon cancers are dependent on Mcl-1 and Bcl-xL for survival; mRNA profiling indicates Mcl-1 and Bcl-xL are indeed more prevalent than other BCL2 homologs in many colon cancers, but resistant HCT-116 is indistinguishable from sensitive lines like Caco-2 and HT-29 (Placzek et al., 2010). Further, the detection of RKO sensitivity to Bfl-1 inhibition highlights the capacity of the designed inhibitors to differentiate BCL2-dependence profiles, even among cancers with similar general characteristics.

More generally, computationally designed inhibitors enable the investigation of the biological roles of specific protein interactions with the high spatio-temporal control that can be achieved with tissue-specific and inducible promoters. Competing approaches offer less control. The distribution of small molecules is difficult to spatially or temporally control *in vivo*, and broadly eliminating the protein of interest with CRISPR or RNAi cannot probe interactions with a specific interface or capture mechanistic intricacies. This work demonstrates that high affinity and specificity protein inhibitors can be designed for each member of a closely-knit protein family, providing a unique opportunity to probe the importance of individual protein interactions.

Chapter 2: Pro-apoptotic BCL2 inhibitors

Introduction

Bak and Bax are the gate-keepers of mitochondrial apoptosis. Homooligomers of Bak and Bax form physical pores in the mitochondrial outer membrane (MOM) and release apoptotic factors into the cytosol, committing the cell to destruction. The molecular details of how cytosolic and MOM-tethered monomers transform into pore-forming oligomers, though widely studied, remain unclear. A subset of BH3-only proteins (BOPs) bind Bak and Bax with micromolar affinity via the canonical hydrophobic cleft shared with pro-survival proteins (Moldoveanu et al., 2013; Walensky et al., 2006) as well as at an alternate "rear pocket" site in the case of Bax (Gavathiotis et al., 2008). These are thought to be transient binding interactions that trigger a conformational change in Bak or Bax; the new conformation may then disfavor BOP-binding and favor homooligomerization. NMR and crystallographic models predict snapshots of Bak or Bax as unbound monomer (Moche et al., 2006, PDB 2JCN; (Suzuki et al., 2000), PDB 1F16) , bound to a BOP but without major structural change (Moldoveanu et al., 2013), PDB 2K7W; (Gavathiotis et al., 2008), PDB 2M5B), and in a presumed transition state in which the C-terminus is extended and the canonical binding groove is empty ((Czabotar et al., 2013), PDB 4BD7 and 4BD8; (Brouwer et al., 2014), PDB 4U2U) or occupied by a BOP (Czabotar et al., 2013), PDB 4BD2); it should be noted that this extended conformation forms domain-swapped dimers in crystallographic models but this complex is thought to be an artifact. Fragments of Bak and Bax have been crystallized in the presumed homodimer conformation that nucleates higher-order oligomer formation and assembles a large, exposed hydrophobic surface to enhance membrane interaction. Termed BH3-in-groove dimer, the BH3 domain of each molecule lies roughly in the hydrophobic cleft of the other (Czabotar et al., 2013), PDB 4BDU; (Brouwer et al., 2014), PDB 4U2V). The affinity of this interaction is unknown.

Pro-survival proteins block apoptosis by two mechanisms: sequestering Bak- and Bax-activating BOPs, and binding Bak or Bax tightly, not transiently. Isolated BH3 peptides from Bak and Bax bind full-length pro-survival proteins via the canonical BH3-binding cleft with binding constants from 1 to 255 nM (Ku et al., 2010b). Although structural information for full-length heterodimers remains elusive, it is inferred that exposure of Bak/Bax's BH3 motif is required for high-affinity pro-survival binding. On the other hand, Barclay et al. (2015) recently showed that the chemically stapled helical BH4 motif of pro-survival protein Bcl-2 binds with 177 nM affinity to monomeric

Bax at the rear binding pocket and inhibits Bax homooligomerization, indicating that exposure of Bax's BH3 domain may not be required for this weaker mode of inhibition by pro-survivals.

While a number of inhibitors exist targeting pro-survival BCL2 proteins, no specific, high-affinity inhibitors are currently available targeting Bak or Bax. Pro-survival proteins bind natural BH3 helices on the order of 1 nM; thus, it comes as little surprise that the plethora of designed BH3-mimetic pro-survival inhibitors bind with similarly high affinity. Analagous BH3-mediated interactions of BOPs with monomeric Bak or Bax via their BH3-binding groove are much weaker, having high nanomolar or micromolar affinity likely due to Bak and Bax's inherent flexibility.

This work presents computationally designed, BH3-mimetic inhibitors of Bak and Bax with 400 pM and 3 nM affinity, between two and four orders of magnitude higher than any natural binding interactions at the BH3-binding interface. The designed inhibitors are specific, binding pro-survival proteins and the off-target pro-apoptotic protein with at least 100-fold weaker affinity. Validating their activity and specificity, the designed proteins inhibit detergent-induced homooligomerization of Bak and Bax *in vitro* and prevent cytochrome *c* release from mitochondria in permeabilized cells treated with the apoptosis-inducing BOP Bim. These first-ever Bak- and Bax-specific inhibitors will be useful molecular tools to further probe BCL2 family interactions in biology. Further, apoptosis inhibitors could be particularly useful in cell engineering. For example, primary CD34+ human hematopoietic stem cells are notoriously difficult to culture and genetically modify *ex vivo* for adoptive cell transfer; continuing work introduces the designed proteins during the *ex vivo* modification step to temporarily stall apoptosis in response to cellular stress and improve survival. Apoptosis inhibitors may also be useful as a transient selection marker for many cell engineering applications. Continuing work aims to improve the efficient generation and expansion of human T-cells genetically modified via CRISPR/Cas9; a single bicistronic mRNA construct encoding gene editing machinery (Cas9 or guide RNA; TALENs) and the designed apoptosis inhibitors could enable active selection of successfully modified T-cells via treatment of the transformed pool with BCL2-specific apoptosis-inducing small molecules.

Results

Computational design and Bak and Bax binding proteins

We recently reported the design, optimization and application of six inhibitors with high affinity for each of six human pro-survival BCL2 proteins (Berger et al., 2016). Though Bak and Bax have opposite function, they are structurally similar and share the canonical BH3-binding hydrophobic cleft. We hypothesized that using similar methods, combining computational protein design and *in vitro* evolution via yeast surface display (YSD), we could generate BH3-mimetic Bak and Bax binders that interact with Bak or Bax's BH3-binding cleft. While BOPs bind with weak affinity and induce conformational change in Bak and Bax, designed proteins with very high affinity should prevent homodimerization and pore formation at the MOM, and ultimately inhibit apoptosis (Figure 10A).

A super-stable *de novo* three-helix bundle scaffold (Procko et al., 2014) was docked into the hydrophobic cleft of Bak and Bax crystallographic, NMR and homology models. Only helix-bound Bak and Bax models with the BH3-binding cleft in an open conformation were used. The Rosetta MotifGraft module was employed to graft a BH3-like helical motif, including five defined hotspots corresponding to conserved BH3 residues, onto any geometrically compatible position on the three-helix bundle backbone, generating thousands of variants on tens of unique docked configurations per Bak/Bax model. Rosetta sequence design calculations (stochastic Monte Carlo sampling) were carried out on each docked configuration to minimize the free energy of the bound complex. Thousands of designs were filtered by calculated Rosetta metrics correlating with binding success: binding energy (ddG), total free energy, shape complementarity, interface size, and number of buried unsatisfied polar atoms.

Genes for 42 designs with optimal scores (11 targeting Bak, 31 targeting Bax) were cloned into yeast for surface display and initially screened for binding Bak or Bax. Several steps were taken to improve the solubility of recombinant Bak and Bax: each was expressed in *E. coli* as a fusion to maltose binding protein (MBP), the N- and/or C-termini were truncated, cysteines were mutated to serine, and biotinylation was carried out *in vivo*, via co-expression with the native biotin ligase BirA, to minimize the overall time to obtain pure protein. Two of 11 (18%) Bak-targeting designs bound Bak with moderate affinity, and both also bound Bax with weak or moderate affinity. Two additional Bak-targeting designs exclusively bound Bax with weak affinity. Of 31 Bax-targeting designs, 14 (45%) bound Bax: two (6%) with high affinity (one also binding Bak with moderate affinity), six (19%) with moderate affinity (one also binding Bak with weak affinity), and six (19%) with weak affinity (one also binding Bak with weak affinity). One additional Bax-targeting design exclusively bound Bak with weak affinity. For all designs,

computational metrics and yeast binding and expression data are summarized in Table 7, and sequences are listed in Table 8.

Designs with greatest affinity and specificity for each target were expressed and purified from *E. coli*, and binding profiles were quantitatively determined with BLI titration experiments (Figure 10B-C). Bak-CDP02 (for Bak-targeting computationally designed protein [ID no.]) bound Bak with 60 ± 20 nM affinity, and Bax-CDP01 (Bax-targeting) bound Bax with 45 ± 4 nM affinity. To compare the designed inhibitors to native interactions with Bak and Bax's BH3 binding cleft, we determined the binding affinity of MBP-fused BH3 peptides from the BOPs Bim and Bid. MBP-BimBH3 bound Bak and Bax at 4,000 ± 2,000 nM and 500 ± 100 nM affinity, and Bid bound Bak and Bax with > 4 μM and 464 ± 4 nM affinity (Table 9). Using computational design alone, we achieved BH3-mimetic binders with one (Bax) and two (Bak) orders of magnitude greater affinity than any known interaction with Bak or Bax's BH3-binding cleft.

Affinity and specificity maturation

To effectively block apoptosis, the designed inhibitors must be specific, as off-target binding to pro-survival BCL2 homologs may induce apoptosis. Therefore, we decided to further optimize the partially-specific binders for greater specificity and affinity using *in vitro* evolution. Site-directed saturation mutagenesis (SSM) was performed on genes for BakCDP02 and BaxCDP01, generating libraries of all possible single amino acid substitutions. Each library was transformed into yeast for surface display and screened via fluorescence-activated cell sorting (FACS) under two conditions: high-affinity binding to labeled target homolog with no competitors, and specific binding to labeled target homolog in the presence of unlabeled competitor pro-survival homologs. Naïve libraries and sorted pools were analyzed with next generation sequencing (NGS) to determine which mutants improved specificity and affinity (Figure 11–figure supplement 1). Previous work showed that screening for specificity alone sometimes selects for highly specific variants with weaker on-target affinity than the initial design (Berger et al., 2016). In theory, selection for specificity only requires improvement in the affinity differential of on- versus off-target homologs, and high on-target affinity is not explicitly selected. To improve both specificity and on-target affinity, we included only those mutants enriched independently for both attributes in each combinatorial library (Figure 11A, B; Table 11). Combinatorial libraries were sorted for specificity six times, with decreasing concentration of target homolog and/or increasing concentration of competitors (sort conditions found in Table 10).

Variants found in the final sort of each library were expressed in *E. coli* and purified, and their binding profiles were qualitatively compared with single-concentration BLI experiments.

The best variants from each library, Bak-EC1M06 (for Bak-targeting enriched combinatorial library 1 mutant [ID no.]) and Bax-EC1M01 (Bax-targeting), exhibited on-target affinity an order of magnitude greater than their CDP precursor and nearly complete specificity (Figure 10B-C). However, each bound tightly to a single remaining pro-survival homolog: Bak-EC1M06 bound Bcl-2 with 40 ± 2 nM affinity, and Bax-EC1M01 bound Bfl-1 with 5 ± 3 nM affinity. Structural data suggest possible explanations for the unique residual cross-reactivities of intermediate and final variants. The loop between helices 4 and 5, positioned at the periphery of the BH3-binding interface, is one residue longer for Bax, Bfl-1 and Mcl-1 than Bak, Bcl-2, Bcl-xL and Bcl-w (Figure 12A). On the other side of the interface, the region spanning helices 2 and 3 (beginning with the C-terminal half of the BH3 motif), Bak is most similar to Bcl-2 at key interface residues, while Bax is most similar to Mcl-1 and/or Bfl-1 (Figure 12B). Excepting loop length, helices 4 and 5 are very structurally similar among all eight pro-apoptotic and pro-survival proteins (see structural models in Figure 12A, sequences in Figure 12C). While the helix 5 sequence is largely conserved likely due to its burial in the core, helix 4 varies considerably, giving each homolog a unique electrostatic profile at key interface positions. Evolved αBAX residue K95 and designed residue E94 likely improve specificity by taking advantage of sequence differences in this region; opposing Bax residue D98 (sequence position 9 in Figure 12C, modeled in Figure 12D) complements evolved αBAX residue K95 and Bax R94 (position 5) complements designed αBAX residue E94, while at least one of the two analogous positions of every other homologs has a different residue type. Crystal structures of αBAX•Bax and αBAK•Bak complexes in progress will be critical to definitive analysis of specificity.

To further enhance specificity and affinity, a second round of *in vitro* evolution was carried out, again including in the second-generation combinatorial libraries only those Bak-EC1M06 or Bax-EC1M01 mutants that improve both affinity and specificity (Figure 11C, D). Five rounds of FACS sorting in specificity-enhancing conditions yielded inhibitors with high affinity and complete specificity (Figure 10B-C). Bak-EC2M01 (Bak-targeting enriched combinatorial library 2 mutant [ID no.]), or αBAK, binds Bak with 400 ± 200 pM affinity and 333-fold specificity. Bax-EC2M01, or αBAX, binds Bax with 3 ± 2 nM affinity and 100-fold specificity (Figure 10B-C). Nearly all mutations made from intermediate EC1M variants to yield the final variants were depleted in the CDP-based SSM, indicating that most mutations made in the second round of evolution are context-dependent

(Figure 11E, F). Each protein exhibits cooperative unfolding when exposed to increasing concentrations of denaturant, suggesting a well-packed core, although denaturation midpoints shift considerably lower with each round of evolution (Figure 13).

Designed inhibitors prevent detergent-induced oligomerization

Next, we sought to validate the mechanism and activity of each designed inhibitor. Bak and Bax oligomerization can be induced *in vitro* by a number of detergents (Bleicken et al., 2010). Using native PAGE to assess the oligomeric state of Bak and Bax, we determined that αBAK and αBAX prevent detergent-induced oligomerization (Figure 14). Compared to Bak or Bax in standard buffer (lane 3), homologs incubated with *n*-dodecyl β-D-maltoside (DDM) form a variety of higher-order oligomers (lane 4). When incubated with 2-times molar excess of inhibitor (lane 5), there is a small but clear shift compared to the migration of Bak and Bax monomer, indicating heterodimerization. When incubated with DDM and inhibitor, a high fraction of total Bak and Bax remains as a heterodimer with the inhibitor, and higher-order oligomers are largely absent (lane 6). Inhibitors are specific, as they do not prevent oligomerization of the off-target homolog (lane 7). Notably, incubation of homodimeric Bax with αBAX, with and without detergent, results in a shift from Bax homodimer bound αBAX to Bax monomer bound αBAX, indicating that αBAX can disrupt Bax homodimers (Figure 14—figure supplement 1). While the inhibitors were designed with the intent to bind monomeric Bak and Bax and block apoptosis induced by subsequent stimuli, the ability to disrupt the BH3-in-groove dimer could extend the window of opportunity for apoptosis inhibition.

Discussion

This work presents the first available inhibitors with high affinity and specificity for pro-apoptotic BCL2 proteins Bak and Bax and provides a novel method to potently block apoptosis. Our computational design calculations, using the stable *de novo* designed scaffold BINDI as a starting point, yielded binders with an order of magnitude higher affinity than any known native interaction at the Bak and Bax BH3-binding interface. *In vitro* evolution via YSD further improved on-target affinity and specificity, yielding Bak and Bax inhibitors with high-picomolar to low-nanomolar affinity and negligible cross-reactivity with non-cognate pro-apoptotic or pro-survival homologs.

Designed protein inhibitors have unique advantages compared to small molecules or gene knock-down or knock-out strategies. When implemented in protein form, the designed inhibitor is active as soon as it reaches the cytosol and binds its target. While gene knock-down blocks translation of new target protein, activity is delayed until existing target protein degrades. Fast inhibition of cell death may be particularly useful when culturing and engineering cells with notoriously low viability and transformation efficiency *in vitro*, such as human stem cells. Further, gene knock-down efficiency is variable and may incompletely eliminate the target protein, and knock-out models can be difficult to generate especially for genes involved in critical cell processes like apoptosis. When implemented as encoding DNA or RNA, designed inhibitors maintain the benefits of gene knock-down strategies (spatiotemporal control) while functionally knocking out target protein activity by binding with very slow off-rates for practically irreversible inhibition. Designed proteins have the unique advantage of modularity and can easily accommodate tags or fusions for detection, subcellular localization or added functionality like targeted degradation. The inhibitors are specific to the BH3 binding groove, and thus can be used to probe interactions with Bak or Bax at alternate binding sites.

Functional tests validate the mechanism and activity of αBAK and αBAX. The designed inhibitors prevent detergent-induced homooligomerization of Bak and Bax, a critical step in the initiation of apoptosis. Ongoing work has confirmed that the inhibitors block the release of cytochrome *c* from mitochondria of engineered cells, mouse embryonic fibroblasts reconstituted with human Bak or Bax, after they are permeabilized and treated with apoptosis-inducing BOP Bim. Common methods to inhibit apoptosis *in vitro*, such as caspase inhibition, act downstream of the apoptotic "point of no return," i.e. Bak- and Bax-mediated pore formation in the MOM. Blocking apoptosis further upstream at Bak and Bax should maintain MOM integrity and thus protect more broadly against both caspase-dependent and -independent cell death associated with MOM permeability (Chipuk et al., 2006). Further, inhibiting Bak and Bax may also provide protection against other cell death mechanisms, as cells lacking Bak and Bax were shown to resist necrotic cell death induced by reactive oxygen species (H_2O_2), calcium overload (ionomycin), and DNA alkylation (methyl methanesulfonate; (Karch et al., 2013).

Designed apoptosis inhibitors can address current bottlenecks limiting production of engineered cells for adoptive therapy: poor *ex vivo* viability, recovery after genetic modification, and efficient selection and expansion of modified cells. Adding inhibitors in protein form during transformation, either in electroporation media or packaged in viral particles alongside gene editing components, could non-specifically boost cell recovery. The

designed inhibitors could also be implemented as a selection tool by linking encoding RNA to gene editing machinery (e.g. Cas9 or guide RNA, TALENs). The transformed cell population would undergo passive selection at a minimum, as apoptosis inhibitors would enable successfully transformed cells to resist death induced by introduction of exogenous donor DNA and endogenous DNA damage. For hardier cell types, additional treatment with apoptosis-inducing small molecules such as staurosporine would actively select for only successfully transformed cells. Current methods for selection of engineered cells require the permanent addition of an otherwise unneeded element to the modified cells: immunomagnetic isolation requires the presence of an inert dummy receptor expressed alongside the chimeric antigen receptor (CAR), tag-mediated isolation requires fusion of a peptide tag sequence to the CAR (E-tag, (Cartellieri et al., 2014); or Strep-tag II, (Liu et al., 2016)), and antibiotic selection requires constitutive expression of an enzyme conferring antibiotic resistance (hygromycin, (Keu et al., 2017)). In contrast, when implemented at the RNA level, designed apoptosis inhibitors provide a transient selection marker that lasts only as long as the RNA and resultant protein survives before degradation, ultimately leaving successfully engineered cells unscathed.

The designed apoptosis inhibitors may also be useful for treatment of diseases in which certain cells die prematurely, such as Parkinson's Disease (dopaminergic neurons), pulmonary fibrosis (type II alveolar epithelial cells), or type I diabetes (beta cells). While the etiologies that ultimately result in cell death are varied and complicated among these and other diseases, apoptosis inhibitors could be used as a first line of defense to mitigate the symptom of cell death alone or in combination with additional drugs that address the root of the pathology. αBAK and αBAX are novel tools for blocking cell death that may be broadly useful in cell engineering applications as well as targeted therapy for degenerative diseases. Altogether, the eight high-affinity, specific inhibitors of pro-survival and pro-apoptotic BCL2 proteins provide a unique molecular toolset to probe the BCL2 family biology as well as useful reagents to study and treat human disease.

Materials and Methods

Computational Methods

General

Rosetta software can be downloaded from www.rosettacommons.org and is available free to academic users. Online documentation can be found at:

http://www.rosettacommons.org/manuals/archive/rosetta3.5_user_guide/index.html

and instructions for RosettaScripts syntax is available at:

http://www.rosettacommons.org/docs/latest/scripting_documentation/RosettaScripts/RosettaScripts

A comprehensive list of command line options for Rosetta can be found at:

www.rosettacommons.org/docs/latest/full-options-list

RosettaScripts framework

All computational protocols were executed from within the RosettaScripts framework, which enables the user to piece together select portions of Rosetta code in order to generate project-specific protocols (Leaver-Fay et al., 2011; Fleishman et al., 2011a). An example of a command line executed to launch ROSETTA employing a RosettaScripts protocol can be found in Appendix I. An example of a RosettaScripts XML protocol, described below under heading *Design with ROSETTA*, can be found in Appendix II.

Manual generation of docked configurations of the BINDI scaffold in the hydrophobic groove of BCL2 homologs

The following crystallographic models of ligand-bound BCL2 homologs, found in the Protein Data Bank, were used to manually graft side chains onto a fixed backbone, as described below: 2PQK (Mcl-1•Bim-BH3), 3PK1 (Mcl-1•Bax-BH3), 3KZ0 (Mcl-1•MB7 peptide), 2XA0 (Bcl-2•Bax-BH3), 4AQ3 (Bcl-2•phenylacylsulfonamide), 4IEH (Bcl-2•sulfonamide), 4LVT (Bcl-2•Navitoclax), 1PQ1 (Bcl-xL•Bim-BH3), 2YQ6 (Bcl-xL•BimSAHB), 2YQ7 (Bcl-xL•BimLOCK), 3PL7 (Bcl-xL•Bax-BH3), 4BPK (Bcl-xL•α/β-Puma-BH3), 4K5A (Bcl-w•DARPin) 3I1H (Bfl-1•Bak-BH3), and 4B4S (Bcl-B•Bim-BH3).

A suitable helical region of the BINDI protein (PDB 4OYD chain B) was aligned to the BH3-motif ligand in crystallographic models of each BCL2 pro-survival homolog, using PyMOL (Schrödinger; PDB IDs noted in Tables 1 and 7). If the target structure was bound to an unnatural ligand, such as a small molecule or α/β-foldamer, the model of the pro-survival homolog was first aligned to an alternative structure bound to a helical BH3 motif, which then served as a guide for structural alignment of BINDI. The structural alignment was visually inspected,

and any docked configurations with backbone clashes between the scaffold protein and BCL2 homolog were discarded. Side chain clashes were tolerated, as they may be resolved later by sequence design of the scaffold and by rotamer repacking on the target. Important interfacial residues from each BH3-motif were transferred, or grafted, to the aligned BINDI scaffold and kept fixed during the subsequent design protocol; these 'hotspot' residues per model are listed in Table 1. A new PDB file containing the partially mutated scaffold bound to the target homolog was saved and used as the input for Rosetta-based design.

Automated generation of docked configurations of the BINDI scaffold in the hydrophobic groove of BCL2 homologs

Additional models of Bcl-w were generated for input into an automated motif grafting protocol described below. The Bcl-w sequence was threaded onto structurally analogous positions in existing crystallographic models of other BCL2 homologs. Only models bound to helical motifs were used: 1PQ1, 2BZW (Bcl-xL•Bad-BH3), 2YJ1 (Bcl-xL•α/β-Puma-BH3), 2YQ6, 2YQ7, 3FDL (Bcl-xL•Bim-BH3), 4A1U (Bcl-xL•designed α/β-foldamer), 4A1W (Bcl-xL•designed α/β-foldamer), 4BPK, 4HNJ (Bcl-xL•Puma-BH3), and 4OYD (BHRF1•BINDI). The TM-align software (Brouwer et al., 2014; Zhang, 2005) was used to generate structural alignments. Each new Bcl-w model then underwent constrained backbone and side chain minimization in the presence of the bound helical motif borrowed from the initial crystallographic model. The Bcl-w•helix complex was then aligned to a common 20-amino-acid truncated BH3-motif (truncatedBH3.pdb; KEKYIAAMLRAIGDIFNAIM) using PyMOL (Schrödinger). New PDB files of each Bcl-w model positioned to bind the common BH3-motif were saved and input as "context" in the automated motif grafting protocol described below.

The following crystallographic and NMR models of Bak and Bax were used as input for the Rosetta MotifGraft module: 1F16, monomeric Bax with its own N-terminus occupying the canonical binding cleft; 4BD2, Bax domain-swapped dimer in complex with BidBH3; 4BD6, Bax domain-swapped dimer in complex with BaxBH3; 2M5B, Bak•BidBH3. Additional models were generated using the TM-align software (###); to predict the conformation of Bak and Bax bound to the helix bundle scaffold, Bak and Bax sequences were structurally aligned with the crystal structure of BHRF1, a viral pro-survival homolog, bound to BINDI (4OYD). Modeled bound peptides (either BH3 domains or Bax's own N-terminus) were replaced with backbone and Cbeta atoms of BINDI residues #-# (4OYD); the backbone conformation and position of bound peptides in this region is very consistent among crystal structures of BH3-bound homologs as well as BINDI-like inhibitor-bound homologs (4OYD, 5JSB, 5JSN). Five residues conserved among BH3 domains and believed to be critical for binding the canonical

hydrophobic cleft were kept constant: BINDI residues I50, L54, I57, G58, D59, corresponding to positions h1, h2, h3, h3+1 and h3+2. All other residues were mutated to alanine. Each Bak•BINDI-BH3 and Bax•BINDI-BH3 complex then underwent constrained backbone and side chain minimization prior to input as "context" (Bak or Bax) and "motif" (bound peptide) in MotifGraft.

Additional conformations of the partially-nonspecific Mcl-1-targeting binder, M-CDP02, were sampled by submitting the M-CDP02 sequence to ROSETTA's ab initio structure prediction protocol (Fowler et al., 2011; Rohl et al., 2004). Of 30,200 generated models, any having greater than 2.5 Å RMSD relative to the starting model of M-CDP02 were discarded. 250 models with the most favorable (lowest) total score in ROSETTA energy units were input as "scaffolds" for the automated motif grafting protocol described below.

Grafting is a 'seeded interface' protein design approach (Correia et al., 2010; Dai et al., 2011; Kim et al., 2009), in which a small motif of known structure that binds to a target site of interest is used to initiate the protein design process. The motif is then grafted (i.e. embedded) into a larger protein scaffold, which both stabilizes the structure of the small motif and contributes additional favorable interactions with the target protein. We have implemented a new computational grafting protocol as the MotifGraft mover in RosettaScripts, described in detail by Silva et al (2016). The input of MotifGraft is composed of three structures: 1) the motif, which is a protein fragment that is intended for grafting in a new protein scaffold; 2) the context, which is the macromolecule interacting with the motif; and 3) the target scaffolds, which are protein scaffolds that the protocol will use to search insertion points for the motif. The goal of MotifGraft is to find fragments in the target scaffolds that are geometrically compatible with the specified motif(s), and then replace those fragments with the motif(s) itself. In this case, the parameters of grafting were settled to perform full backbone alignment of the input motif, with a maximum RMSD of the backbone of 3.0 Å and RMSD for the endpoints of 2.0 Å. No clashes between the grafted design and the context protein were allowed. This module can be implemented within the RosettaScripts framework; an example can be found in Appendix III.

Design with Rosetta

An example RosettaScripts XML file used for computational design after manual or automated motif-grafting can be found in Appendix II. The script is annotated with brief descriptions, and the indicated pieces of ROSETTA code were implemented in the order listed in the "<PROTOCOLS>" section below. Designs were generated and then filtered by the indicated metrics.

Recombinant protein expression and purification

Designed constructs targeting pro-survival homologs were codon-optimized for *E. coli* and commercially synthesized by Integrated DNA Technologies. Genes were assembled from oligo primers with Phusion polymerase (New England Biolabs) and cloned into the *E. coli* expression vector pET29b (Novagen), adding a C-terminal 6-histidine tag. Designed constructs targeting pro-apoptosis homologs were codon-optimized for *E. coli*, commercially synthesized by Gen9, and cloned into pETCON for yeast surface display via fusion to Aga2p, or pET29b for expression in *E. coli*.

Pro-survival homologs (Bcl-2 full-length; Bcl-xL full-length; Bcl-w 1-182; Mcl-1 172-327; Bfl-1 1-153; Bcl-B 1-165) were cloned into vectors for genetic fusion of a C-terminal 6-histidine tag, and with or without an N-terminal fusion to MBP (6H-modified pMAL-c5x or pET29b vectors, respectively). Each homolog was also expressed with a C-terminal Avi-GS-6H tag (GLNDIFEAQKIEWHEGSHHHHHH; modified pMAL-c5x and pET29b vectors). Pro-apoptosis homologs (Bak 16-186; Bax 1-166 C62S C126S) were cloned into the pMAL-c5x plasmid for N-terminal fusion to MBP, and modified with either a 6H or Avi-6H tag at the C-terminus.

All proteins were expressed via IPTG induction (0.5 mM) in TBII media (MP Biomedicals). Cells were pelleted, resuspended in high-salt Buffer 1 (20 mM Tris, 500 mM NaCl, 20 mM imidazole, pH 8), lysed via sonication, and centrifuged at high speed. Protein was purified from cleared lysates with metal affinity chromatography: 0.5 mL NiNTA-agarose resin (Qiagen) was added per 1L expression culture; resin was collected, washed and eluted (20 mM Tris, 150 mM NaCl, 300 mM imidazole, pH 8) over a 20 mL gravity column (Biorad). Proteins were further purified via SEC (Superdex 75 10/300 GL, GM), and fractions contain monomeric protein were collected and concentrated via centrifugal filtration with a 3 kDa MW cutoff (Millipore). Avi-tagged proteins were enzymatically biotinylated *in vitro* with BirA (Avidity) followed by metal affinity purification, or *in vivo* via co-expression of BirA (*E. coli* expression strain CVB101; Avidity). Aliquots of purified protein were snap-frozen in liquit nitrogen and stored at -80 ºC.

Protein optimization via yeast surface display

Library generation

Designed proteins were optimized by yeast surface display. SSM libraries were generated with overlap PCR (Otwinowski and Minor, 1997; Procko et al., 2013), using Phusion polymerase and custom degenerate primers to introduce mutations to NNK at each codon. Mutations with highest enrichment in the sorted SSM (fitness for the

attribute promoted by the sort condition, either specific binding or high-affinity on-target binding) were combined in combinatorial libraries, generated by oligo assembly with primers having degenerate codons. For pro-survival targeting designs, only specific binding was assayed. For pro-apoptosis targeting designs, specificity and on-target affinity were independently assayed, and mutants independently enriched for both attributes were included in subsequent combinatorial libraries. The diversity of all combinatorial libraries was limited to less than 4×10^7 variants. GeneMorph II Random Mutagenesis kit (Agilent Technologies) was used to introduce up to three random mutations in F-ECM04 and B-ECM01 genes.

DNA libraries comprising genes for the initial designed protein sequence and related variants were cloned into the pETCON plasmid (Fleishman et al., 2011b; McCoy et al., 2007), transformed into yeast, and expressed as fusions with N-terminal Aga2p for surface display and a C-terminal myc-tag for detection in the EBY100 strain (Berger et al., 2016; Brouwer et al., 2014; Chao et al., 2006; Fleishman et al., 2011b; Procko et al., 2013). Yeast libraries were grown in minimal media selective for the yeast strain (-ura) and the transforming plasmid (-trp), and protein expression was induced with 2% galactose. Surface expression was detected with anti-myc-FITC (Immunology Consultants Laboratory), and binding to biotinylated Bcl-2 proteins after co-incubation for 0.5-2 hr at 22 ºC was detected with phycoerythrin-streptavidin (Invitrogen). Yeast were sorted with an Influx (BD) or SH800 (Sony) cell sorter and either plated on solid media for isolating and sequencing individual clones (Bcl-w-targeting design screen, combinatorial and epPCR libraries), or pelleted for batch DNA extraction and deep sequencing (SSM libraries).

Deep sequencing analysis

Yeast (2 x 1.0 OD units) were lysed with 125 U/ml Zymolase at 37 ºC for 5 h, and DNA was harvested (Zymoprep kit from Zymo Research). Genomic DNA was digested with 2 U/µl Exonuclease I and 0.25 U/µl Lambda exonuclease (New England Biolabs) for 90 min at 30 ºC, and plasmid DNA purified with a QIAquick kit (Qiagen). DNA was deep sequenced with a MiSeq sequencer (Illumina): genes were PCR amplified using primers that annealed to external regions within the plasmid, followed by a second round of PCR to add flanking sequences for annealing to the Illumina flow cell oligonucleotides and a 6 bp sample identification sequence. High-fidelity Phusion polymerase was used for PCR, and round 1 was run for 12 cycles. PCR round 2 was monitored qualitatively with qPCR (SYBR Safe), and cycles proceeded until amplification was exponential but was stopped before signal plateau. Barcodes were read on a MiSeq sequencer using either a 300-cycle or 600-cycle reagent kit (Illumina), and

sequences were analyzed with adapted scripts from Enrich (Fowler et al., 2011; Skubak et al., 2004) or custom scripts. Enrichment ratios, i.e. the fitness fold-change of each mutant in the sorted population compared to naïve pool, were calculated using the following formula:

Equation 1: $$\text{Enrichment ratio} = \log_2 \left[\frac{mutant\ fraction\ in\ sorted\ population}{mutant\ fraction\ in\ naive\ pool}\right]$$

Deep sequencing data, both raw and processed files, have been deposited in the National Center for Biotechnology Information Gene Expression Omnibus repository with accession number GSE80194.

Protein characterization

Biolayer interferometry

Purified designed proteins were screened for binding to BCL2 homologs with bio-layer interferometry (BLI). Data were collected on an Octet RED96 (Forte Bio) and processed using the instrument's integrated software. All proteins were diluted from concentrated stock in binding buffer (10 mM HEPES [pH 7.4], 150 mM NaCl, 3 mM EDTA, 0.05% surfactant P20, 0.5% non-fat dry milk). Streptavidin-coated biosensors were dipped in wells containing biotinylated BCL2 proteins (25 nM) in binding buffer for 3-5 minutes for immobilization. After baseline measurement in buffer alone, binding kinetics were monitored by dipping the biosensors in wells containing defined concentrations of the designed protein (association), then dipping sensors back into baseline wells (dissociation). Titrations were done in triplicate and kinetic constants were determined from the mathematical fit of a 1:1 binding model.

Circular dichroism

CD spectra were recorded with a J-1500 Circular Dichroism Spectrometer (JASCO), at a protein concentration of 10 μM in DPBS free of $MgCl_2$ and NaCl (Life Technologies). GuHCl melt data were collected at 25°C.

Crystal structure determination and refinement

Designs with C-terminal 6-His tags and untagged pro-survival homologs were expressed independently, and lysates of cognate pairs were co-purified with NiNTA affinity chromatography and SEC. Initial crystallization trials employed commercial screens using a MOSQUITO robot. Two conditions from Wizard I & II screen (indexes F4 and F6) yielded small crystals from the αMCL1•Mcl-1 complex that were reproducible in the mosquito tray but were not transferable to larger 24-well trays. Precipitant and pH optimizations using MOSQUITO trays yielded

diffracting crystals in buffer conditions 1-1.3 M sodium citrate, 100 mM CHES, pH 9.5, which were then cryoprotected with paratone oil prior to flash freezing. 30% Jeffamine ED-2001, 100 mM HEPES, pH 7.0 (index D3) yielded crystals for αBCL2•Bcl-2, which were looped directly from the mother liquid and flash froze in liquid nitrogen. Data was collected either using an in house Rigaku MicroMax^{TM}-007HF rotating anode generator equipped with a Saturn CCD detector or from beam line BL 5.0.2 at the Advance Light Source synchrotron facility at the Laurence Berkeley National laboratories. Datasets were integrated and scaled using HKL2000 (Otwinowski and Minor, 1997; Winn et al., 2011). Structures were determined using molecular replacement (PHASER, RRID:SCR_014219; McCoy et al., 2007, Potterton et al., 2003) with 4LVTA and 2XA0A (Bcl-2), 3KZOA (Mcl-1) and computational models of αMCL1 and αBCL2. Refinements (by REFMAC5, RRID:SRC_014225; Emsley and Cowtan, 2004; Skubak et al., 2004) were conducted using the CCP4 program suite (Winn et al., 2011; SCR_007255) with CCP4i interface (Potterton et al., 2003). Model-building was carried out with COOT (Emsley and Cowtan, 2004; RRID:SRC_014222). The crystal structure factors and coordinates of αMCL1•Mcl-1 (PDB 5JSB) and αBCL2•Bcl-2 (PDB 5JSN) have been deposited in the Protein Data Bank.

Protein cross-linking and mass-spectrometric analysis

17 µg 3KZO-Y49 plus 22 µg Mcl1 were mixed in HB150 buffer (40 mM HEPES, 150 mM NaCl, 1 mM DTT, pH 7.5) in a final volume of 90.5 µL. Cross-linker concentration was brought to 0.86 mM by adding 14.5 mM DSS (disuccinimidyl suberate), DSG (disuccinimidyl glutarate) or BS3 bis(sulfosuccinimidyl)suberate. The reaction was allowed to proceed for 2 minutes at 25^{o}C before quenching with 10 µL 500 mM NH_4HCO_3. Cross-linked proteins were reduced with 10 mM dithiothreitol (DTT) at 37^{o}C for 30 minutes followed by 30 minutes alkylation at room temperature with 15 mM iodoacetamide (IAA). 25% volume of distilled water was added to the reactions prior to digestion with trypsin at a substrate-to-enzyme ratio of 60:1 overnight at room temperature with shaking. Digested samples were acidified with 5M HCl prior to being stored at -80°C until analysis. MS analysis was performed on a Q-Exactive (Thermo Fisher Scientific) and analyzed using the Kojak (version 1.4.2) cross-link identification software as previously described (Zelter et al., 2015; Hoopmann, et al. 2015).

Native PAGE

5 µg of Bak or Bax (N-terminal fusion to MBP, C-terminal Avi-GS-6H tag, *in vivo* biotinylated, and purified via metal affinity and subsequent SEC) were incubated at room temperature with a 2-times molar excess of

specific inhibitor, control inhibitor (non-cognate), or an equal volume of TBS. After 10 minutes, N-dodecyl-beta-maltoside (DDM) was added to a final concentration of 1% (Bak) or 2% (Bax), or an equal volume of TBS as control, vortexed and incubated another 30 minutes at room temperature. 2X native load dye (30 mM Tris-HCl, 20% [v/v] glycerol, 0.02% [w/v] bromophenol blue, pH 6.8) was added, vortexed and the entire volume loaded onto a NativePAGE 4-16% Bis-Tris acrylamide gels (Fisher). Gel was run at 150V until the dye front reached the bottom of the gel, approximately 2.5 hours, in native running buffer (3 g Tris base, 14.4 g glycine in 1 L water, pH 8.5).

In vitro studies in mammalian cell lines

MEF-derivative cell line generation

Mouse embryonic fibroblasts were generated from E13-E14.5 embryos derived from *CreERT2/Bcl-x$^{fl/fl}$/Mcl-1$^{fl/fl}$* C57BL/6 mice (Kelly et al., 2014) and immortalized (at passage 2-4) with SV40 large T antigen. Retroviral expression constructs in the pMIG vector (Murine Stem Cell Virus-IRES-GFP) expressing each FLAG-tagged pro-survival protein were transiently transfected using Lipofectamine (Invitrogen), into Phoenix ecotropic packaging cells. Filtered virus-containing supernatants were used to infect the MEFs by spin inoculation as previously described (Lee et al., 2008). Cells stably expressing each pro-survival protein were selected by sorting GFP^{+ve} cells 24 hours after spin inoculation and protein expression verified by Western blotting using an anti-FLAG antibody (Sigma-Aldrich, RRID:AB_439687). Following verification of exogenous pro-survival protein expression, each cell line was treated with 1 M Tamoxifen (Sigma-Aldrich) to enable deletion of endogenous Mcl-1 and Bcl-xL. Deletion of endogenous Mcl-1 and Bcl-xL was shown by Western blotting using anti-Mcl-1 (Rockland Clone, RRID:AB_2266446) and anti-Bcl-xL (BD Transduction Laboratories, RRID:AB_398070) antibodies. All Western blots were probed with anti-actin antibody (Sigma-Aldrich, RRID:AB_476697) to verify uniform loading. Cells were maintained in DME Kelso medium supplemented with 10% (v/v) fetal bovine serum, 250 mM L-asparagine and 50 mM 2-mercaptoethanol.

HeLa-derivative cell line generation

HeLa cells (originally obtained from ATCC, RRID:CVCL_0030) were generously provided by Dusty Miller at the Fred Hutchinson Cancer Research Center (Seattle, WA). HeLa cells were transfected with pSFFV vectors encoding human Mcl-1, Bcl-2, Bcl-xL, or empty vector (Neo) and selected with 1 mg/ml geneticin for 48 hours. Cells were maintained afterwards in DMEM with 10% (v/v) fetal bovine serum (FBS) supplemented with 500 μg/ml geneticin. Increased expression of pro-survival BCL2 proteins was confirmed by Western blotting using anti-

Bcl-2 (Santa Cruz Biotechnology, RRID:AB_626736), anti-Bcl-xL (Santa Cruz Biotechnology, RRID:AB_630917), and anti-Mcl-1 (GeneTex, RRID:AB_377762) antibodies.

Melanoma, glioblastoma and colon cancer cell lines

Melanoma cell lines (LOX-IMVI, RRID:CVCL_1381; SK-MEL-5, RRID:CVCL_0527) were purchased from the National Cancer Institute (NCI). Glioblastoma cells lines were generously provided by Paul Mischel at the Ludwig Institute for Cancer Research (San Diego, CA); U87 (originally obtained from ATCC; RRID:CVCL_0022) were modified to express EGFR and variant EGFRvIII as described by Wang, et al. 2015. SW620 (originally obtained from ATCC, RRID:CVCL_0547), HCT-116 (ATCC, RRID:CVCL_0291), DLD1 (ATCC, RRID:CVCL_0248), RKO (ATCC, RRID:CVCL_0504), HT-29 (ATCC, RRID:CVCL_0320), Caco-2 (ATCC, RRID:CVCL_0025), and SW48 (ATCC, RRID:CVCL_1724) colon cancer cell lines were generously provided by John Mariadason at the Olivia Newton-John Cancer Research Institute.

Lentiviral infection

Inducible αMCL1 and αBFL1 constructs were generated in a lentiviral vector described in Aubrey *et al.* (2015). Ligand expression is linked via the T2A peptide to mCherry fluorescent reporter protein. Lentiviral particles were produced by transient transfection of 293T cells (AATC, RRID:CVCL_0063) with plasmid DNA along with the packaging constructs pMDL, pRSV-rev and pVSV-G using calcium chloride precipitation. Viral supernatants were then filtered prior to target cell transduction. For infection of MEFs and colon cancer cell lines, equal volume of virus-containing supernatant was added to target cells pre-incubated with 10 ng/L polybrene, and centrifuged at 2500 rpm for 2 hours at 32^{o}C. Following spin inoculation, cells were then incubated overnight at 37^{o}C. Cells expressing the doxycycline-inducible constructs were then selected by sorting mCherry^{+ve} cells. Expression of the HA-tagged designed protein was confirmed with Western blotting using an anti-HA antibody (Roche, RRID:AB_390918). MEFs were maintained in DME Kelso medium supplemented with 10% (v/v) FBS, 250 mM L-asparagine and 50 mM 2- mercaptoethanol. Colon cancer cell lines were maintained in DMEM/F-12 supplemented with 10% (v/v) FBS.

For constitutive expression of αBCL2, αBCLXL, αBCLW, αMCL1 and αBFL1, genes were first codon optimized for human expression including a 5' Kozak sequence (GCCACC) and 3' FLAG tag, then cloned into the SparQ lentivector containing GFP reporter gene downstream of an internal ribosome entry site (QM530A-1; System

Biosciences). Lentiviral particles were produced by transient transfection of 293T cells with plasmid DNA along with packaging constructs pMD2.G and psPAX using calcium chloride precipitation. Viral supernatants were harvested 48 or 72 hours after transfection, filtered and used immediately or stored in aliquots at -80^{o}C.

MEF cytochrome c *release assay*

Small molecule inhibitors used for cytochrome *c* release and survival assays were purchased from ChemiTek (ABT-263 and ABT-199) or prepared according to published methods (A-1331852; Leverson et al., 2015a; Wang et al., 2013). Mouse embryonic fibroblasts ($1x10^6$) were pelleted and lysed in 0.05% (w/v) digitonin containing lysis buffer (20 mM Hepes-pH 7.2, 100 mM KCl, 5 mM $MgCl_2$, 1 mM EDTA, 1 mM EGTA, 250 mM Sucrose), supplemented with protease inhibitors (Roche) for 3 min on ice. Crude lysates containing the mitochondria were incubated with 10 μM ligand at 30 ^{o}C for 1 hour before pelleting. The supernatant was retained as the soluble fraction (S), while the pellet, containing the mitochondria (P), was solubilized in lysis buffer (20 mM Tris-pH 7.4, 135 mM NaCl, 1.5 mM $MgCl_2$, 1 mM EGTA, 10 % (v/v) glycerol and 1 % (v/v) Triton X-100. Both soluble and pellet fractions were subsequently analyzed by Western blotting using an anti-cytochrome *c* antibody (BD Biosciences, RRID:AB_396417).

Short-term survival assays

MEF and colon cancer cells were aliquoted in 96-well tissue culture plates in 50 μL culture media at 20,000 cells per mL. Cells were treated with doxycycline at a final concentration of 1 mg/mL to induce protein expression, and/or small molecule drugs at the indicated final concentrations and a final total volume of 100 μL per well. Viability was assayed after 24 hours with Cell Titer Glo (Promega). For drug titrations, ABT-263 and A-1331852 were serially diluted 2-fold from 250 nM to 2 nM (eight concentrations in total) and combined with doxycycline (to induce expression of αMCL1) or media (drug only). EC_{50} values were determined with nonlinear regression.

HeLa, melanoma, and glioblastoma cell lines were seeded at 3,000 – 5,000 cells per well in 96 well plates in 100 μl culture medium. Cells were transduced the next day with 100 μl lentiviral supernatant to induce expression of each designed inhibitor. For experiments using combinations of three inhibitors, 75 μl media was removed before virus addition to accommodate the appropriate volume of virus. Viability was assayed at 72 hours post-infection

with Cell Titer Glo (Promega). Expression of the FLAG-tagged constructs was confirmed by flow cytometry (GFP) and western blotting with an anti-FLAG antibody (Sigma-Alrich, RRID:AB_439685).

Long-term survival assays

MEF and colon cancers were seeded in 6-well tissue culture plates in 2 mL culture media at 150 cells per mL. The next day and every 48 hours following, doxycycline was added at a final concentration of 1 μg/mL to each well, while nothing was added to control wells. After seven to ten days, media was aspirated and colonies were stained (5:4:1 MeOH:H_2O:AcOH, 0.25% Coomassie Blue R-250) and counted.

Immunoprecipitation

Cells were harvested, washed with PBS, and extracted with ice-cold Chaps buffer (40 mM Tris-HCl, pH 7.5, 150 mM NaCl, 1 mM EDTA, 2% CHAPS, and Complete Protease Inhibitors [Roche]) for 20 minutes, on ice. Extracts were spun down at 10,000 g for 10 min and supernatants were removed and used for SDS-PAGE analysis. Expression of proteins of interest was analyzed using antibodies against Bcl-2, Bcl-xL, Mcl-1 (as above), Bfl-1 (ProsSci, Inc., RRID:AB_735550), Bim (BD Biosciences, RRID:AB_397305), and tubulin (Sigma-Aldrich, RRID:AB_477593). For immnoprecipitation experiments, 1,000 μg protein lysates were pre-cleared and then incubated with 3 μg Bim antibody for 2 hours at 4°C, followed by addition of Protein A/G Plus agarose beads (Santa Cruz Bioechnology) and overnight incubation with rotation at 4°C. Negative control reactions used normal IgG. Immunoprecipitates were washed four times with lysis buffer and eluted with loading buffer at 95°C, 2 times for 10 min, followed by SDS-PAGE analysis.

Cell line authentication and mycoplasma testing

For colon cancer cell lines, authentication was performed using the Promega StemElite ID System at the Queensland Institute of Medical Research (QMIR, Queensland, Australia) DNA Sequencing and Fragment Analysis Facility (January 2013). All colon cancer cell lines and parent MEF cell lines tested negative for mycoplasma by the MycoAlert Mycoplasma Detection Kit (Lonza). HeLa, melanoma and glioblastoma cell lines have not been authenticated in our hands, and each tested negative for mycoplasma by the MycoFluor Mycoplasma Detection Kit (ThermoFisher).

MEF and HeLa cells were retrovirally infected with constructs for constitutive expression of BCL2 pro-survival homologs and selected with FACS (MEF) or geneticin (HeLa). In MEFs, endogenous Mcl-1 and Bcl-xL were deleted via Cre-Lox recombination (Kelly et al., 2014). Engineered MEF and HeLa cells, colon cancer,

glioblastoma and melanoma cells were lentivirally infected with constructs for constitutive or inducible expression of designed inhibitors (Aubrey et al., 2015). Infected cells were selected with antibiotics or FACS, and stable cell lines were cultured.

Survival assays

For short-term survival assays, engineered MEFs and colon cancer cells were treated with doxycycline to induce designed protein expression and/or small molecule drugs at indicated final concentrations. Viability was assayed after 24 hours. Engineered HeLa, melanoma and glioblastoma cells were transiently transduced with designed inhibitors. Viability was assayed after 72 hours.

To assay long-term survival, MEF and colon cancers were sparsely plated, then treated with doxycycline to induce designed protein expression the next day and approximately every 48 hours for the next seven to ten days. Media was aspirated and colonies were stained and manually counted.

References

Aubrey, B.J., Kelly, G.L., Kueh, A.J., Brennan, M.S., O'Connor, L., Milla L., Wilcox, S., Tai, L., Strasser, A., Herold., M.J. (2015). An inducible lentiviral guide RNA platform enables the identification of tumor-essential genes and tumor-promoting mutations *in vivo*. Cell Rep *10*, 1422-1432.

Barclay, L.A., Wales, T.E., Garner, T.P., Wachter, F., Lee, S., Guerra, R.M., Stewart, M.L, Braun, C.R., Bird, G.H., Gavathiotis, E., et al. (2015) Mol Cell *57*, 873-886.

Berger, S., Procko, E., Margineantu, D., Lee, E.F., Shen, B.W, Zelter A., Silva, D.A., Chawla, K., Herold, M.J., Garnier, J.M. et al. (2016). Computationally designed high specificity inhibitors delineate the roles of BCL2 family proteins in cancer. eLife *5*, e20352.

Bleicken, S., Classen, M., Padmavathi, P.V.L., Ishikawa, T., Zeth, K., Steinhoff, H.J., and Bordignon, E. (2010). Molecular details of Bax activation, oligomerization, and membrane insertion. J Biol Chem *285*, 6636–6647.

Brouwer, J.M., Westphal, D., Dewson, G., Robin, A.Y., Uren, R.T., Bartolo, R., Thompson, G.V., Colman, P.M., Kluck, R.M., and Czabotar, P.E. (2014). Bak core and latch domains separate during activation, and freed core domains form symmetric homodimers. Molecular Cell *55*, 938–946.

Cartellieri, M., Koristka, S., Arndt, C., Feldmann, A., Stamova, S., Bonin, von, M., Töpfer, K., Krüger, T., Geib, M., Michalk, I., et al. (2014). A novel ex vivo isolation and expansion procedure for chimeric antigen receptor engrafted human T cells. PLoS One *9*, e93745.

Certo, M., Moore, V.D.G., Nishino, M., Wei, G., Korsmeyer, S., Armstrong, S.A., and Letai, A. (2006). Mitochondria primed by death signals determine cellular addiction to antiapoptotic BCL-2 family members. Cancer Cell *9*, 351–365.

Chao, G., Lau, W.L., Hackel, B.J., Sazinsky, S.L., Lippow, S.M., and Wittrup, K.D. (2006). Isolating and engineering human antibodies using yeast surface display. Nat Protoc *1*, 755–768.

Chen, L., Willis, S.N., Wei, A., Smith, B.J., Fletcher, J.I., Hinds, M.G., Colman, P.M., Day, C.L., Adams, J.M., and Huang, D.C.S. (2005). Differential targeting of prosurvival Bcl-2 proteins by their BH3-only ligands allows complementary apoptotic function. Mol Cell *17*, 393–403.

Chipuk, J.E., Bouchier-Hayes, L., and Green, D.R. (2006). Mitochondrial outer membrane permeabilization during apoptosis: the innocent bystander scenario. Cell Death Differ *13*, 1396–1402.

Correia, B.E., Ban, Y.-E.A., Holmes, M.A., Xu, H., Ellingson, K., Kraft, Z., Carrico, C., Boni, E., Sather, D.N., Zenobia, C., et al. (2010). Computational design of epitope-scaffolds allows induction of antibodies specific for a poorly immunogenic HIV vaccine epitope. Structure *18*, 1116–1126.

Czabotar, P.E., Westphal, D., Dewson, G., Ma, S., Hockings, C., Fairlie, W.D., Lee, E.F., Yao, S., Robin, A.Y., Smith, B.J., et al. (2013). Bax crystal structures reveal how BH3 domains activate Bax and nucleate its oligomerization to induce apoptosis. Cell *152*, 519–531.

Dai, H., Smith, A., Meng, X.W., Schneider, P.A., Pang, Y.-P., and Kaufmann, S.H. (2011). Transient binding of an activator BH3 domain to the Bak BH3-binding groove initiates Bak oligomerization. J Cell Biol *194*, 39–48.

DeBartolo, J., Dutta, S., Reich, L., and Keating, A.E. (2012). Predictive Bcl-2 family binding models rooted in experiment or structure. J Mol Biol *422*, 124–144.

Desagher, S., Osen-Sand, A., Montessuit, S., and Magnenat, E. (2001). Phosphorylation of bid by casein kinases I and II regulates its cleavage by caspase 8. Mol Cell *8*, 601-611.

Dutta, S., Chen, T.S., and Keating, A.E. (2013). Peptide ligands for pro-survival protein Bfl-1 from computationally guided library screening. ACS Chem Biol *8*, 778–788.

Dutta, S., Gullá, S., Chen, T.S., Fire, E., Grant, R.A., and Keating, A.E. (2010). Determinants of BH3 binding specificity for Mcl-1 versus Bcl-xL. J Mol Biol *398*, 747–762.

Emsley, P., and Cowtan, K. (2004). Coot: model-building tools for molecular graphics. Acta Crystallogr D Biol Crystallogr *60*, 2126-2132.

Essafi, A., Fernández de Mattos, S., Hassen, Y.A., Soeiro, I., Mufti, G.J., Thomas, N.S.B., Medema, R.H., and Lam, E.W.-F. (2005). Direct transcriptional regulation of Bim by FoxO3a mediates STI571-induced apoptosis in Bcr-Abl-expressing cells. Oncogene *24*, 2317–2329.

Fleishman, S.J., Leaver-Fay, A., Corn, J.E., Strauch, E.M., Khare, S.D., Koga, N., Ashworth, J., Murphy, P., Richter, F., Lemmon, G., et al. (2011a) RosettaScripts: a scripting language interface to the Rosetta macromolecular modeling suite. PLoS One *6,* e20161.

Fleishman, S.J., Whitehead, T.A., Ekiert, D.C., Dreyfus, C., Corn, J.E., Strauch, E.-M., Wilson, I.A., and Baker, D. (2011b). Computational design of proteins targeting the conserved stem region of influenza hemagglutinin. Science *332*, 816–821.

Foight, G.W., Ryan, J.A., Gullá, S.V., Letai, A., and Keating, A.E. (2014). Designed BH3 Peptides with High Affinity and Specificity for Targeting Mcl-1 in Cells. ACS Chem. Biol. *9*, 1962–1968.

Fowler, D.M., Araya, C.L., Gerard, W., and Fields, S. (2011). Enrich: software for analysis of protein function by enrichment and depletion of variants. Bioinformatics *27*, 3430–3431.

Fricker, M., Prey, J.O.A., Tolkovsky, A.M., and Ryan, K.M. (2010). Phosphorylation of Puma modulates its apoptotic function by regulating protein stability. Cell Death Dis *1*, e59–e59.

Gavathiotis, E., Suzuki, M., Davis, M.L., Pitter, K., Bird, G.H., Katz, S.G., Tu, H.-C., Kim, H., Cheng, E.H.Y., Tjandra, N., et al. (2008). BAX activation is initiated at a novel interaction site. Nature *455*, 1076–1081.

Hind, C.K., Carter, M.J., Harris, C.L., Chan, H.T.C., James, S., and Cragg, M.S. (2015). Role of pro-survival molecule Bfl-1 in melanoma. Int J Biochem Cell B *59*, 94–102.

Hoopmann, M.R., Zelter, A., Johnson, R.S., Riffle, M., MacCoss, M.K., Davis, T.N., Moritz, R.L. (2015). Kojak: efficient analysis of chemically cross-linked protein complexes. J Proteome Res *14*, 2190-2198.

Karch, J., Kwong, J.Q., Burr, A.R., Sargent, M.A., and Elrod, J.W. (2013). Bax and Bak function as the outer membrane component of the mitochondrial permeability pore in regulating necrotic cell death in mice. eLife.

Kelly, G.L., Grabow, S., Glaser, S.P., Fitzsimmons, L., Aubrey, B.J., Okamoto, T., Valente, L.J., Robati, M., Tai, L., Fairlie, W.D., et al. (2014). Targeting of MCL-1 kills MYC-driven mouse and human lymphomas even when they bear mutations in *p53*. Genes Dev *28*, 58-70.

Kelly, P.N., and Strasser, A. (2011). The role of Bcl-2 and its pro-survival relatives in tumourigenesis and cancer therapy. Cell Death and Differentiation *18*, 1414–1424.

Keu, K.V., Witney, T.H., Yaghoubi, S., Rosenberg, J., Kurien, A., Magnusson, R., Williams, J., Habte, F., Wagner, J.R., Forman, S., et al. (2017). Reporter gene imaging of targeted T cell immunotherapy in recurrent glioma. Sci Transl Med *9*, eaag2196.

Kim, H., Tu, H.-C., Ren, D., Takeuchi, O., Jeffers, J.R., Zambetti, G.P., Hsieh, J.J.D., and Cheng, E.H.Y. (2009). Stepwise activation of BAX and BAK by tBID, BIM, and PUMA initiates mitochondrial apoptosis. Mol Cell *36*,

487–499.

Ku, B., Liang, C., Jung, J.U., and Oh, B.-H. (2010). Evidence that inhibition of BAX activation by BCL-2 involves its tight and preferential interaction with the BH3 domain of BAX. Cell Res *21*, 627–641.

Kuwana, T., Bouchier-Hayes, L., Chipuk, J.E., Bonzon, C., Sullivan, B.A., Green, D.R., and Newmeyer, D.D. (2005). BH3 domains of BH3-only proteins differentially regulate Bax-mediated mitochondrial membrane permeabilization both directly and indirectly. Mol Cell *17*, 525–535.

Latha, K., Li, M., Chumbalkar, V., Gururaj, A., Hwang, Y., Dakeng, S., Sawaya, R., Aldape, K., Cavenee, W.K., Bogler, O., et al. (2012). Nuclear EGFRvIII-STAT5b complex contributes to glioblastoma cell survival by direct activation of the Bcl-XL promoter. Int J Cancer *132*, 509–520.

Leaver-Fay, A., Tyka, M., Lewis, S.M., Lange, O.F., Thompson, J., Jacak, R., Kaufman, K., Renfrew, P.D., Smith, C.A., Sheffler, W., et al. (2011). ROSETTA3: an object-oriented software suite for the simulation and design of macromolecules. Methods Enzymol. *487*, 545-574.

Letai, A., Bassik, M.C., Walensky, L.D., and Sorcinelli, M.D. (2002). Distinct BH3 domains either sensitize or activate mitochondrial apoptosis, serving as prototype cancer therapeutics. Cancer Cell *2*, 183-192.

Leverson, J.D., Boghaert, E.R., Ackler, S.L., Catron, N.D., Chen, J., Dayton, B.D., Ding, H., Enschede, S.H., Fairbrother, W.J., Huang, D.C.S., et al. (2013). ABT-199, a potent and selective BCL-2 inhibitor, achieves antitumor activity while sparing platelets. Nature Medicine *19*, 202–208.

Leverson, J.D., Phillips, D.C., Mitten, M.J., Boghaert, E.R., Diaz, D., Tahir, S.K., Belmont, L.D., Nimmer, P., Xiao, Y., Ma, X.M., et al. (2015a). Exploiting selective BCL-2 family inhibitors to dissect cell survival dependencies and define improved strategies for cancer therapy. Sci Transl Med *7*, 279ra40.

Leverson, J.D., Zhang, H., Chen, J., Tahir, S.K., Phillips, D.C., Xue, J., Nimmer, P., Jin, S., Smith, M., Xiao, Y., et al. (2015b). Potent and selective small-molecule MCL-1 inhibitors demonstrate on-target cancer cell killing activity as single agents and in combination with ABT-263 (navitoclax). Cell Death Dis *6*, e1590.

Liu, L., Sommermeyer, D., Cabanov, A., Kosasih, P., Hill, T., and Riddell, S.R. (2016). Inclusion of Strep-tag II in design of antigen receptors for T-cell immunotherapy. Nat Biotechnol *34*, 430–434.

Llambi, F., Moldoveanu, T., Tait, S.W., Bouchier-Hayes, L., Temirov, J., McCormick, L.L.,, Dillon, C.P., and Green, D.R. (2011). A unified model of mammalian BCL-2 protein family interactions at the mitochondria. Mol Cell *44*, 517-531.

London, N., Gullá, S., Keating, A.E., and Schueler-Furman, O. (2012). In silico and in v itro elucidation of BH3 binding specificity toward Bcl-2. Biochemistry *51*, 5841–5850.

Mason, K.D., Carpinelli, M.R., Fletcher, J.I., Collinge, J.E., Hilton, A.A., Ellis, S., Kelly, P.N., Ekert, P.G., Metcalf, D., Roberts, A.W., et al. (2007). Programmed anuclear cell death delimits platelet life span. Cell *128*, 1173–1186.

McCoy, A.J., Grosse-Kunstleve, R.W., Adams, P.D., Winn, M.D., Storoni, L.C., and Read, R.J. (2007). Phaser crystallographic software. J Appl Crystallogr *40*, 658-674.

Moldoveanu, T., Grace, C.R., Llambi, F., Nourse, A., Fitzgerald, P., Gehring, K., Kriwacki, R.W., and Green, D.R. (2013). BID-induced structural changes in BAK promote apoptosis. Nat Struct Mol Biol *20*, 589–597.

Nagane, M., Pan, G., Weddle, J.J., Dixit, V.M., Cavenee, W.K., and Huang, H.J. (2000). Increased death receptor 5 expression by chemotherapeutic agents in human gliomas causes synergistic cytotoxicity with tumor necrosis factor-related apoptosis-inducing ligand in vitro and in vivo. Cancer Res *60*, 847–853.

Nakano, K., and Vousden, K.H. (2001). PUMA, a novel proapoptotic gene, is induced by p53. Mol Cell *7*, 683-694.

Otwinowski, Z., and Minor, W. (1997). Processing of X-ray diffraction data collected in oscillation mode. Macromolecular Crystallography, Pt A *276*, 307–326.

Petros, A.M., Gunasekera, A., Xu, N., Olejniczak, E.T., Fesik, S.W. (2004). Defining the p53 DNA-binding domain/Bcl-x(L)-binding interface using NMR. FEBS Lett *559*, 171-174.

Placzek, W.J., Wei, J., Kitada, S., Zhai, D., Reed, J.C., and Pellecchia, M. (2010). A survey of the anti-apoptotic Bcl-2 subfamily expression in cancer types provides a platform to predict the efficacy of Bcl-2 antagonists in cancer therapy. Cell Death Dis *1*, e40–e49.

Potterton, E., Briggs, P., Turkenburg, M., and Dodson, E. (2003). A graphical user interface to the CCP4 program suite. Acta Crystallogr D Biol Crystallogr *59*, 1131–1137.

Procko, E., Berguig, G.Y., Shen, B.W., Song, Y., Frayo, S., Convertine, A.J., Margineantu, D., Booth, G., Correia, B.E., Cheng, Y., et al. (2014). A computationally designed inhibitor of an Epstein-Barr viral Bcl-2 protein induces apoptosis in infected cells. Cell *157*, 1644–1656.

Procko, E., Hedman, R., Hamilton, K., Seetharaman, J., Fleishman, S.J., Su, M., Aramini, J., Kornhaber, G., Hunt, J.F., Tong, L., et al. (2013). Computational design of a protein-based enzyme inhibitor. J Mol Biol *425*, 3563–3575.

Roberts, A.W., Seymour, J.F., Brown, J.R., Wierda, W.G., Kipps, T.J., Khaw, S.L., Carney, D.A., He, S.Z., Huang, D.C.S., Xiong, H., et al. (2012). Substantial susceptibility of chronic lymphocytic leukemia to BCL2 inhibition: results of a phase I study of navitoclax in patients with relapsed or refractory disease. J Clin Oncol *30*, 488–496.

Rohl, C.A., Strauss, C., Misura, K., and Baker, D. (2004). Protein structure prediction using Rosetta. Method Enzymol *383*, 66-93.

Rong, Y.P., Bultynck, G., Aromolaran, A.S., Zhong, F., Parys, J.B., De Smedt, H., Mignery, G.A., Roderick, H.L., Bootman, M.D., Distelhorst, C.W. (2009). The BH4 domain of Bcl-2 inhibits ER calcium release and apoptosis by binding the regulatory and coupling domain of the IP3 receptor. Proc Natl Acad Sci USA *106*, 14397-14402.

Shamas-Din, A., Brahmbhatt, H., Leber, B., and Andrews, D.W. (2011). BH3-only proteins: orchestrators of apoptosis. Biochim Biophys Acta. *1813*, 508–520.

Silva, D.A., Correia, B.E., Procko, E. (2016). Motif-driven design of protein-protein interfaces. Methods Mol Biol *1414*, 285-304.

Skubak, P., Murshudov, G.N., and Pannu, N.S. (2004). Direct incorporation of experimental phase information in model refinement. Acta Crystallogr D Biol. Crystallogr *60*, 2196–2201.

Souers, A.J., Leverson, J.D., Boghaert, E.R., Ackler, S.L., Catron, N.D., Chen, J., Dayton, B.D., Ding, H., Enschede, S.H., Fairbrother, W.J., Huang, D.C.S., et al. (2013). ABT-199, a potent and selective BCL-2 inhibitor, achieves antitumor activity while sparing platelets. Nature Med *19*, 202–208.

Suzuki, M., Youle, R.J., and Tjandra, N. (2000). Structure of Bax: coregulation of dimer formation and intracellular localization. Cell *103*, 645–654.

Tse, C., Shoemaker, A.R., Adickes, J., Anderson M.G., Chen, J., Jin, S., Johnson, E.F., Marsh K.C., Mitten, M.J., Nimmer, P., et al. ABT-263: a potent and orally bioavailable Bcl-2 family inhibitor. (2008). Cancer Res *68*, 3421-3428.

Tsujimoto, Y., and Croce, C.M. (1986). Analysis of the structure, transcripts, and protein products of bcl-2, the gene involved in human follicular lymphoma. Proc Natl Acad Sci USA *83*, 5214-5418.

van Delft, M.F., Wei, A.H., Mason, K.D., Vandenberg, C.J., Chen, L., Czabotar, P.E., Willis, S.N., Scott, C.L., Day, C.L., Cory, S., et al. (2006). The BH3 mimetic ABT-737 targets selective Bcl-2 proteins and efficiently induces apoptosis via Bak/Bax if Mcl-1 is neutralized. Cancer Cell *10*, 389–399.

Walensky, L.D., Pitter, K., Morash, J., Oh, K.J., Barbuto, S., Fisher, J., Smith, E., Verdine, G.L., and Korsmeyer, S.J. (2006). A Stapled BID BH3 helix directly binds and activates BAX. Mol Cell *24*, 199–210.

Wang, L., Doherty, G., Wang, X., Tao, Z.F., Brunko, M., Kunzer, A.R., Wendt, M.D., Song, X., Frey, R., and Hansen, T.M. (2013). 8-carbamoyl-2-(2,3-disubstituted pyrid-6-yl)-1,2,3,4-tetrahydroisoquinoline derivatives as apoptosis - inducing agents for the treatment of cancer and immune and autoimmune diseases. United States patent WO2013139890 A1.

Wang, L.M., Lu, K.V., Zhu, S., Dia, E.Q., Vivanco, I., Shackleford, G.M., Cavenee, W.K., Mellinghoff, I.K., Cloughesy, T.F., Sawyers, C.L., et al. (2006). Mammalian target of rapamycin inhibition promotes response to epidermal growth factor receptor kinase inhibitors in PTEN-deficient and PTEN-intact glioblastoma cells. Cancer Res *66*: 7864-7869.

Weller, M., Malipiero, U., Aguzzi, A., Reed, J.C., and Fontana, A. (1995). Protooncogene bcl-2 gene transfer abrogates Fas/APOU-1 antibody-mediated apoptosis of human malignant glioma cells and confers resistance to chemotherapeutic drugs and therapeutic irradiation. J Clin Invest *95*, 2633-2643.

Willis, S.N., Fletcher, J.I., Kaufmann, T., van Delft, M.F., Chen, L., Czabotar, P.E., Ierino, H., Lee, E.F., Fairlie, W.D., Bouillet, P., et al. (2007). Apoptosis initiated when BH3 ligands engage multiple Bcl-2 homologs, not Bax or Bak. Science *315*, 856–859.

Winn, M.D., Ballard, C.C., Cowtan, K.D., Dodson, E.J., Emsley, P., Evans, P.R., Keegan, R.M., Krissinel, E.B., Leslie, A.G.W., McCoy, A., et al. (2011). Overview of the CCP4 suite and current developments. Acta Crystallogr D Biol Crystallogr. *67*, 235-242.

Zelter, A., Bonomi, M., Kim, J., Umbreit, N.T., Hoopmann M.R., Johnson, R., Riffle, M., Jaschob, D., MacCoss, M.J., Moritz, R.L., et al. (2015). The molecular architecture of the Dam1 kinetochore complex is defined by cross-linking based structural modeling. Nat Comm *6*, 8673.

Zhang, H., Xue, J., Hessler, P., Tahir, S.K., Chen, J., Jin, S., Souers, A.J., Leverson, J.D., and Lam, L.T. (2015). Genomic analysis and selective small molecule inhibition identifies BCL-X(L) as a critical survival factor in a subset of colorectal cancer. Mol Cancer *14*, 126.

Zhang, Y, and Skolnick, J. (2005). TM-align: a protein structure alignment algorithm based on the TM-score. Nucleic Acids Res *33*, 2302–2309.

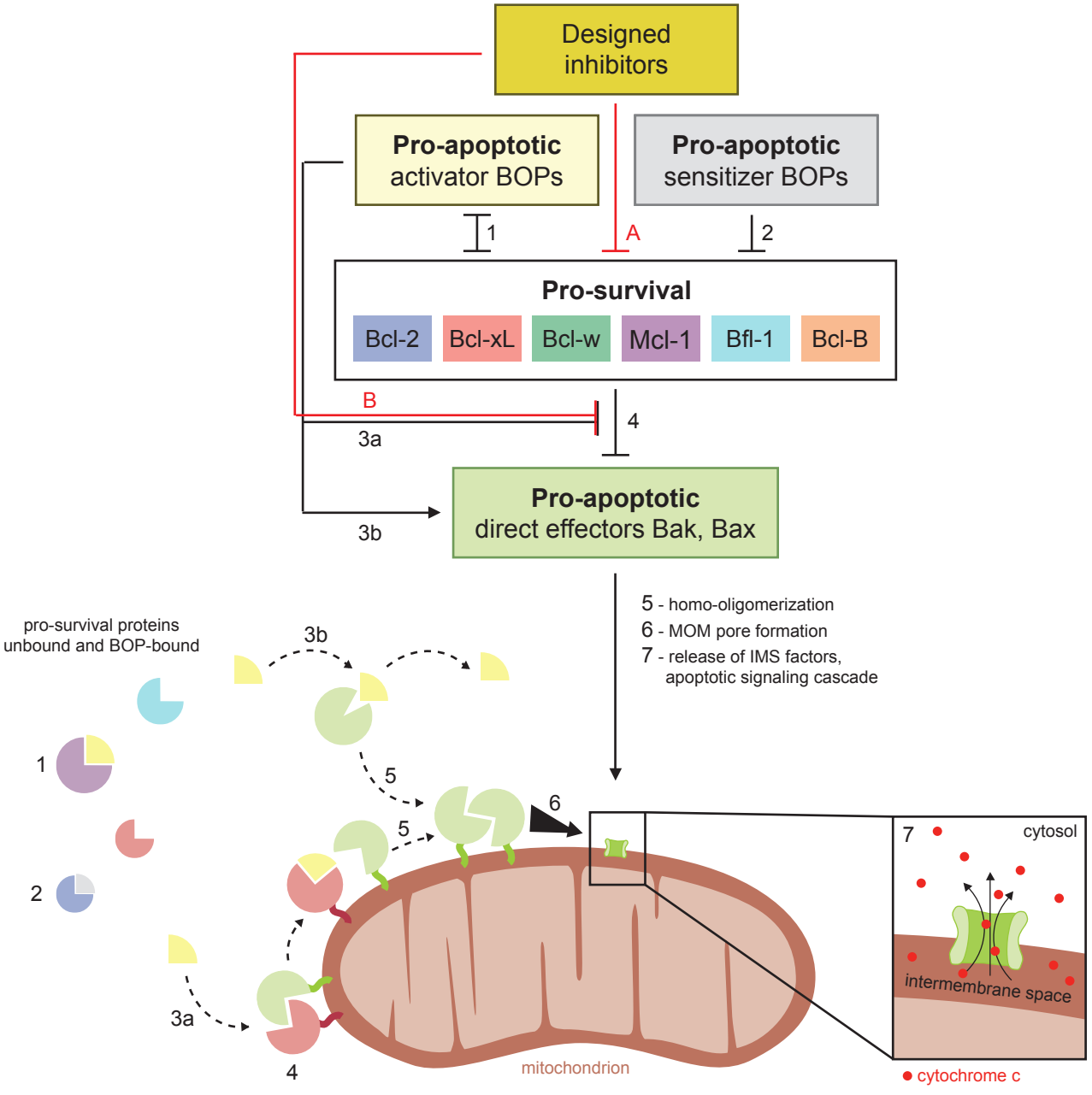

Figure 1. Schematic of BCL2 family interactions. BCL2 proteins are categorized by their net effect on cell fate and the presence of shared structural domains. BH3-only proteins (BOPs) are sequestered by pro-survival homologs (labels 1 and 2), and some BOPs may activate the direct effectors Bak and Bax by disrupting their inhibition by pro-survival proteins (3a) and/or promoting their homo-oligomerization (3b). Pro-survival proteins, which are typically overexpressed in cancer, bind and inhibit Bak and Bax (4), which would otherwise homo-oligomerize upon activation (5) and form pores in the mitochondrial outer membrane (MOM; 6). MOM permeabilization allows the release of cytochrome c and other factors from the intermembrane space (IMS) and thus initiates the apoptotic signaling cascade (7). Designed inhibitors have a net pro-apoptotic effect by binding pro-survival proteins, which may both limit sequestration of BOPs (A) and disrupt inhibition of Bak and Bax (B).

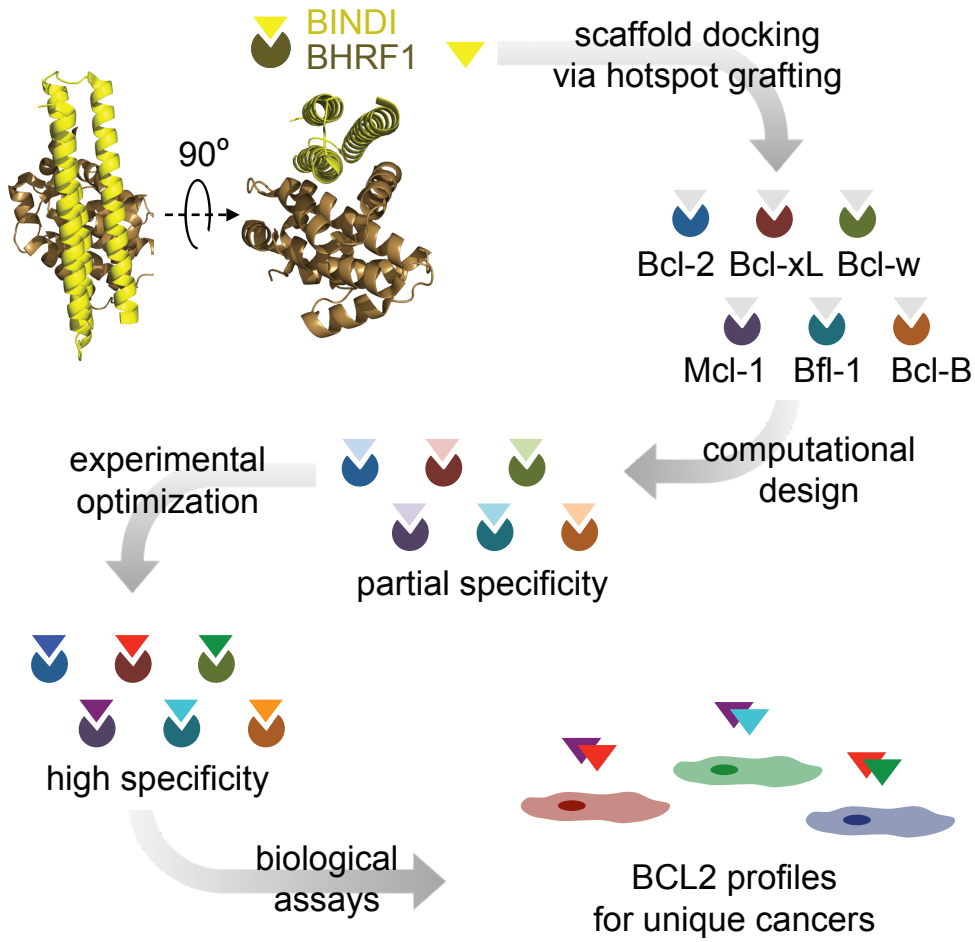

Figure 1—figure supplement 1. Design strategy. BINDI, a de novo three-helix bundle inhibitor of BHRF1, was employed as a scaffold protein to engineer altered specificities toward each of six human pro-survival proteins. BINDI was first computationally docked into the binding groove of each BCL2 homolog and interface residues were computationally designed, yielding high affinity inhibitors with at least partial specificity. Some designs were further optimized for specificity and affinity via mutagenesis and in vitro evolution. Specific, optimized inhibitors were used to study BCL2 profiles of different cancers.

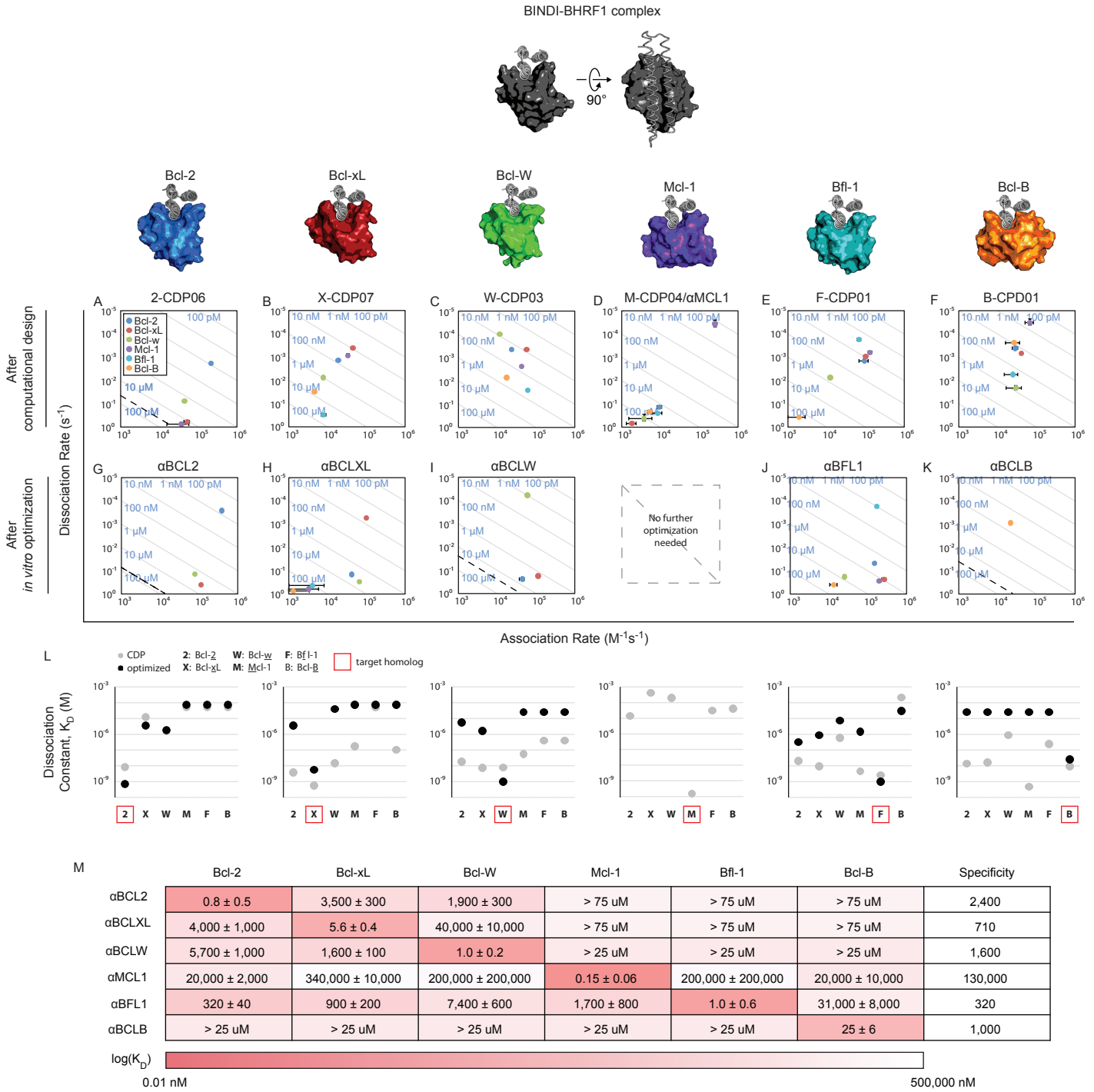

Figure 2. Binding profiles for highly specific, high affinity inhibitors. On and off rates were determined by BLI with multiple-concentration binding titrations for each computationally designed protein (A-F) and optimized variants (G-K; mean ± SD; n=3). Diagonal lines represent dissociation constants (KD) as labeled. Dashed lines indicate affinities at which binding signals were too weak to be accurately measured; dissociation constants for interactions not plotted are assumed to be greater than these thresholds. (L) KD values for computational designs (gray) and optimized inhibitors (black). (M) KD values for final optimized inhibitors (mean ± SD; n=3).

Figure 2—figure supplement 1. Computational design and screening methods. (A) BINDI (gray) was docked to the hydrophobic binding groove of Bcl-xL (red) by alignment to a bound BH3 peptide (not shown). The docked pose undergoes successive rounds of design with ROSETTA, in which BINDI residues within 8 Å (Cβ atoms indicated by yellow spheres) and then 12 Å (cyan spheres) of the interface are available for computational mutation, while hotspot residues (pink spheres) are held constant. (B) Hotspots (pink) are borrowed from native BH3 motifs or designed peptides, transferred to the BINDI scaffold and restricted from mutation during design (termed 'side chain grafting'). (C) A novel motif-grafting method samples all possible docked configurations of the BINDI scaffold (multiple colors) in the Bcl-w (green) binding groove. (D) The docked position of Bcl-w-targeting design W-CDP03 (green cartoon) is shifted one helical turn relative to (E) BINDI (gray cartoon) and exhibits better shape complementarity to Bcl-w (green surface). (F) Selected computationally designed proteins (CDPs) are qualitatively compared with single-concentration BLI assays. Design M-CDP02 is partially specific for Mcl-1, and M-CDP04 is highly specific. (G) Binding constants (K_D) are accurately determined with multiple-concentration BLI titrations. Biotinylated Mcl-1 was immobilized to a streptavidin-coated sensor and incubated with the indicated concentrations of soluble αMCL1. Raw data is purple, fitted curves are black. (H) K_D values of CDPs, intermediate ECMs, and Bim BH3 (as a fusion to maltose binding protein) were determined with BLI (mean ± SD; n=3), and binding constants of competing small molecule and peptide inhibitors (citations noted below). (I) Computationally designed proteins (all gray, except M-CDP04/αMCL1 in black which required no further optimization) and their optimized successors (ECMs dashed; best variants solid black) were denatured with guanidinium hydrochloride. CD signal at 222 nM was measured and loss of signal used to calculate the fraction folded. Mean CD signal ± SD from three scans. (1) Souers et al., 2013; (2) Leverson et al., 2015a; (3) Leverson et al., 2015b; (4) Tse et al., 2008; (5) Dutta et al., 2010; (6) Foight et al., 2014; (7) Dutta et al., 2013.

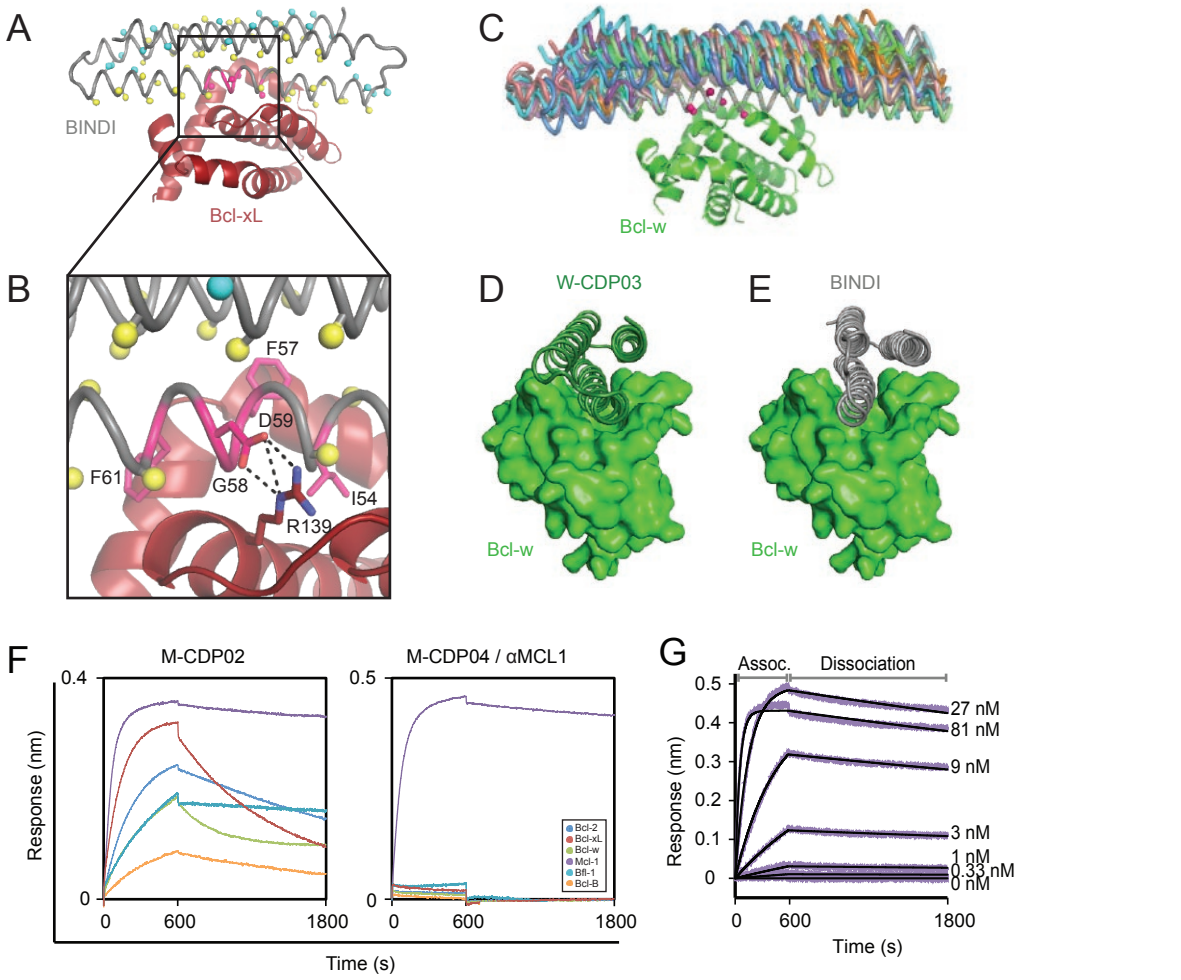

H

	Bcl-2	Bcl-xL	Bcl-w	Mcl-1	Bfl-1	Bcl-B	Specificity
2-CDP06	9 ± 1	12,000 ± 1,000	1,700 ± 100	> 50,000	> 50,000	> 50,000	190
X-CDP07	4 ± 1	0.59 ± 0.07	14.9 ± 0.5	17 ± 1	> 50,000	107 ± 9	7
W-CDP03	30 ± 20	7 ± 1	8 ± 1	57 ± 8	500 ± 300	410 ± 80	< 1
F-CDP01	27 ± 8	11 ± 1	600 ± 80	4.6 ± 0.6	2 ± 2	100,000 ± 100,000	2
F-ECM04	100 ± 6	540 ± 30	3,800 ± 500	300 ± 100	1.1 ± 0.7	4,000 ± 4,000	91
10-CDP01	17 ± 3	20 ± 4	2,000 ± 500	0.46 ± 0.09	520 ± 30	8 ± 1	< 1
10-ECM01	12,500 ± 400	7,800 ± 300	19,000 ± 2,000	3,700 ± 100	2,400 ± 900	80 ± 50	30
BIM BH3	0.17	0.75	1.56	0.61	7	20	N/A
ABT-199 (1)	< 0.01	48	245	> 444	N/A	N/A	4,800
A-13311852 (2)	6	0.01	4	142	N/A	N/A	400
A-1210477 (3)	132	660	2280	0.415	660	N/A	320
ABT-263 (2)	0.044	0.055	7	> 224	354	N/A	N/A
ABT-737 (4)	< 1	< 0.5	0.9	> 1000	N/A	N/A	N/A
MB1 (5)	1000	1000	1000	4	1000	N/A	250
MS1 (6)	2300	1600	1300	1.9	5000	N/A	690
FA1 (7)	N/A	33	N/A	6	0.3	N/A	20
XH11 (5)	73	2.9	81	1000	1000	N/A	25

log(K_D)
0.01 nM
500,000 nM

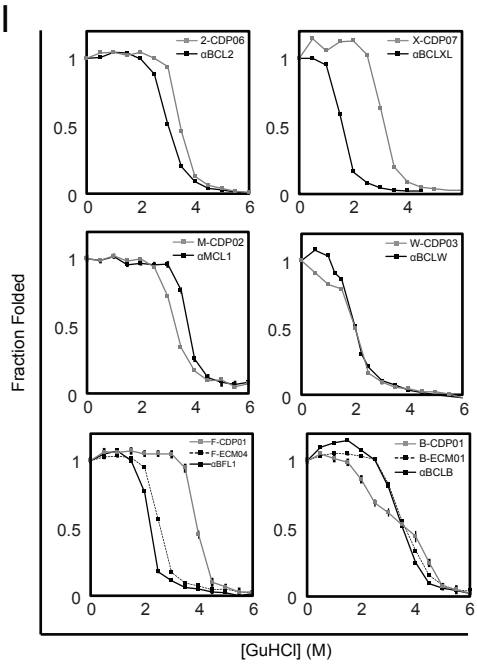

Figure 2—figure supplement 1. Computational design and screening methods (continued).

Figure 2—figure supplement 2. Computational docking calculations: CDPs. CDPs were computationally docked into the canonical binding groove of each pro-survival BCL2 homolog, sampling both local (close to the input bound conformation) and global (entire protein surface) environments. (A) Binding energy (ddG) and RMSD from the input bound conformation were calculated for each of thousands of docked configurations and plotted (global docking models in gray, local in black). The average of the 100 lowest-scoring docked conformations were calculated for local (local minimum; black dashed line) and global (global minimum; gray dashed line) docking. (B) Absolute binding energy (local minimum) and relative binding energy (difference between local and global minima) are plotted and compared to experimental binding data.

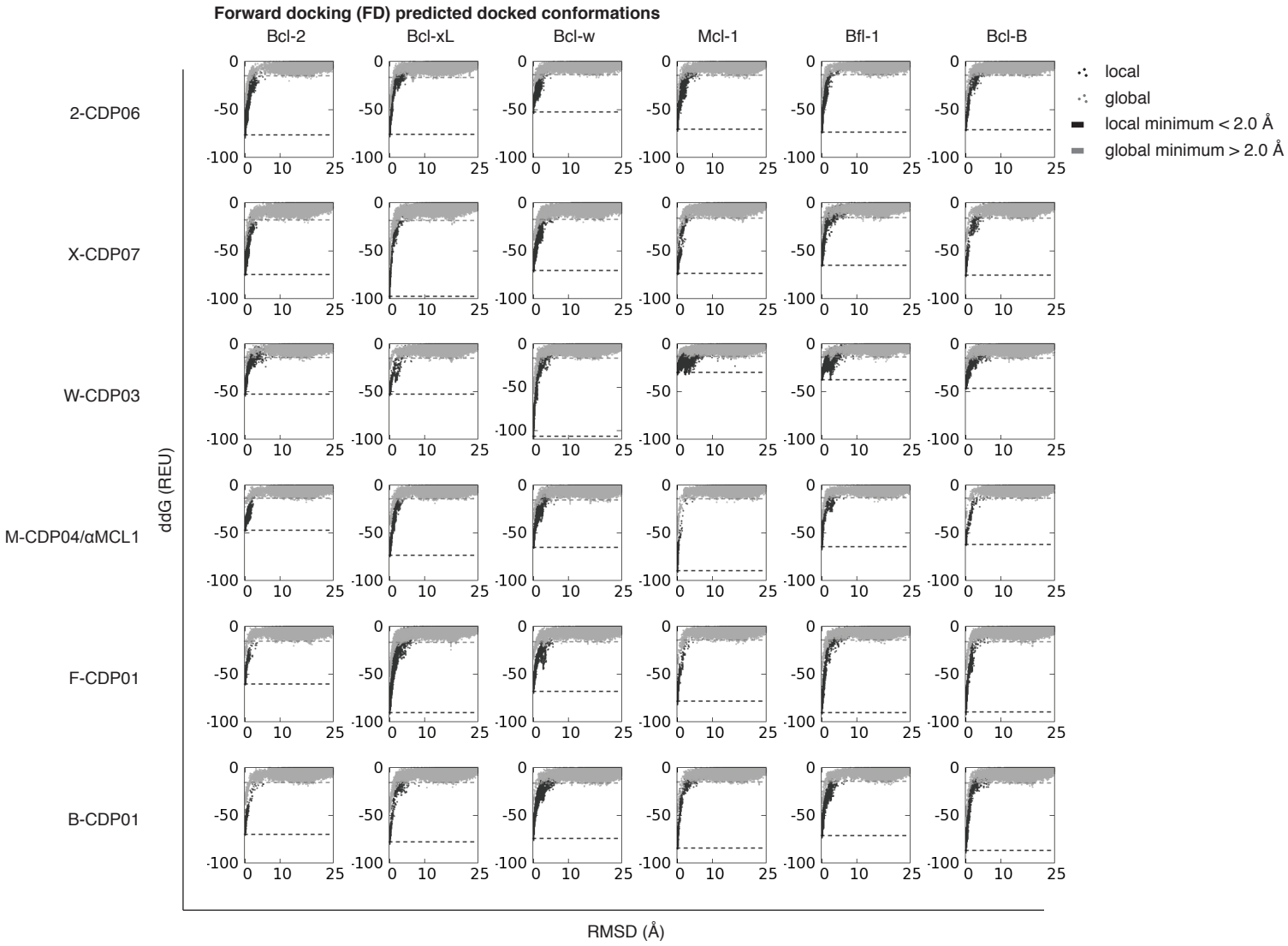

Absolute binding energy (local FD ddG minimum)

	Bcl-2	Bcl-xL	Bcl-w	Mcl-1	Bfl-1	Bcl-B
2-CDP06	-76.4	-76.0	-52.8	-70.8	-73.4	-71.5
X-CDP07	-74.7	-97.7	-70.3	-73.6	-65.3	-75.7
W-CDP03	-52.8	-52.8	-106.1	-30.2	-37.6	-46.7
M-CDP04/αMCL1	-47.1	-73.4	-65.0	-89.9	-64.6	-62.5
F-CDP01	-60.6	-90.2	-68.0	-78.6	-90.6	-89.9
B-CDP01	-69.8	-77.9	-74.4	-84.6	-70.9	-86.7

Relative binding energy (local vs. global minima)

	Bcl-2	Bcl-xL	Bcl-w	Mcl-1	Bfl-1	Bcl-B
2-CDP06	-61.5	-59.5	-38.8	-56.2	-59.4	-57.3
X-CDP07	-57.0	-79.4	-52.8	-57.6	-49.9	-59.8
W-CDP03	-38.6	-37.7	-89.8	-16.8	-23.7	-32.0
M-CDP04/αMCL1	-33.3	-58.9	-49.4	-75.7	-51.5	-49.0
F-CDP01	-45.1	-73.7	-52.0	-64.1	-76.3	-73.9
B-CDP01	-54.2	-62.2	-58.1	-69.6	-56.4	-70.6

Dissociation constants (K_D)

	Bcl-2	Bcl-xL	Bcl-w	Mcl-1	Bfl-1	Bcl-B
2-CDP06	9 ± 1	12,000 ± 1,000	1,700 ± 100	> 50,000	> 50,000	> 50,000
X-CDP07	4 ± 1	0.59 ± 0.07	14.9 ± 0.5	17 ± 1	> 50,000	107 ± 9
W-CDP03	30 ± 20	7 ± 1	8 ± 1	57 ± 8	500 ± 300	410 ± 80
M-CDP04/αMCL1	20,000 ± 2,000	340,000 ± 10,000	200,000 ± 200,000	0.15 ± 0.06	200,000 ± 200,000	20,000 ± 10,000
F-CDP01	27 ± 8	11 ± 1	600 ± 80	4.6 ± 0.6	2 ± 2	100,000 ± 100,000
B-CDP01	17 ± 3	20 ± 4	2,000 ± 500	0.46 ± 0.09	520 ± 30	8 ± 1

Figure 2—figure supplement 2. Computational docking calculations: CDPs (continued).

Figure 2—figure supplement 3. Computational docking calculations: optimized inhibitors. Optimized, specific inhibitors were computationally docked into the canonical binding groove of each pro-survival BCL2 homolog, sampling both local (close to the input bound conformation) and global (entire protein surface) environments. (A) Binding energy (ddG) and RMSD from the input bound conformation were calculated for each of thousands of docked configurations and plotted (global docking models in gray, local in black). The average of the 100 lowest-scoring docked conformations were calculated for local (local minimum; black dashed line) and global (global minimum; gray dashed line) docking. (B) Absolute binding energy (local minimum) and relative binding energy (difference between local and global minima) are plotted and compared to experimental binding data.

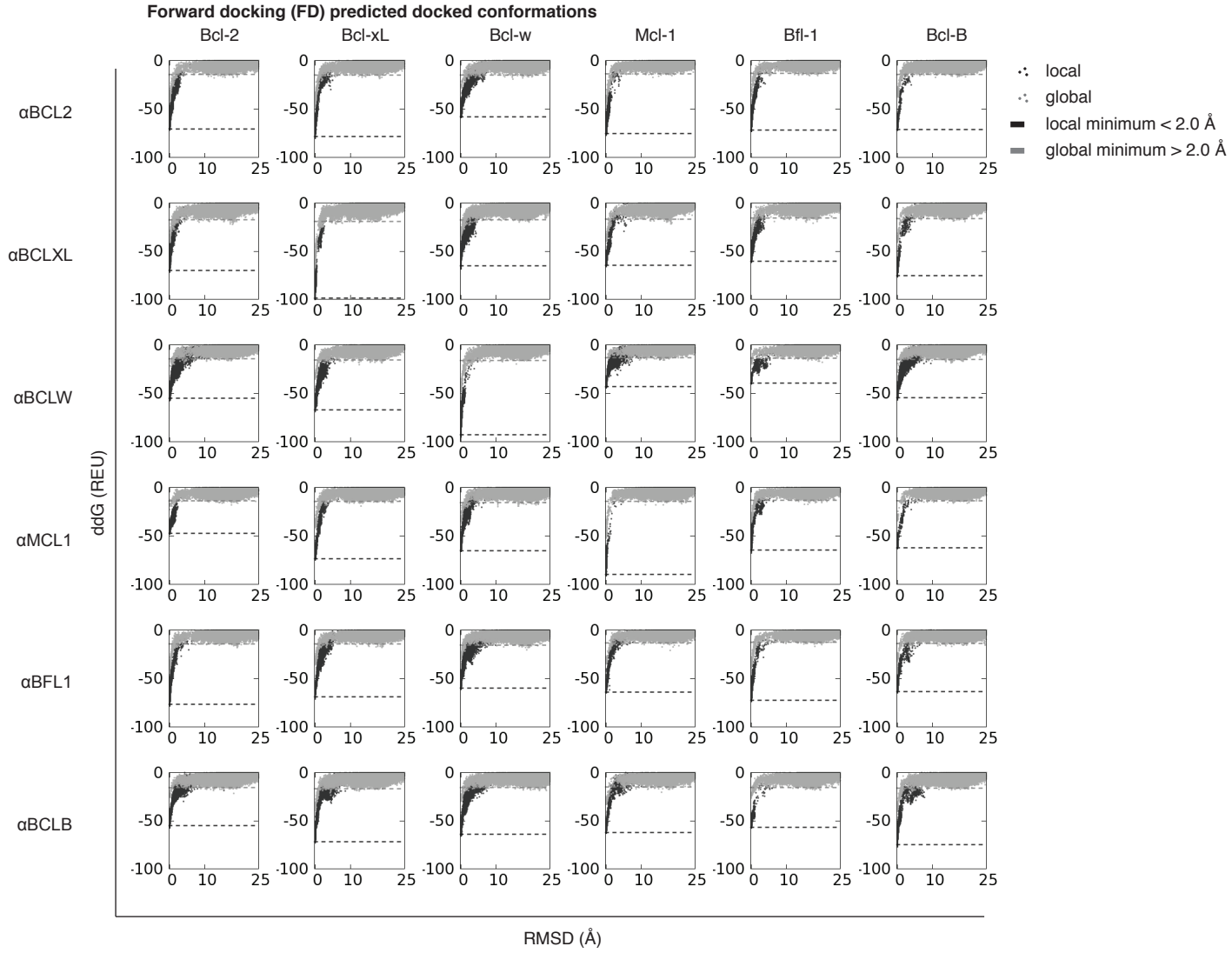

Absolute binding energy (local FD ddG minimum)

	Bcl-2	Bcl-xL	Bcl-w	Mcl-1	Bfl-1	Bcl-B
αBCL2	-70.3	-78.5	-57.8	-75.3	-71.9	-71.2
αBCLXL	-69.7	-99.0	-65.1	-64.7	-60.6	-74.2
αBCLW	-55.1	-67.0	-92.7	-43.3	-39.6	-54.5
M-CDP04/αMCL1	-47.1	-73.4	-65.0	-89.9	-64.6	-62.5
αBFL1	-76.7	-68.8	-59.7	-64.0	-72.3	-63.7
αBCLB	-55.2	-71.9	-64.3	-62.2	-56.9	-74.9

Relative binding energy (local vs. global minima)

	Bcl-2	Bcl-xL	Bcl-w	Mcl-1	Bfl-1	Bcl-B
αBCL2	-55.7	-63.7	-42.9	-61.7	-58.9	-56.7
αBCLXL	-52.2	-80.0	-47.5	-48.2	-45.0	-57.8
αBCLW	-40.7	-51.4	-76.6	-30.1	-25.9	-39.5
M-CDP04/αMCL1	-33.3	-58.9	-49.4	-75.7	-51.5	-49.0
αBFL1	-62.5	-54.6	-44.5	-50.8	-59.7	-49.7
αBCLB	-39.6	-55.2	-48.8	-47.3	-41.5	-58.9

Dissociation constants (K_D)

	Bcl-2	Bcl-xL	Bcl-w	Mcl-1	Bfl-1	Bcl-B
αBCL2	0.8 ± 0.5	3,500 ± 300	1,900 ± 300	> 75 uM	> 75 uM	> 75 uM
αBCLXL	4,000 ± 1,000	5.6 ± 0.4	40,000 ± 10,000	> 75 uM	> 75 uM	> 75 uM
αBCLW	5,700 ± 1,000	1,600 ± 100	1.0 ± 0.2	> 25 uM	> 25 uM	> 25 uM
M-CDP04/αMCL1	20,000 ± 2,000	340,000 ± 10,000	200,000 ± 200,000	0.15 ± 0.06	200,000 ± 200,000	20,000 ± 10,000
αBFL1	320 ± 40	900 ± 200	7,400 ± 600	1,700 ± 800	1.0 ± 0.6	31,000 ± 8,000
αBCLB	> 25 uM	> 25 uM	> 25 uM	> 25 uM	> 25 uM	25 ± 6

Figure 2—figure supplement 2. Computational docking calculations: CDPs (continued).

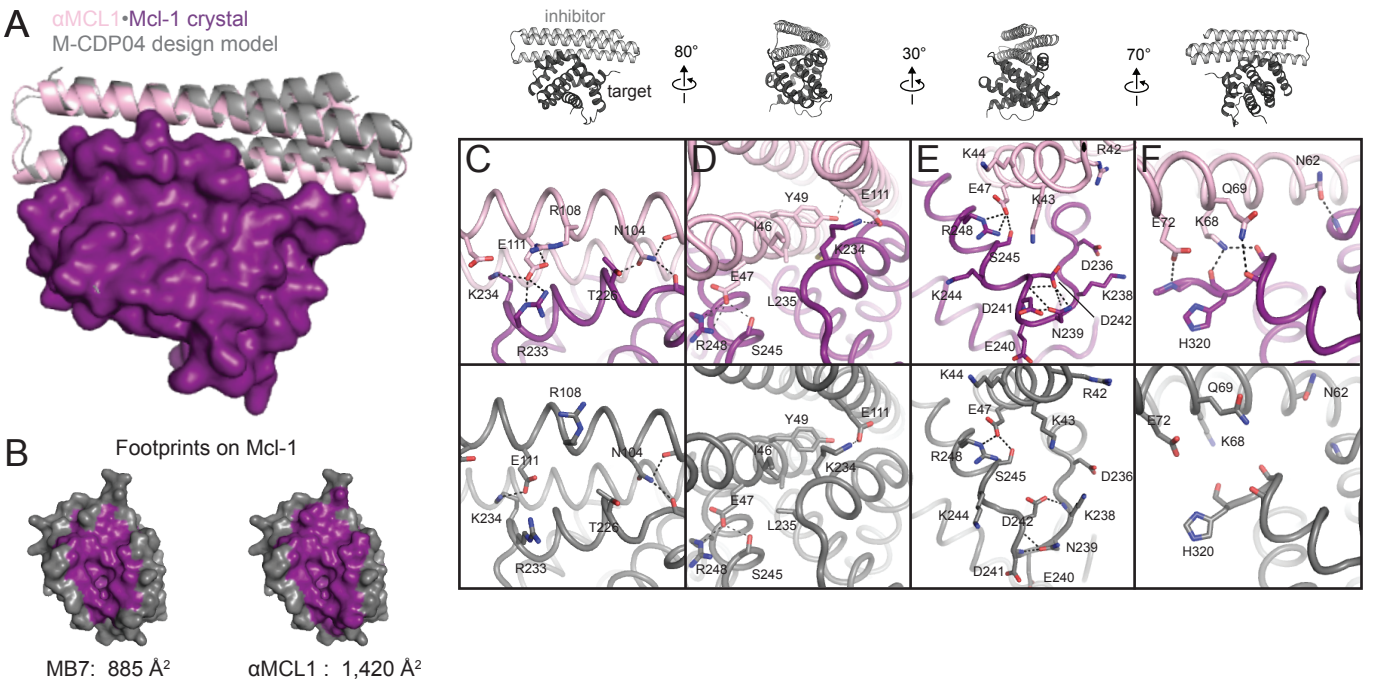

Figure 3. The crystal structure of αMCL1•Mcl-1 is very close to the design model. (A) Alignment of the design model M-CDP04 (gray cartoon) and crystal structure (Mcl-1, purple surface; αMCL1, pink cartoon). (B) Buried contact surfaces on Mcl-1 bound to a BH3-like motif (designed peptide MB7; PDB 3KZ0) and αMCL1. (C-F) Comparison of crystal structure (top panels) with the design model (bottom panels): (C) αMCL1 computationally designed residues E111, R108 and N104 complement nearby Mcl-1 residues. (D) αMCL1 residue 46 was mutated from glutamate (BINDI scaffold) to isoleucine to accommodate the hydrophobic Mcl-1 binding pocket. (E) Designed residues R42, K43 and K44 promote long-range electrostatic complementarity to the negatively-charged loop region of Mcl-1. α MCL1 residue E47 (borrowed from Bim) makes ionic interactions with Mcl-1 residues S245 and R248. (F) Designed residues K68, Q69, and E72, and Bim residue N62, make polar interactions with the Mcl-1 backbone. Though the design model does not place αMCL1 near enough to Mcl-1 to make these interactions, our design calculations selected residues with long-range electrostatic complementarity.

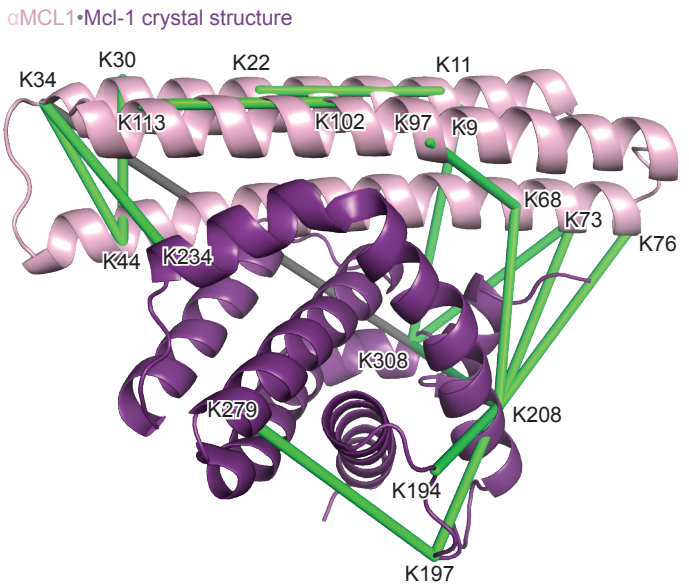

Figure 3—figure supplement 1. Structural analysis of the αMCL1•Mcl-1 complex via lysine-specific chemical cross-linking. Cross-linking studies of αMCL1 bound to Mcl-1 were consistent with the design model and crystal structure. The protein complex was incubated with three different cross-linking agents; DSS and BS3 have spacer arms of 11.4 Å, and DSG has a 7.7 Å spacer arm. These agents link lysine residues whose alpha carbons are within ~30 Å or ~26 Å, respectively. The proteins were trypsin-digested and peptides analyzed by mass spectrometry. 38 of 44 cross-links mapped to the model are below the 30 Å limit for the cross-linking agents. In the crystal structure (chains A and B used for analysis; Mcl-1 is purple and αMCL1 is light pink in cartoon representation), electron density was observed for additional residues not included in the design model, allowing additional cross-links to be mapped to the structure. 41 out of 49 cross-links mapped to the crystal structure are below the 30 Å limit. As distances increase, residues are less likely to be linked by all three reagents. For residues linked by all three reagents, 20/20 agree with the crystal structure (18/18 agree with the model); for residues linked by two of the reagents, 10/11 agree with the crystal structure (10/11 agree with the model); and for residues linked by only one of the reagents, 11/18 agree with the crystal structure (10/15 agree with the model). Overall, cross-links with the greatest confidence (i.e. detected by at least two different cross-linking agents, shown as green lines) are in excellent agreement with the structure, and these data have insufficient resolution to distinguish the model from the crystal structure; only one of these cross-links (gray line) violates the 30 Å limit.

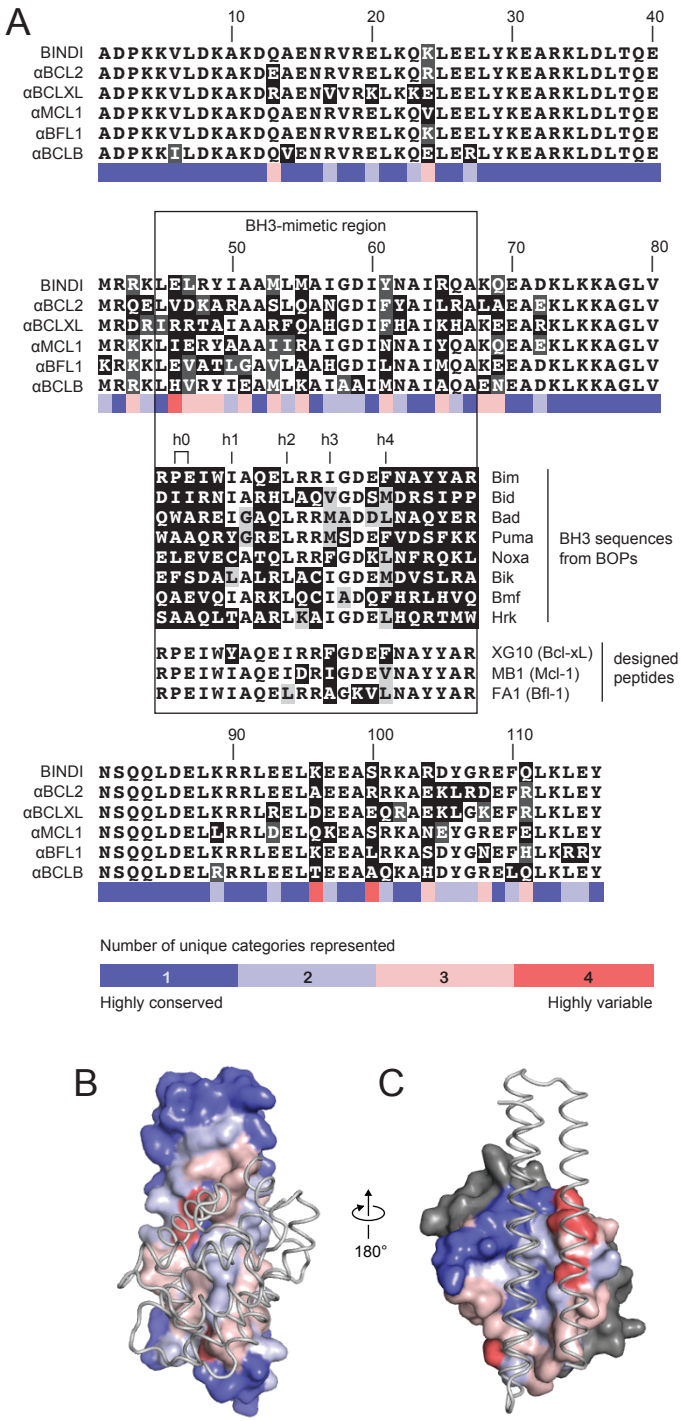

Figure 4. Comparison of design sequences with BH3-mimetic peptides and natural BH3 motifs. (A) Sequences of optimized inhibitors are aligned, excluding αBCLW, which binds to Bcl-w using a shifted interaction surface. The BH3-mimetic region of designed inhibitors is compared to natural BH3 sequences and synthetic peptides designed for indicated specificities. Non-consensus residues are shaded gray if similar to consensus and black if different. (B) Conservation was assessed by counting the number of unique categories of amino acids (polar, charged, etc.) represented across each position. Conservation scores were mapped onto each position of BINDI (surface) bound to BHRF1 (gray ribbon; PDB 4OYD). (C) Conservation scores from a sequence alignment of BCL2 proteins are mapped to BHRF1 (surface) bound to BINDI (gray ribbon).

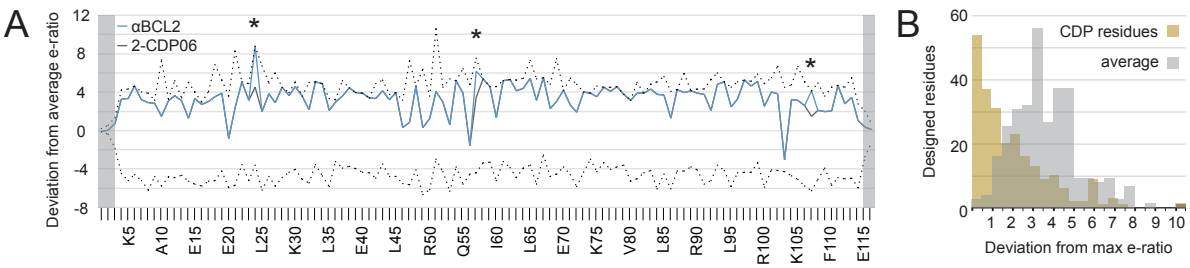

Figure 5. Analysis of computational design success. (A) Deep sequencing analysis of the naïve and sorted 2-CDP06 SSM library enabled quantitative analysis of the fitness of each single amino acid substitution for specificity and affinity toward Bcl-2. Per position, the enrichment ratio (abbreviated e-ratio; a fitness score) of each 2-CDP06 residue (black) was compared to the average value for all 20 amino acids (normalized to zero). Maximum deviations from average are represented by dashed lines, positive values indicate the best score and negative the worst. SSM-guided mutations from 2-CDP06 to αBCL2 (blue) are starred. Gray shading indicates positions with insufficient sequencing data. (B) Deviation from maximum e-ratio was calculated for each designable residue of the five mutagenized CDPs, pooled, and the distribution of deviations plotted (gold; full SSM heatmaps in Figure 5—figure supplement 1); distribution of average deviations from maximum is shown in gray.

Figure 5—figure supplement 1. Sequence analysis of SSM libraries. (A) SSM libraries were generated based on the indicated CDPs and sorted for high affinity and specificity to each target BCL2 homolog. Sequence fitness landscapes show enriched mutations (blue) that favor high affinity and/or specific binding and depleted mutations (orange) that do not. Mutations selected for a combinatorial library are boxed. Red boxes indicate mutations present in the optimized variant from each combinatorial library, and green boxes indicate mutations present in the best optimized variants from epPCR libraries. (B) For each computationally designed protein (black) and optimized variant (corresponding colors), at each position, the designed protein residue's enrichment ratio was compared to the average value for all 20 amino acids, and this deviation from average is plotted. The x-axis represents the average enrichment ratio normalized to zero (deviation from average = 0), and the gray lines indicate the maximum and minimum deviation from average represented at each position. CDPs scored above average (> 0) at most positions, indicating that designed sequences were close to optimum. As expected, mutations incorporated in each optimized variant had more favorable enrichment ratios than their corresponding designed residues, except αBFL1 M53V, which could be preferred in context of other mutations. (C) An SSM library was generated based on the partially-specific Mcl-1-targeting design M-CDP02 (see Figure S2F) and sorted for high affinity and specificity to each indicated BCL2 homolog. Sequence fitness landscapes show enriched (blue) and depleted (orange) mutations. Red boxes highlight the enrichment of aberrant mutations to proline and stop codons.

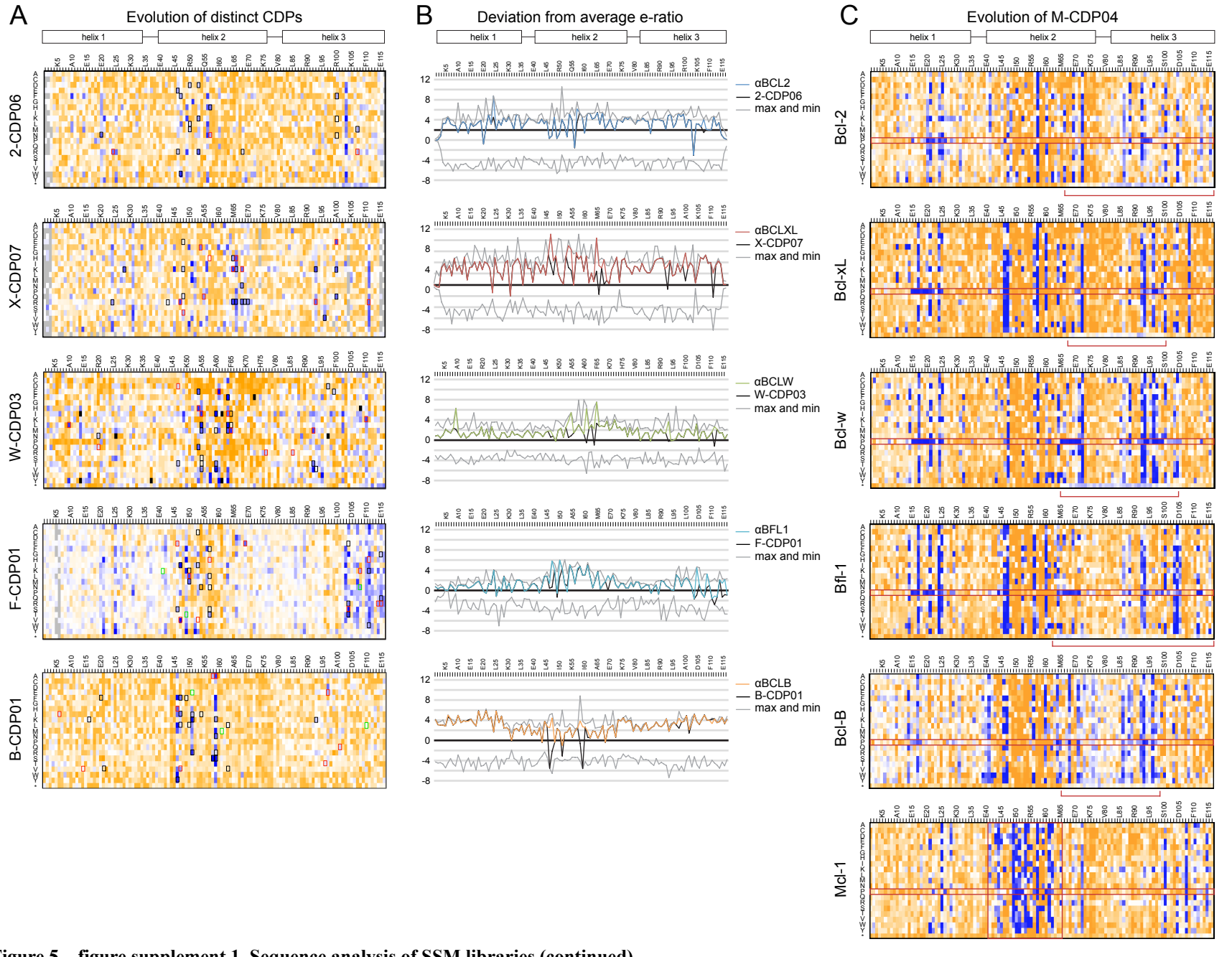

Figure 5—figure supplement 1. Sequence analysis of SSM libraries (continued).

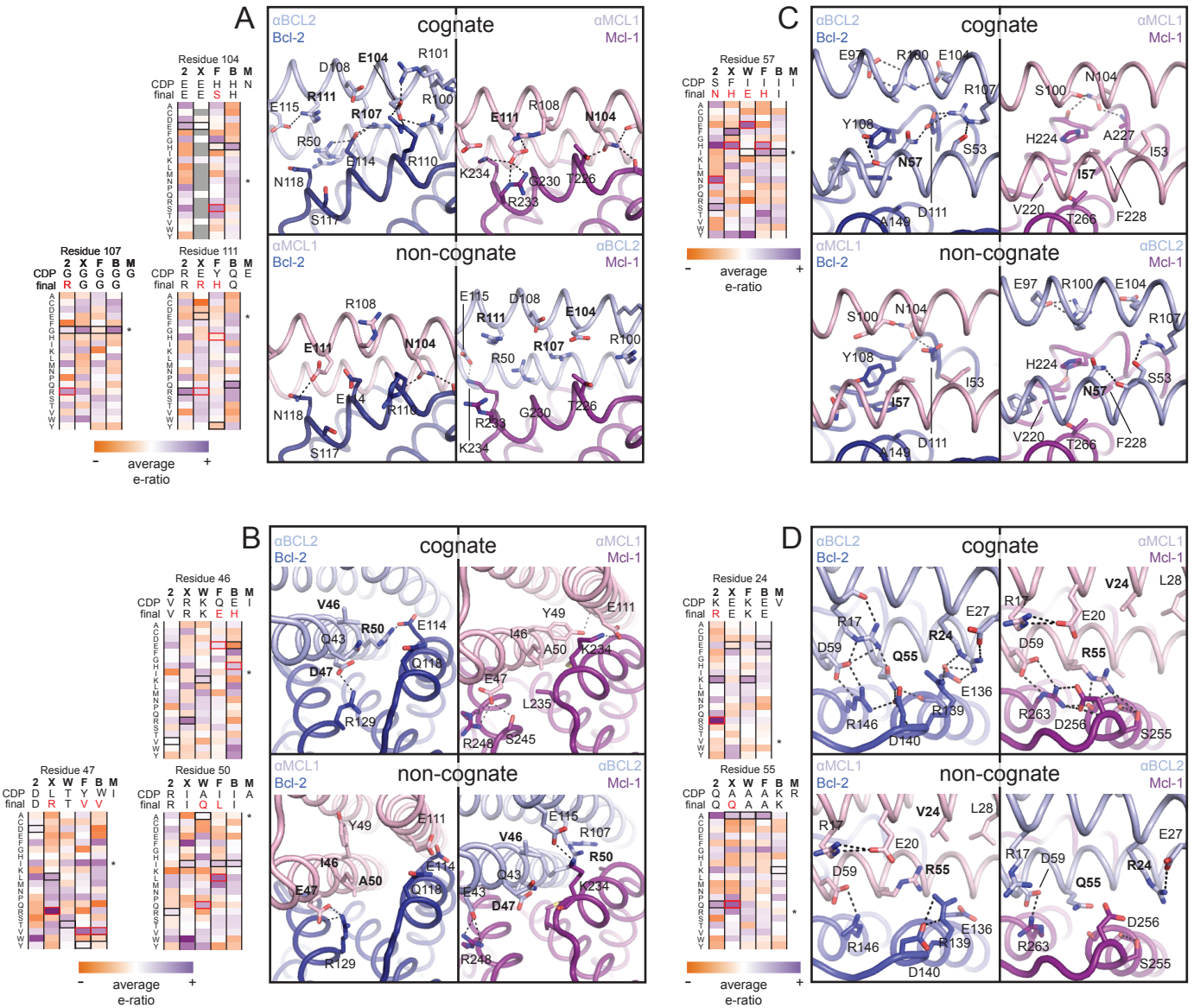

Figure 6. Determinants of binding specificity. αMCL1•Mcl-1 and αBCL2•Bcl-2 crystal structures (upper panels, high complementarity) and non-cognate binding pairs modeled in Rosetta (lower panels, poor complementarity) were aligned. For select positions on the three-helix bundle scaffold, normalized enrichment of each mutant (indicated by amino acid code) toward specific binding to each homolog (indicated at the top of each column) are shown for comparison Black outlines indicate the identity of the homolog-specific CDP, and red outlines indicate the identity of the homolog-specific optimized inhibitor (if different from CDP). Stars indicate the identity of M-CDP04/αMCL1 (no in vitro evolution required, and thus no deep sequencing data available). Gray fill indicates positions with insufficient sequencing data. Analogous αBCLW residues were included for helix 2 (sequence shifted +4 relative to others). (A) Designed αBCL2 residues E104 and R111 and αMCL1 N104 and E111 illustrate computational design success. Each contributes polar contact(s) with its target homolog, and deep sequencing data show these residues deplete binding toward one or more competitor homologs to improve specificity. αMCL1 E111 opposes Bcl-2 E114. SSM-guided α BCL2 mutation G107R contributes additional polar contacts with Bcl-2. (B) Designed αBCL2 residue R50 is tolerated by a more spacious Bcl-2 binding pocket and interacts with Bcl-2 E114. Designed αBCL2 residue D47 is partially satisfied by Bcl-2 R129. Both αBCL2 R50 and D47 fit poorly in the more hydrophobic analogous region of Mcl-1. (C) Evolved αBCL2 residue N57 introduces polar atoms in the hydrophobic interface but is partially satisfied by Bcl-2 D111. (D) Evolved αBCL2 residue R24 and designed Q55 make polar contacts with Bcl-2. αMCL1 R55, borrowed from Bim, caps an Mcl-1 helix and opposes Bcl-2 residue R139.

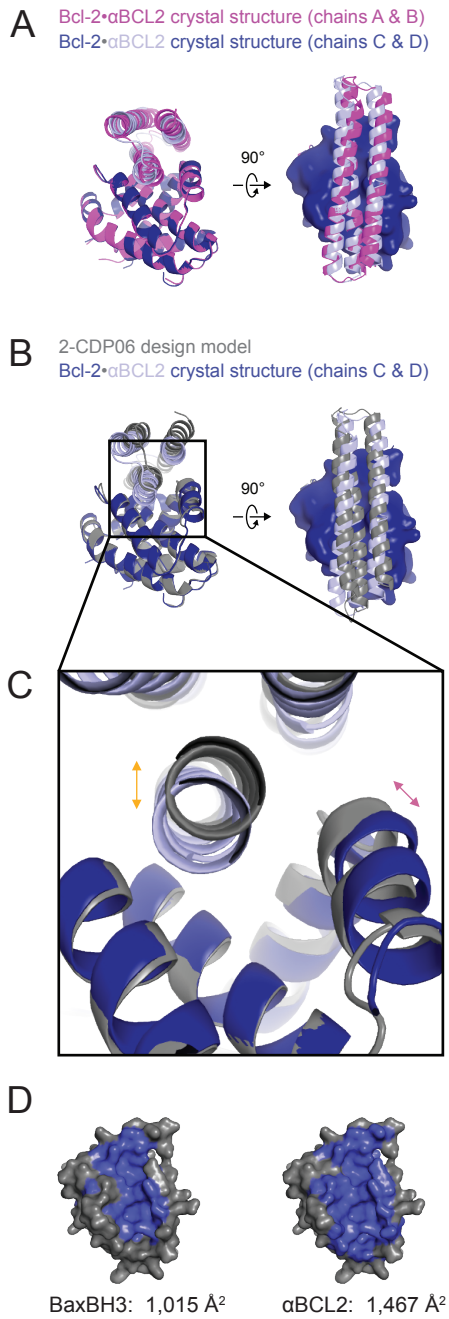

Figure 6—figure supplement 1. The crystal structure of the αBCL2•Bcl-2 complex. (A) Alignment of the two non-crystallographic symmetry (NCS)-related Bcl-2 molecules show the binding modes of the two NCS-related α BCL2 molecules differ slightly (1.9 Å RMSD). (B) Alignment of Bcl-2 molecules of the design model and crystal structure (chain C) show that design model 2-CDP06 and crystal structure αBCL2 have significantly different binding modes (4.0 Å RMSD, average from crystal structure chains A and C). (C) Magnification of the Bcl-2 binding pocket. The design model Bcl-2, based on PDB 4LVT, has a binding pocket slightly closed relative to the Bcl-2 crystal structure (pink arrow), and 2-CDP06 is positioned further from Bcl-2 than the αBCL2 crystal structure (orange arrow). Backbone restriction during design likely prohibited Bcl-2-targeting designs from accessing the closer bound conformation. (D) The buried contact surfaces of Bcl-2 bound to a representative BH3 motif (BaxBH3; PDB 2XA0) and α BCL2.

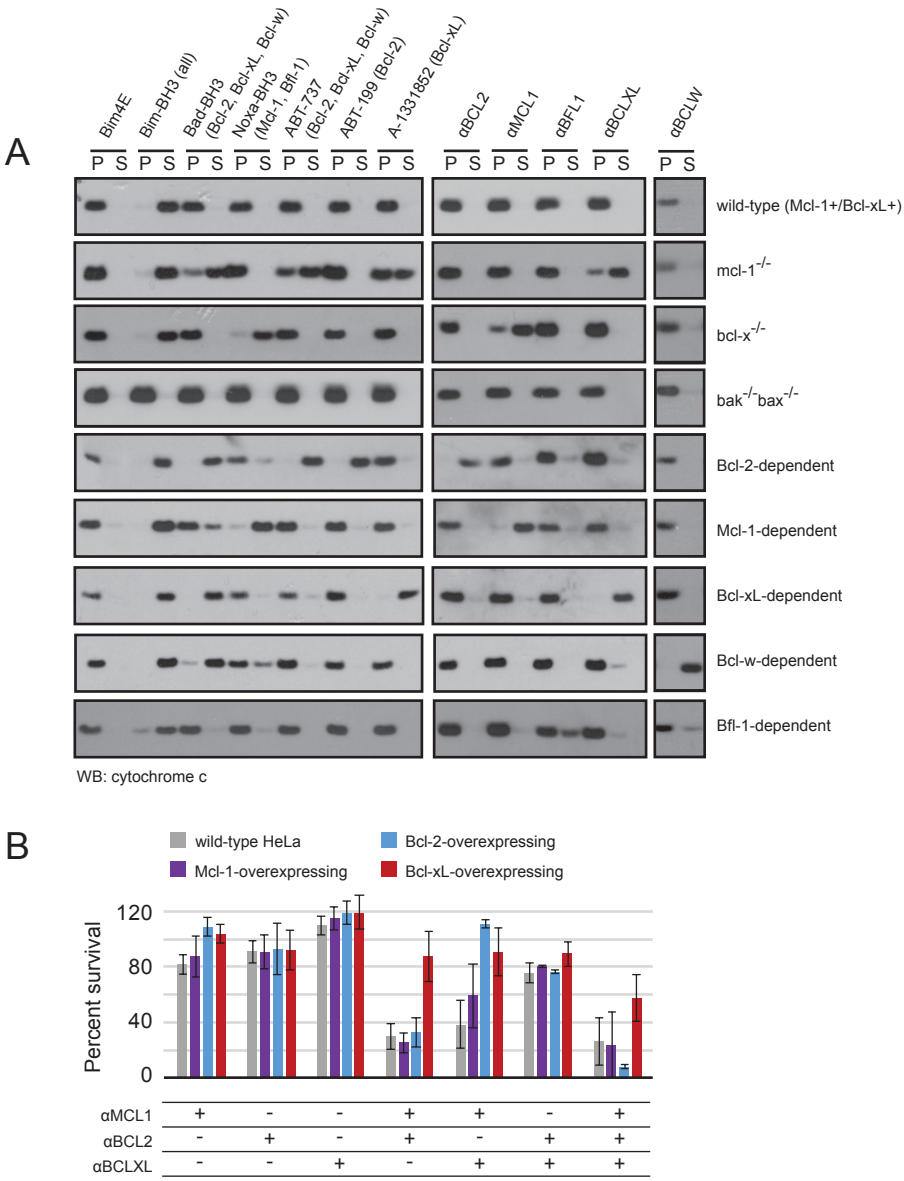

Figure 7. Designed inhibitors induce apoptosis in vitro by engaging the BH3-binding grooves of specific pro-survival homologs. (A) Western blot for cytochrome c in pelleted (P) and soluble (S) fractions of engineered MEFs after permeabilization and treatment with 10 mM BCL2 inhibitors. Bim-BH3, which binds all pro-survival homologs, is a positive control. Bim-BH3 peptide with four mutations to glutamate at interface residues (Bim4E) is a negative control. BOPs Bad and Noxa, and small molecule drugs tested have the indicated binding specificities in parentheses. (B) HeLa cells were transduced with constructs for designed inhibitor expression, and viability was assayed after 72 hours (mean ± SD; n=2 for Bcl-2+ double and triple combinations, n=3 for all others).

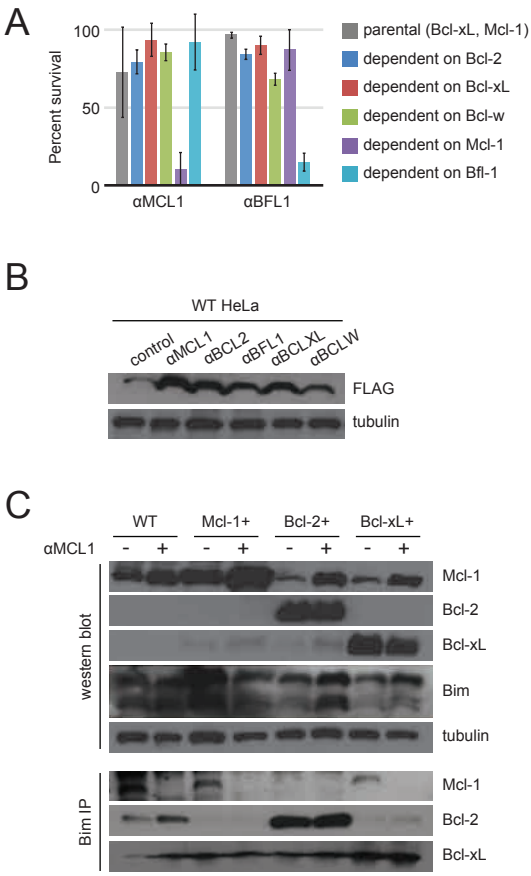

Figure 7—figure supplement 1. Long-term MEF survival and HeLa co-immunoprecipitation studies. (A) Long-term survival of engineered MEFs (pro-survival protein dependence as indicated) was assayed by counting colonies after seven to ten days of doxycycline-induced expression of αMCL1 or αBFL1 (mean ± SD; for αMCL1, n=3; for αBFL1, n=2). (B) Expression of FLAG-tagged designed inhibitors in transduced HeLa cells validated with Western blotting. (C) Bim coIP experiments in wild-type and engineered HeLa cells, with and without expression of α MCL1. Expression of αMCL1 caused a dramatic increase in the quantities of Mcl-1 protein present in all cell lines, consistent with previous studies showing increased Mcl-1 half-life in the presence of BH3-peptides (Lee et al., 2008). Bound αMCL1 may stabilize Mcl-1 or occlude Mule (Mcl-1 ubiquitin ligase E3), which binds and ubiquitinates Mcl-1 via a BH3 motif. Despite elevating Mcl-1 protein levels, αMCL1 expression potently induces apoptosis in the expected cell contexts.

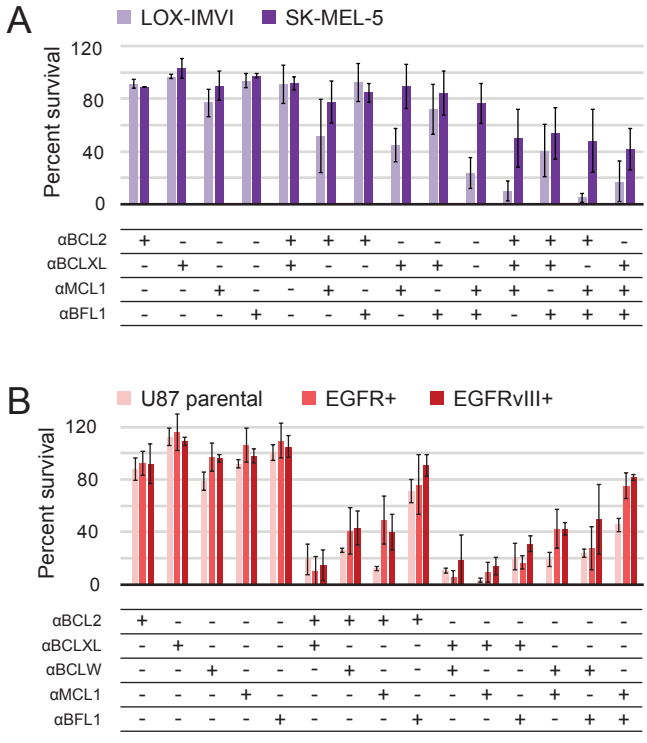

Figure 8. Determination of functional BCL2 profiles in melanoma and glioblastoma cell lines. (A) Melanoma and (B) glioblastoma cell lines were transduced with constructs for designed inhibitor expression and viability was assayed after 72 hours (mean ± SD; for melanoma, n=2 to 4; for glioblastoma, n=4). See also Figure 8¬–supplement 1D.

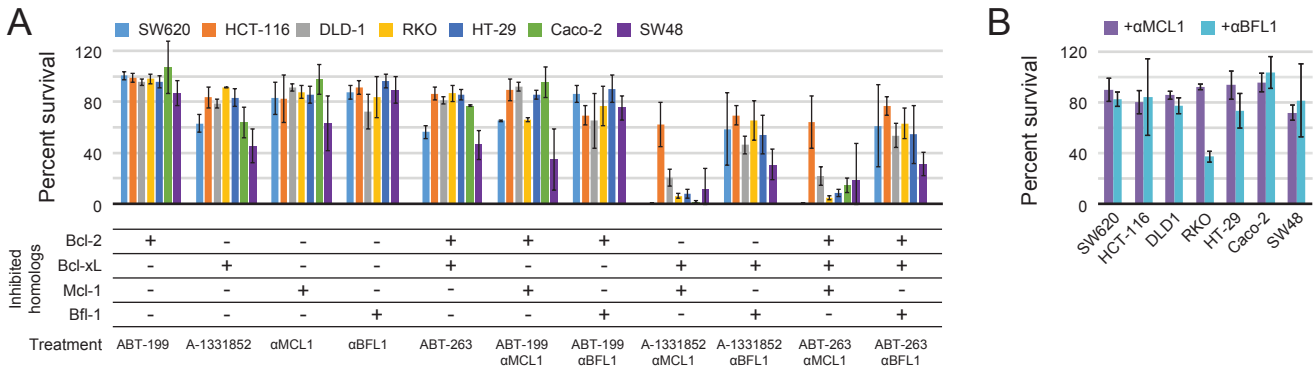

Figure 9. Determination of functional BCL2 profiles in colon cancer cell lines. (A) Colon cancers were treated with small molecule drugs (2 μM) and/or doxycycline to induce expression of designed inhibitors, as indicated, and viability was assayed after 24 hours (mean ± SD; n=3). (B) Long-term survival was assessed after expression of αMCL1 or αBFL1 (mean ± SD; n=3).

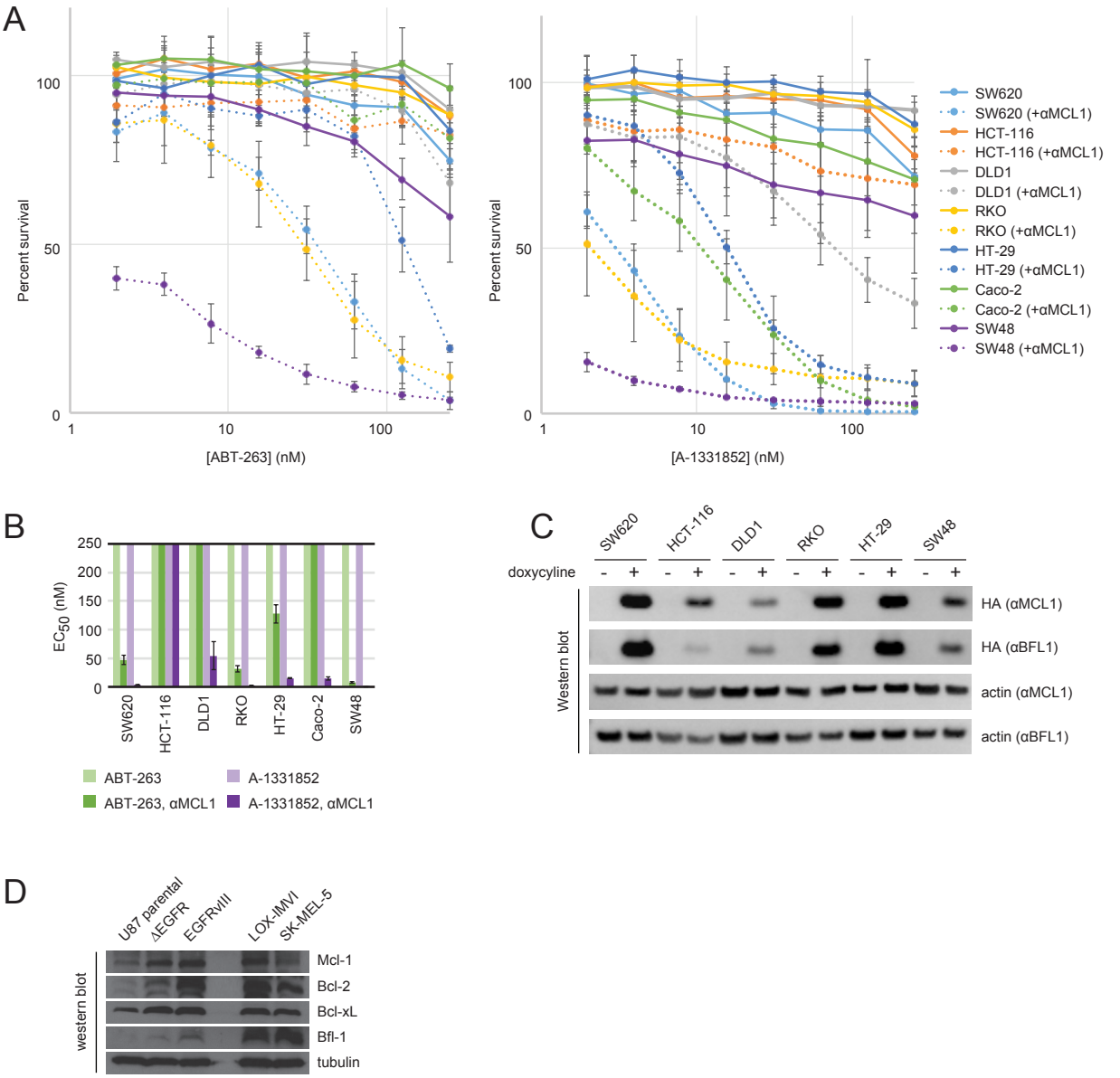

Figure 9—figure supplement 1. Drug titrations and long-term survival assays in colon cancers. (A) Drug titrations for EC50 determination of ABT-263 and A-1331852 in colon cancer lines, with (dotted lines) and without (solid lines) expression of □MCL1 (mean ± SD, n=3). (B) Long-term survival of colon cancers was assayed by counting colonies after seven to ten days of doxycycline-induced expression of □MCL1 or □BFL1 (mean ± SD, n=3). (C) Western blotting confirms expression of HA-tagged □MCL1 and □BFL1 in transformed cell lines (actin loading control). (D) Western blotting assays expression of pro-survival proteins in glioblastoma and melanoma cell lines.

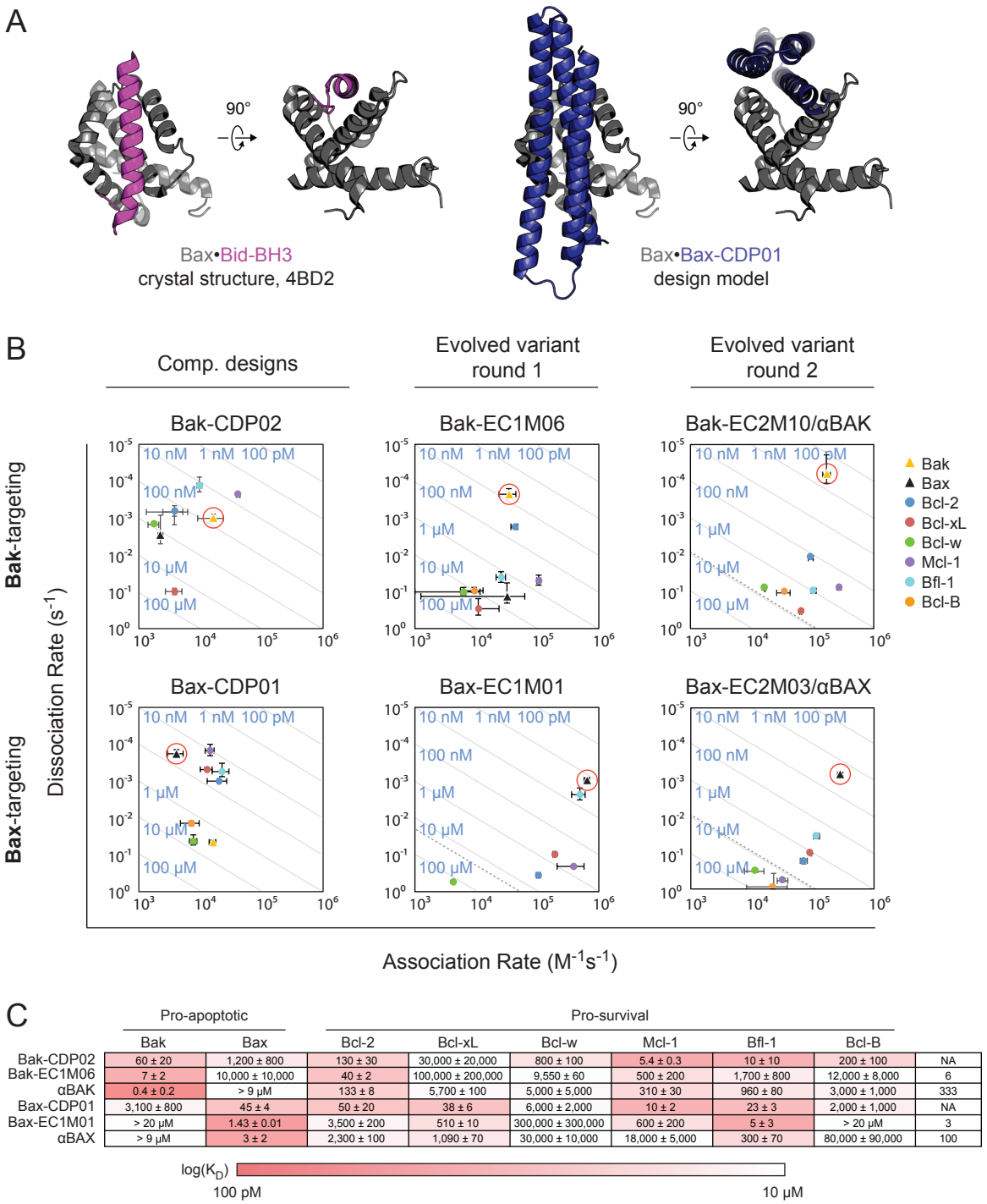

C

	Pro-apoptotic		Pro-survival						
	Bak	Bax	Bcl-2	Bcl-xL	Bcl-w	Mcl-1	Bfl-1	Bcl-B	
Bak-CDP02	60 ± 20	1,200 ± 800	130 ± 30	30,000 ± 20,000	800 ± 100	5.4 ± 0.3	10 ± 10	200 ± 100	NA
Bak-EC1M06	7 ± 2	10,000 ± 10,000	40 ± 2	100,000 ± 200,000	9,550 ± 60	500 ± 200	1,700 ± 800	12,000 ± 8,000	6
αBAK	0.4 ± 0.2	> 9 µM	133 ± 8	5,700 ± 100	5,000 ± 5,000	310 ± 30	960 ± 80	3,000 ± 1,000	333
Bax-CDP01	3,100 ± 800	45 ± 4	50 ± 20	38 ± 6	6,000 ± 2,000	10 ± 2	23 ± 3	2,000 ± 1,000	NA
Bax-EC1M01	> 20 µM	1.43 ± 0.01	3,500 ± 200	510 ± 10	300,000 ± 300,000	600 ± 200	5 ± 3	> 20 µM	3
αBAX	> 9 µM	3 ± 2	2,300 ± 100	1,090 ± 70	30,000 ± 10,000	18,000 ± 5,000	300 ± 70	80,000 ± 90,000	100

log(K_D)
100 pM
10 µM

Figure 10. Targeting the BH3-binding cleft of Bak and Bax. (A) The BH3 domain of BOP Bid interacts with the canonical BH3-binding groove of Bax (PDBID 4BD2). The BINDI helix bundle scaffold was docking into the BH3-binding groove of Bax. (B) On and off rates were determined by BLI with multiple-concentration binding titrations for each computationally designed protein and optimized variants (mean ± SD; n=3). Diagonal lines represent dissociation constants (KD) as labeled. Dashed lines indicate affinities at which binding signals were too weak to be accurately measured; dissociation constants for interactions not plotted are assumed to be greater than these thresholds. (C) KD values for CDPs, intermediate, and final optimized variants (mean ± SD; n=3).

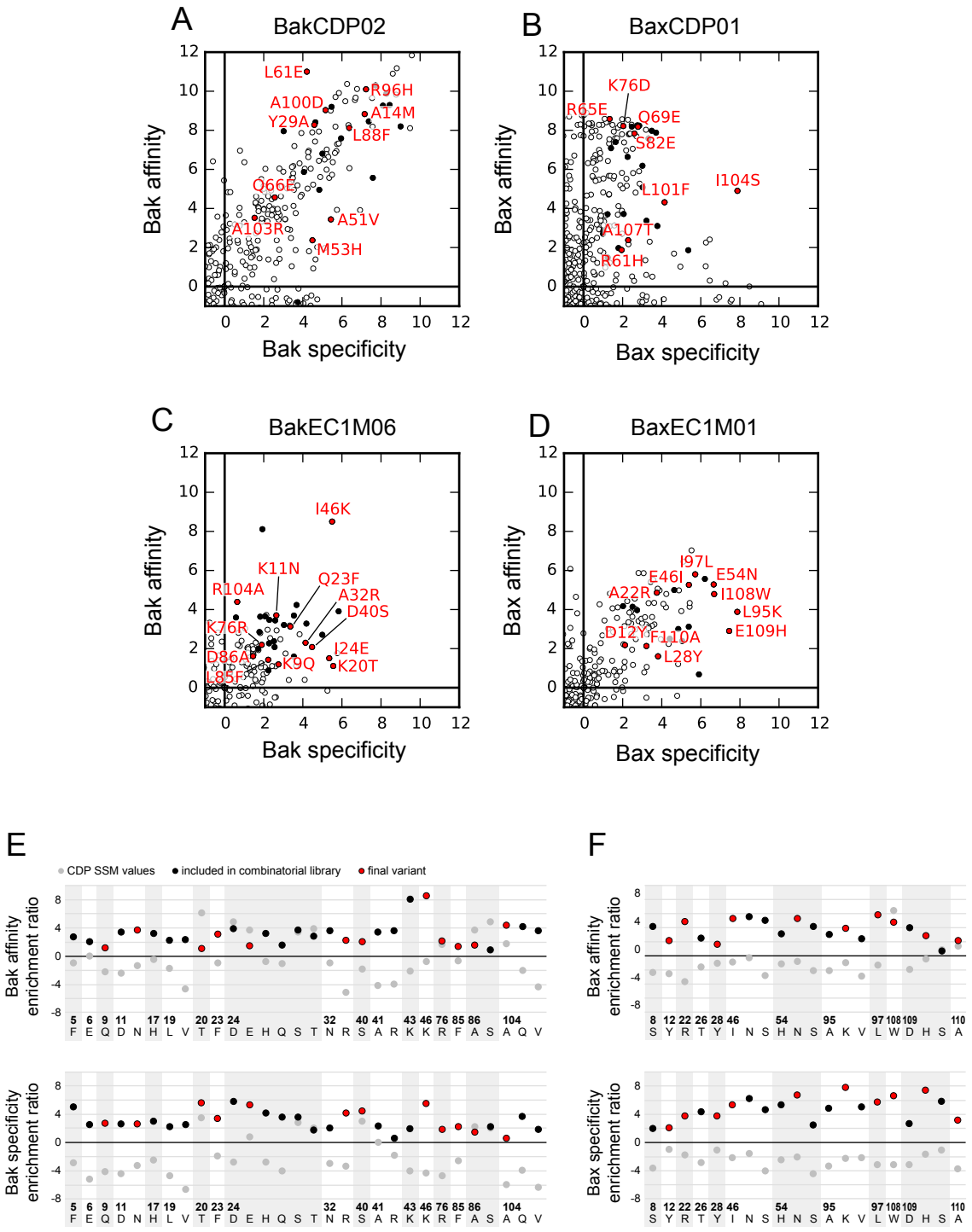

Figure 11. Selection of combinatorial mutants informed by SSM NGS data. Deep sequencing analysis of naïve and sorted SSM libraries, based on original CDPs (A,B) and intermediate EC1Ms (C,D) enabled quantitative analysis of the fitness of each single amino acid substitution for specificity or affinity toward Bak or Bax. (E,F) Enrichment ratios of mutations selected from each EC1M SSM for inclusion in the second-generation combinatorial libraries were compared to enrichment ratios of the same mutations relative to the original CDPs (values from the first generation SSM); mutations enriched in the EC1M SSMs were largely depleted in the CDP SSMs, and thus are likely context-dependent.

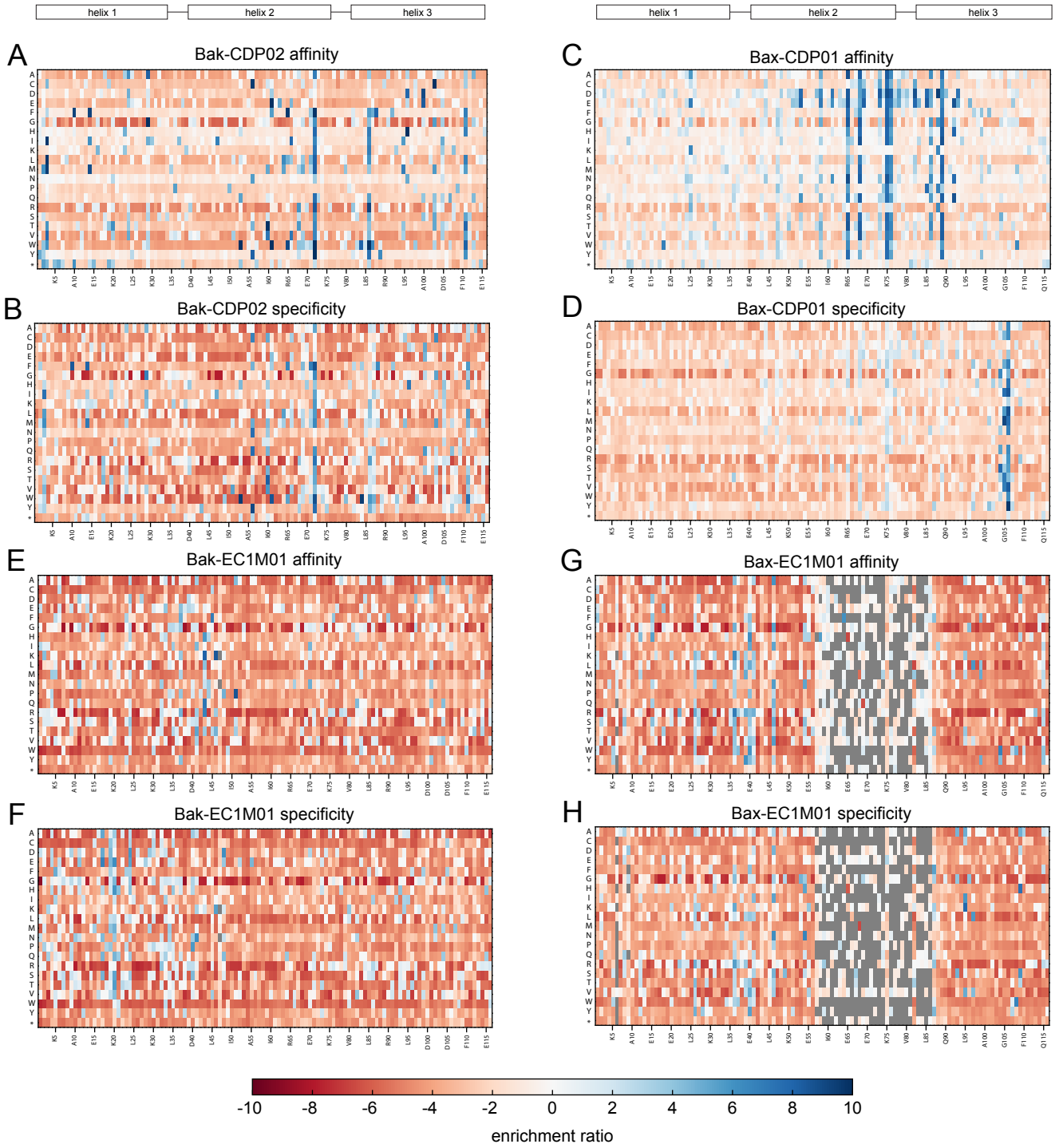

Figure 11—figure supplement 1. Bak- and Bax-targeting SSM heatmaps. SSM libraries based on Bak-CDP02 (A, B), Bax-CDP01 (C, D), Bak-EC1M06 (E, F) and Bax-EC1M01 (G, H) were screened for binding to labeled target homolog alone or in the presence of unlabeled pro-survival competitors. FACS-sorted pools were analyzed with NGS, and enrichment ratios were calculated as in Equation 1 (see Materials and Methods). Enrichment or depletion of each mutant represents its fitness for high-affinity (A, C, E, G) or specific binding (B, D, F, H). Gray indicates positions where NGS data were poor quality and thus omitted from analysis.

Figure 12. Specificity analysis of Bak- and Bax-targeting designed proteins. (A) Comparison of α3 and α4 of helix-bound models homologs of Bcl-2 (5JSNa), Bcl-xL (3R85a), and Bak (2M5B; left, bound to representative helix SOUL-BH3 [3R85e]) with Mcl-1 (5JSBa), Bfl-1 (4ZEQa) and Bax (4BD2a; right, bound to representative helix Bid-BH3 [4BD2c]). While helices α3 and α4 are structurally similar, the loop between them is one residue shorter for Bcl-2, Bcl-xL and Bak than Mcl-1, Bfl-1 and Bax, perhaps contributing to Bak-EC1M06 and αBAK's cross-reactivity with Bcl-2, and Bax-EC1M01 and αBAX's cross-reactivity with Bfl-1. (B,C) The denoted sequences of each homolog are aligned and colored by the indicated residue type. Black boxes indicate positions that would likely contact a bound helix, and dashed boxes indicate positions that may contact a bound helix depending on its side chain identity. (B) Structural evidence of the unique cross-reactivities is found on the opposite side of the BH3-binding cleft at positions spanning α2 and α3, where Bak is most similar to Bcl-2 and Bax is most similar to Mcl-1 and Bfl-1, especially at interface positions. (C) The sequence of α5 is highly conserved among homologs, likely because it is buried in the core of the protein. However, α4 has considerable sequence diversity at interface positions, and thus the designed inhibitors likely take advantage of this region to gain specificity. (D) For example, αBAX residue K95 complements Bax residue D98 and αBAX E94 complements Bax R94; no other homolog has this exact electrostatic profile at these positions.

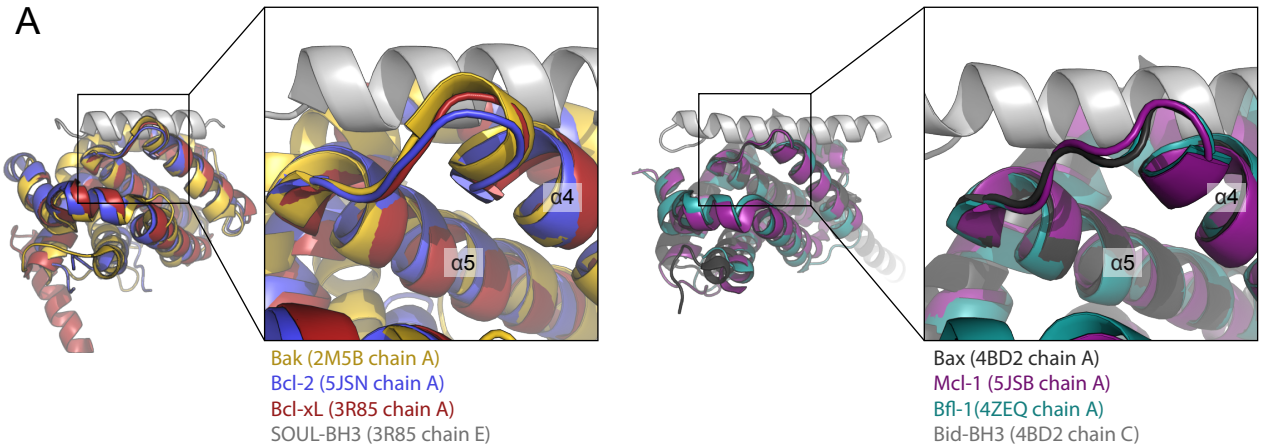

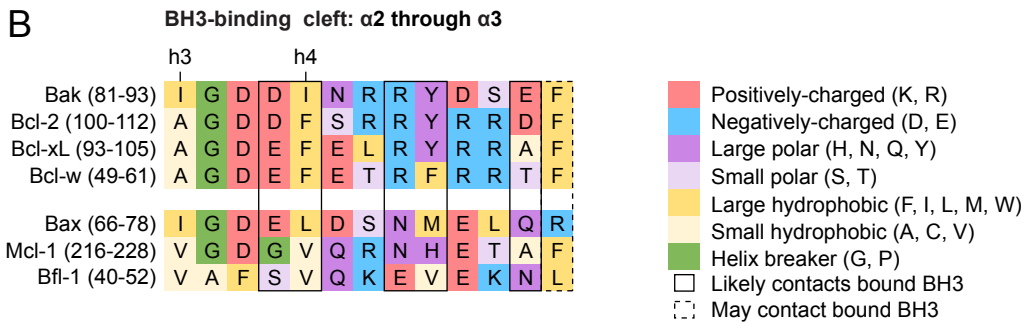

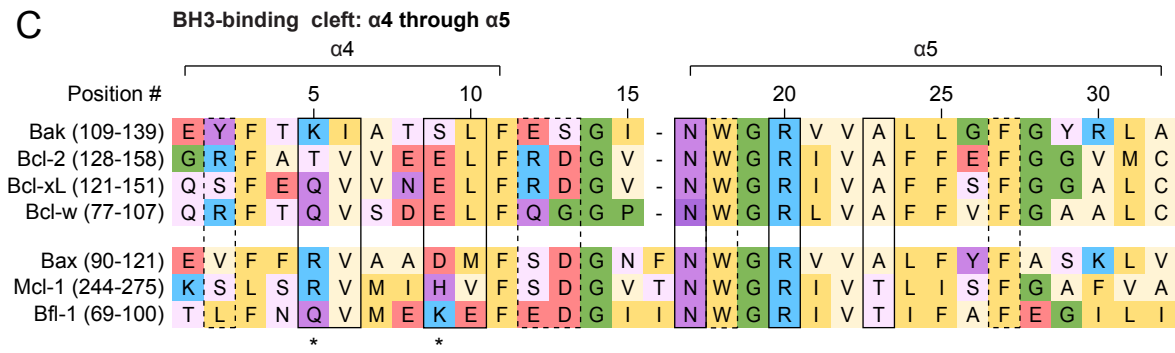

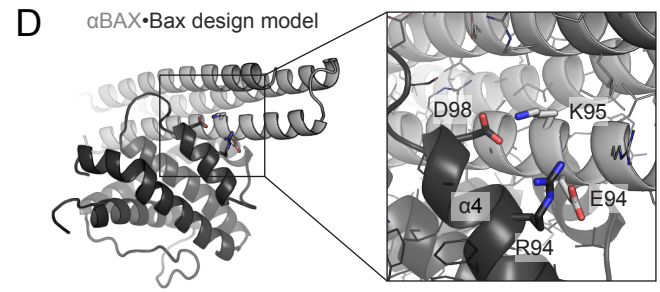

Figure 12. Specificity analysis of Bak- and Bax-targeting designed proteins (continued).

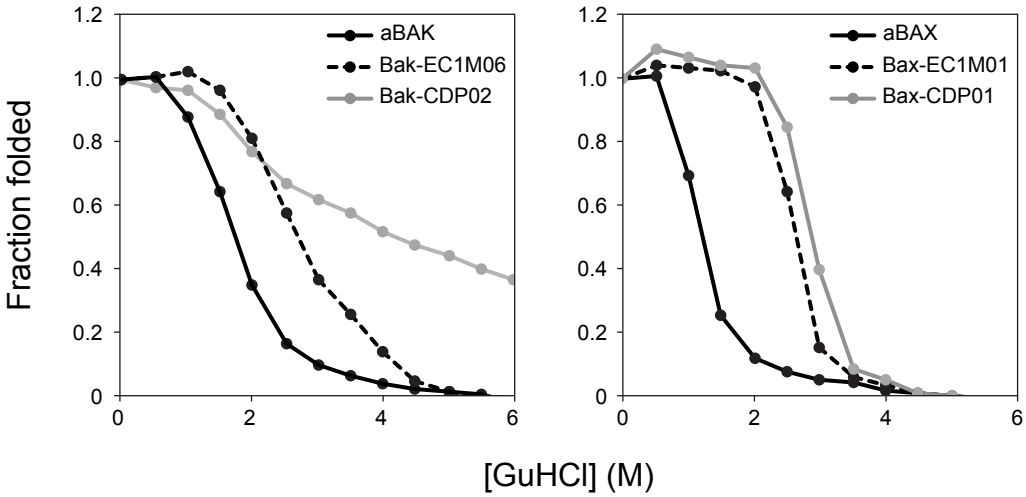

Figure 13. Biochemical characterization of Bak- and Bax-targeting inhibitors. Computationally designed proteins (gray) and their optimized successors (EC1Ms dashed; best variants solid black) were denatured with guanidinium hydrochloride. CD signal at 222 nM was measured and loss of signal used to calculate the fraction folded. Values reported are the result of three accumulations averaged at acquisition.

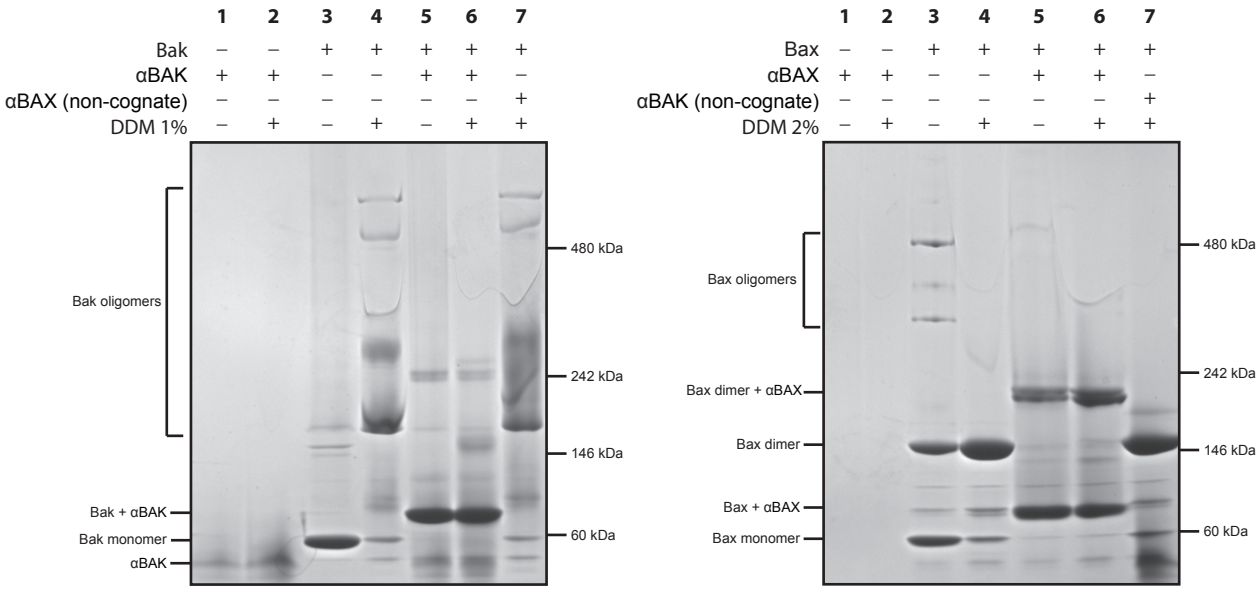

	Molecular weight	Isoelectric point
MBP-Bak-AH monomer	66.5 kDa	5.27
MBP-Bak-AH homodimer	133 kDa	
αBAK monomer	14.9 kDa	6.27
MBP-Bak-AH-αBAK heterodimer	81.4 kDa	5.52
MBP-Bak-AH-αBAK heterotetramer	162.8 kDa	
MBP-Bax-AH monomer	64.1 kDa	5.17
MBP-Bax-AH homodimer	128.2 kDa	
αBAX monomer	15.0 kDa	9.47
MBP-Bax-AH-αBAX heterodimer	79.1 kDa	5.86
MBP-Bax-AH-αBAX heterotetramer	158.2 kDa	

Figure 14. αBAK and αBAX prevent and detergent-induced homooligomerization of Bak and Bax. 5 ug Bak (A) or Bax (B) were incubated with a 2-fold molar excess of specific inhibitor or non-cognate inhibitor (control) for 10 minutes at room temperature. DDM, or an equal volume of buffer, was then added to 1% (Bak) or 2% (Bax) and incubated another 45 minutes at room temperature before loading on a native PAGE bis-tris gel to assess the oligomerization state of Bak and Bax. NativeMark protein standard was run to approximate molecular weight distribution. Molecular weights and isoelectric points of monomers and relevant oligomers are listed for reference.

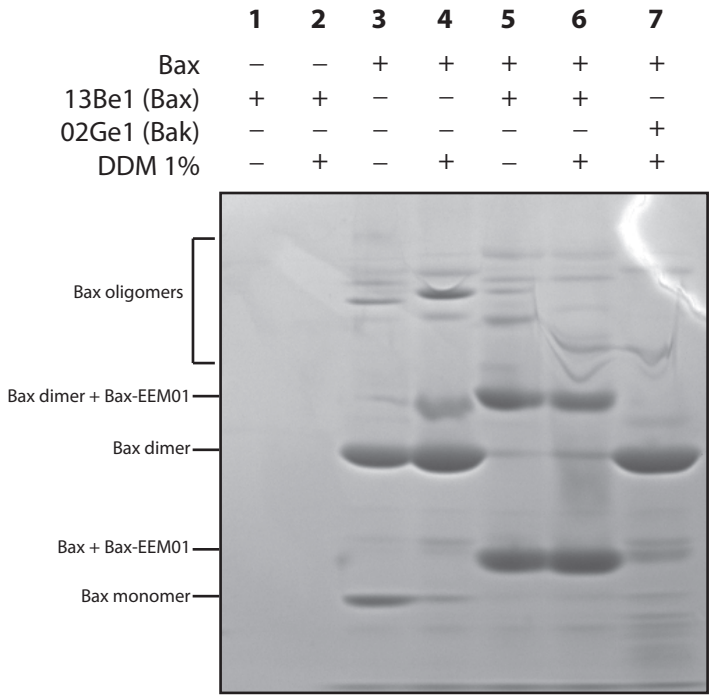

Figure 14¬—figure supplement 1. Bax-EEM01 disrupts Bax homodimers. The best variant from an error-prone PCR (epPCR) library based on Bax-EC1M01, Bax-EEM01 (Bax-targeting enriched epPCR mutant [ID no.]) disrupts Bax homodimers. Bax tends to dimerize over time in solution; the MBP-Bax-AH sample used for this assay was majority dimer, indicated by a larger band corresponding to dimer molecular weight compared to monomer. Lanes 5 and 6, where Bax-EEM01 was added at a 1:1 molar ratio to Bax with and without DDM, show that the heterodimer (Bax + Bax-EEM01) band is significantly brighter than the presumed heterotetramer (2Bax + 2Bax-EEM01) bands in the same lanes and brighter than reference Bax monomer in lane 2. This suggests that Bax-EEM01, a 3 nM Bax binder (data not shown), not only binds Bax monomer but can disrupt the Bax homodimer. Bak-EEM01, the best Bak-targeting epPCR mutant, does not bind Bax and has no effect on homooligomerization.

Tables

Table 1. Summary of pro-survival-targeting computational designs selected for protein production and biochemical analysis.

Design	Target PDB	PDB description	Residues kept fixed (numbered as on BINDI scaffold)	Residues borrowed from	Binds target?	Binding energy (ddg)	Shape complementarity (Sc)	Buried unsatisfied polar atoms (unsat)
2-CDP01	2XA0	Bcl-2•Bax-BH3	L54, I57, G58, D59, F61	Bad-BH3	+	-35.2669	0.509289	10
2-CDP02	2XA0	Bcl-2•Bax-BH3	L54, I57, G58, D59, F61	Bad-BH3	+	-41.0808	0.529427	9
2-CDP03	4AQ3	Bcl-2•phenylacyl sulfonamide	A51, L54, G58, D59	BINDI	+	-29.2064	0.580547	2
2-CDP04	4IEH	Bcl-2/Bcl-XL•N-heteroaryl sulfonamide	Y49, A51, L54, G58, D59, N62	BINDI	-	-24.6658	0.528941	7
2-CDP05	4IEH	Bcl-2/Bcl-XL•N-heteroaryl sulfonamide	A51, L54, G58, D59	BINDI	-	-17.011	0.554712	5
2-CDP06	4LVT	Bcl-2•navitoclax	L54, G58, D59	BINDI	+	-25.7035	0.467105	5
2-CDP07	4LVT	Bcl-2•navitoclax	L54, G58, D59, N62	BINDI	+	-25.7202	0.466163	11
X-CDP01	1PQ1	Bcl-XL•Bim-BH3	I50, A51, L54, G58, D59	Bim-BH3	+	-40.5426	0.613795	9
X-CDP02	1PQ1	Bcl-XL•Bim-BH3	Y49, I50, A51, L54, G58, D59	Bim-BH3, BINDI	+	-37.9138	0.575281	7
X-CDP03	2YQ6	Bcl-XL•BimSAHB	I50, A51, L54, I57, G58, D59, N62	Bim-BH3	+	-32.0914	0.622902	8
X-CDP04	2YQ6	Bcl-XL•BimSAHB	Y49, I50, A51, L54, I57, G58, D59, N62	Bim-BH3, BINDI	+	-34.2881	0.554852	4
X-CDP05	2YQ6	Bcl-XL•BimSAHB	Y49, I50, A51, L54, I57, G58, D59, N62	BINDI	+	-32.6508	0.603245	11
X-CDP06	2YQ7	Bcl-XL•BimLOCK	A52, I54, F57, G58, D59, F61	XG10 peptide[1]	+	-44.9274	0.643131	6
X-CDP07	2YQ7	Bcl-XL•BimLOCK	A52, I54, F57, G58, D59, F61	XG10 peptide[1]	+	-47.9744	0.61353	4
X-CDP08	2YQ7	Bcl-XL•BimLOCK	A52, I54, F57, G58, D59, F61	XG10 peptide[1]	+	-31.7966	0.631045	7
X-CDP09	3PL7	Bcl-XL•Bax-BH3	L50, S51, L54, K55, I57, G58, D59, D62	Bax-BH3	-	-24.8947	0.637508	7
X-CDP10	4BPK	Bcl-XL•Puma-α/β-foldamer	I50, A51, L54, G58, D59	BINDI	+	-40.6185	0.587325	3
X-CDP11	4BPK	Bcl-XL•Puma-α/β-foldamer	Y49, I50, A51, L54, I57, G58, D59, N62	BINDI	+	-31.2246	0.549465	4
W-CDP01	1PQ1*	Bcl-XL•Bim-BH3	L54, I57, G58, D59, F61, N62	Bim-BH3	+	-29.6374	0.563108	7
W-CDP02	2YJ1*	Bcl-XL•Puma-α/β-foldamer	L54, I57, G58, D59, F61, N62	Bim-BH3	+	-28.4893	0.557322	10
W-CDP03	3FDL*	Bcl-XL•Bim-BH3	L54, I57, G58, D59, F61, N62	Bim-BH3	+	-29.7158	0.532155	4
W-CDP04	4K5A	Bcl-w•DARPIN	G58, D59	BINDI	-	-19.4883	0.435829	3
W-CDP05	4K5A	Bcl-w•DARPIN	Y49, G58, D59	BINDI	-	-25.4117	0.522469	5
M-CDP01	2PQK	Mcl-1•Bim-BH3	E47, I50, A51, L54, R55, I57, G58, D59, F61, N62	Bim-BH3	+	-38.3045	0.665342	8
M-CDP02	2PQK	Mcl-1•Bim-BH3	E47, I50, A51, L54, R55, I57, G58, D59, F61, N62	Bim-BH3, BINDI	+	-37.4996	0.678787	8
M-CDP03	3KZ0	Mcl-1•MB7	E47, A50, A51, I54, R55, I57, G58, D59, N61, N62, Y65	MB7 peptide	+	-31.2833	0.660599	11
M-CDP04	3KZ0	Mcl-1•MB7	E47, A50, A51, I54, R55, I57, G58, D59, N61, N62, Y65; Y49	MB7 peptide; BINDI	+	-31.1976	0.656449	5
M-CDP05	3PK1	Mcl-1•Bax-BH3	T47, L50, S51, L54, I57, G58, D59, L61, D62, M65	Bax-BH3	+	-30.7442	0.694437	5
F-CDP01	3I1H	Bfl-1•Bak-BH3	I50, A51, L54, I57, G58, D59, N62	Bak-BH3	+	-28.74	0.671393	5
B-CDP01	4B4S	Bcl-B•Bim-BH3	I50, A51, L54, I57, G58, D59, N62	Bim-BH3	+	-29.0724	0.700157	5

*Bcl-w models were generated by threading the aligned Bcl-w sequence onto the crystal structure of the Bcl-2 pro-survival homolog with indicated PDBID

[1]XG10 is a synthetic peptide designed for specificity to Bcl-xL, as described in Dutta et al., 2010.

Table 2. Sequences of pro-survival-targeting computational designs and optimized variants.

>2-CDP01
ADPKKVLDKAKDQAENVVRKLKQELEELYKEARKLDLTQDMREKIKLRAEAAELQAIGDIFQAILQAKMEAKKLYDAGLVNSQQLDELKRRLEELAKEAEDRAAKLGKEFLQKLEY
>2-CDP02
ADPKKVLDKAKDRAENAVRELKQKLEELYKEARKLDLTQDMRNKLIMKAIAAELRAIGDIFQAILEAKAEAKKLLDAGLVNSQQFDELKRRLEELEEEAAERARKLGDEFRQKLEY
>2-CDP03
ADPKKVLDKAKDQAENRVRELKQKLEELYKEARKLDLTQEMRRELKERALAARLQAVGDIFYAILQAKSEADKLKKAGLVNSQQLDELKRRLEELAEEAQRKARDYGIEFALKLEY
>2-CDP04
ADPKKVLDKAKDQAENRVRELKQKLEELYKEARKLDLTQEMREKLQEQALAAWLNAAGDIIEAISRALQEADKLKKAGLVNSQQLDELKRRLEELAEEAARKAEKYGEEFKKKLEY
>2-CDP05
ADPKKVLDKAKDQAENRVRELKQKLEELYKEARKLDLTQEMRAELNARFAAATLAAAGDIINAISEALAEADKLKKAGLVNSQQLDELKRRLEELAQEAERKAEEYGQEFLLKLEY
>2-CDP06
ADPKKVLDKAKDEAENRVRELKQKLEELYKEARKLDLTQEMRQELVDKARAASLQASGDIFYAILRALAEAEKLKKAGLVNSQQLDELKRRLEELAEEARRKAEKLGDEFRLKLEY
>2-CDP07
ADPKKVLDKAKDDAENRVRELKQKLEELYKEARKLDLTQEERDELKLKAIAASLQASGDIYNAILRALEEARKLKKAGLVNSQQLDELKRRLEELAEEAQRKANKLGDEFRLKLEY
>aBCL2
ADPKKVLDKAKDEAENRVRELKQRLEELYKEARKLDLTQEMRQELVDKARAASLQANGDIFYAILRALAEAEKLKKAGLVNSQQLDELKRRLEELAEEARRKAEKLRDEFRLKLEY
>X-CDP01
ADPKKVLDKAKDQAENRVRELKQKLEELYKEARKLDLTQEMRRELQARYIAAMLAAAGDIMEAIQQAKNEADKLKKAGLVNSQQLDELKRRLEELAKEAARKAEDYGREFQLKLEY
>X-CDP02
ADPKKVLDKAKDQAENRVRELKQKLEELYKEARKLDLTQEMRKELVARYIAAMLAAAGDIVQAIQDAKNEADKLKKAGLVNSQQLDELKRRLEELAKEAARKATDYGREFQLKLEY
>X-CDP03
ADPKKVLDKAKDQAENRVRELKQKLEELYKEARKLDLTQEMRRELRNRAIAAILQAIGDLLNAIQQAKDEADKLKKAGLVNSQQLDELKRRLEELQNEAAEKAADYGEEFWLKLEY
>X-CDP04
ADPKKVLDKAKDQAENRVRELKQKLEELYKEARKLDLTQEDRKRLLLQYIAAMLAAIGDLENAIRWAKREADKLKKAGLVNSQQLDELKRRLEELAKEAAEKAADYGEEFNLKLEY
>X-CDP05
ADPKKVLDKAKDQAENRVRELKQKLEELYKEARKLDLTQEMRRQLRDQYIAAMLAAIGDLLNAIMQAKREADKLKKAGLVNSQQLDELKRRLEELEEEAAQKAADYGQEFLLKLEY
>X-CDP06
ADPKKVLDKAKDRAENRVRELKKKLEKLYKEARKLDLTQEQRNKIINAAMAAMIAAFGDIFHAIQEAKEEAKKLKKAGLVNSQQLDELKRRLDELDEEAAQRAEKLGKEFNLKFEY
>X-CDP07
ADPKKVLDKAKDRAENVVRKLKKELEELYKEARKLDLTQEMRDRIRLAAIAARIAAFGDIFHAIMEALEEARKLKKAGLVNSQQLDELKRRLEELDEEAAQRAEKLGKEFELKLEY
>X-CDP08
ADPKKVLDKAKDRAENRVRKLKKELEKLYKEARKLDLTQEQRDRIINAAIAAMIAAFGDIFHAIMEAKEEARKLKKAGLVNSQQLDELKRRLDELDEEAAQRAEKLGKEFRLKFEY
>X-CDP09
ADPKKVLDKAKDQAENRVRELKQKLEELYKEARKLDLTQEMRKKLIQKALSALLKAIGDILDAIARAKAEADKLKKAGLVNSQQLDELKRRLEELLKEAARKALDYGREFWLKLEY
>X-CDP10
ADPKKVLDKAKDQAENRVRELKQKLEELYKEARKLDLTQEMRRELRERYIAAMLAAAGDLWYAITQAKREADKLKKAGLVNSQQLDELKRRLEELLEEAARKAEDYGEEFRLKLEY
>X-CDP11
ADPKKVLDKAKDQAENRVRELKQKLEELYKEARKLDLTQEMRRELRDRYIAAMLAAIGDLFNAIQWAKQEADKLKKAGLVNSQQLDELKRRLEELAEEAARKAEDYGEEFKLKLEY
>X-ECM01
ADPKKVLDKAKDRAENVVRKLKKELEELYKEARKLDLTQEMRDRIRRAAIAARIQAHGDIFHAIKHALREARKLKKAGLVNSQQLDELKRRLEELDEEAEQRAEKLGKEFELKLEY
>X-ECM02
ADPKKVLDKAKDRAENVVRKLKKELEELYKEARKLDLTQEMRDRIRRTAIAARFQAHGDIFHAIKEAKREARKLKKAGLVNSQQLDELKRRLEELDEEAEQRAEKLGKEFELKLEY
>X-ECM03
ADPKKVLDKAKDRAENVVRKLKKELEELYKEARKLDLTQEMRDRIRRAAIAARFAAHGDIFHAIKEAKEEARKLKKAGLVNSQQLDELKRRLRELDEEAEQRAEKLGKEFRLKLEY
>X-ECM04 (XINDI)
ADPKKVLDKAKDRAENVVRKLKKELEELYKEARKLDLTQEMRDRIRRTAIAARFQAHGDIFHAIKHAKEEARKLKKAGLVNSQQLDELKRRLRELDEEAEQRAEKLGKEFRLKLEY
>W-CDP01
ADPKKVFDKAKDKAENQVRYLKQRLEELYKEARKKDLTQEQRRKLKEKYLAAKLAAILAAIGDAFNALAEARELHKQGKVNKQQLDELAKRLDRLAEEAIQKAEDYAREFAYKLEY
>W-CDP02
ADPKKVLDKARDQALKRLEEMRKKLEESYKEARKKDLTQEERRKLEEKYAEAMKRAAEDIYNMIQQALKEAEKEKKAGQVNSQQLDKLREDLNNKLIAAALAAIGDAFNMAANLRT
>W-CDP03
ADPKKVFDEAKDRAENNVRRLKQKLEELYKEARKKDLTQEEREKLKEKYKTAMAAAALAAIGDAFNALLKARKLHKNGQVNEQQLEELARRLQELAKEAFQKAKDYANEFEYKLEY
>W-CDP04
ADPKKVLDKAKDQAENRVRELKQKLEELYKEARKLDLTQEMRLKLIQKAYVALASAAGDNEAAIIQAKQEADKLKKAGLVNSQQLDELKRRLEELAKEAERKAEDYGREFQLKLEY
>W-CDP05
ADPKKVLDKAKDQAENRVRELKQKLEELYKEARKLDLTDEMRTKLLQKYAAALVSAYGDNWKAIKQAKQEADKLKKAGLVNSQQLDELKRRLEELSKEAERKAEDYGREFRLKLEY
>W-ECM01 (aBCLW)
ADPKKVFDELKDRAENNVRRLKQKLEELYKEARKKDLTQEEREKLKTKYKTAMQLAALAAEGDIMNALLKARKLHKNGQVNEQQLEELARRLMELAKEAFQKAKDYANEFKYKLEY
>M-CDP01
ADPKKVLDKAKDQAENRVRELKQELEELYKKARKLDLTQEERRKLEEEAIAALLRAIGDIYNAIQQALNEADKLKKAGLVNSQQLDELKRRLEELKKEASKKARDYGLEFFEKLDY
>M-CDP02
ADPKKVLDKAKDQAENRVRELKQELEELYKEARKLDLTQEERRKLEESYIAAMLRAIGDIFNAIMQAKNEADKLKKAGLVNSQQLDELRRRLEELRKEASLKAEDYGREFQEKLEY
>M-CDP03
ADPKKVLDKAKDQAENRVRELKQDLERLYKEARKLDLTQEMRRKLQEKAAAAMIRAIGDINNAIYQALQEADKLKKAGLVNSQQLDELKRRLEELQKEASRKAQAYGEEFMLKLEY
>M-CDP04 (aMCL1)
ADPKKVLDKAKDQAENRVRELKQVLEELYKEARKLDLTQEMRKKLIERYAAAIIRAIGDINNAIYQAKQEAEKLKKAGLVNSQQLDELLRRLDELQKEASRKANEYGREFELKLEY
>M-CDP05
ADPKKVLDKAKDQAENRVRELKQKLEELYKEARKLDLTQEERHRLETKALSALLAAIGDILDAIMQALQEAAKLKKAGLVNSQQLDELKRRLEELRKEASRKARDYGREFWLKLDY
>F-CDP01
ADPKKVLDKAKDQAENRVRELKQKLEELYKEARKLDLTQEMRKKLQYAAIGAMLAAIGDILNAIMQAKQEADKLKKAGLVNSQQLDELKRRLEELKEEALRKAHDYGSEFYLKLEY
>F-ECM01
ADPKKVLDKAKDQAENRVRELKQKLEELYKEARKLDLTQEMRKKLEIAALGAVLAAHGDILNAIMQAKEEADKLKKAGLVNSQQLDELKRRLEELKEEALRKASDYGKEFHLKRQY
>F-ECM02
ADPKKVLDKAKDQAENRVRELKQKLEELYKEARKLDLTQEMRKKLEIAALGAVLAAHGDILNAIMQAKEEADKLKKAGLVNSQQLDELKRRLEELKEEALRKASDYGKEFHLKRRY
>F-ECM03
ADPKKVLDKAKDQAENRVRELKQKLEELYKEARKLDLTQEMRKKLEVAALGAVLAAHGDILNAIMQAKEEADKLKKAGLVNSQQLDELKRRLEELKEEALRKASDYGKEFHLKRQY
>F-ECM04
ADPKKVLDKAKDQAENRVRELKQKLEELYKEARKLDLTQEMRKKLEVAALGAVLAAHGDILNAIMQAKEEADKLKKAGLVNSQQLDELKRRLEELKEEALRKASDYGKEFHLKRRY
>F-ECM05
ADPKKVLDKAKDQAENRVRELKQKLEELYKEARKLDLTQEMRKKLQIAALGAMLAAIGDILNAIMQAKEEADKLKKAGLVNSQQLDELKRRLEELKEEALRKASDYGKEFHLKRQY
>F-ECM06
ADPKKVLDKAKDQAENRVRELKQKLEELYKEARKLDLTQEMRKKLQIAALGAMLAAIGDILNAIMQAKEEADKLKKAGLVNSQQLDELKRRLEELKEEALRKASDYGSEFHLKREY
>F-ECM07
ADPKKVLDKAKDQAENRVRELKQKLEELYKEARKLDLTQEMRKKLQIAALGAMLAAIGDILNAIMQAKEEADKLKKAGLVNSQQLDELKRRLEELKEEALRKASDYGSEFHLKLEY
>aBFL1
ADPKKVLDKAKDQAENRVRELKQKLEELYKEARKLDLTQEKRKKLEVATLGAVLAAHGDILNAIMQAKEEADKLKKAGLVNSQQLDELKRRLEELKEEALRKASDYGNEFHLKRRY
>B-CDP01
ADPKKVLDKAKDQAENRVRELKQELERLYKEARKLDLTQEMRRKLEWRYIAAMLKAIGDILNAIAQAENEADKLKKAGLVNSQQLDELRRRLEELAKEAARKAHDYGREFQLKLEY
>B-ECM01

ADPKKILDKAKDQVENRVRELKQELERLYKEARKLDLTQEMRRKLHVRYIAAMLKAIAAILNAIAQAENEADKLKKAGLVNSQQLDELRRRLEELTEEAAQKAHDYGREFQLKLEY
>B-ECM02
ADPKKILDKAKDQVENRVRELKQELERLYKEARKLDLTQEMRRKLHVRYIAAMLKAIASILNAIAQAENEADKLKKAGLVNSQQLDELRRRLEELTEEAAQKAHDYGREFQLKLEY
>B-ECM03
ADPKKILDKAKDQVENRVRELKQELERLYKEARKLDLTQEMRRKLHVRYIAAMLKAIADILNAIAQAENEADKLKKAGLVNSQQLDELRRRLEELTEEAARKAHDYGREFQLKLEY
>B-ECM04
ADPKKILDKAKDQVENRVRELKQELERLYKEARKLDLTQEMRRKLHWRYIAAMLKAIADILNAIAQAENEADKLKKAGLVNSQQLDELRRRLEELTEEAARKAHDYGREFQLKLEY
>aBCLB
ADPKKILDKAKDQVENRVRELKQELERLYKEARKLDLTQEMRRKLHVRYIEAMLKAIAAIMNAIAQAENEADKLKKAGLVNSQQLDELRRRLEELTEEAAQKAHDYGRELQLKLEY

Table 3. Crystallographic data collection and refinement statistics.

Crystal	aMCL1·Mcl-1	aBCL2·Bcl-2
Data Collection		
Beamline	ALS502	Saturn CCD
Wavelength	1.000	1.5418
Space group	$P2_1$	$P4_1$
Cell dimensions		
a (Å)	61.92	65
b (Å)	92.25	65
c (Å)	162.01	134.31
β (°)	92.39	90
R_{merge}(%)[a,*]	9.4 (80.9)	5.0 (52.8)
$I/\sigma I$	17.3(1.09)	25.8(1.39)
$CC_{1/2}$	0.596	0.508
Completeness (%)	95.5(61.2)	96.6(69.7)
Redundency	8.0(3.4)	6.0(2.1)
B(iso)(Å^2)	55.87	39.97
Refinement		
Resolution (Å)	49.5 – 2.74	32 – 2.1
Unique reflections	43179	35816
R_{work} (%)[c,*]	19.3(33.4)	15.9(24.7)
R_{free} (%)[c,*]	23.1(38.4)	20.8(32.7)
Protein atoms[d]	13123	4441
Solvent molecules	10	150
Protein *B* factors (Å^2)	92.31	55.26
Solvent *B* factors (Å^2)	69.64	51.48
RMSD bond length (Å)	0.019	0.0189
RMSD bond angle (°)	1.998	1.992
Twinning operator h, k, l	NA[b]	0.673
Twinning operator –h, k, -l	NA[b]	0.327
Ramachandran (%)		
Core region	97.19	98.84
Allowed region	1.60	0.96
Outliers	1.21	0.19

* Highest resolution shell values in parenthesis.

[a] $R_{merge} = \|I_{hi} - \langle I_h \rangle\| / I_{h,}$ where I_{hi} is the ith measurement of reflection h, and $\langle I_h \rangle$

[b] Not applicable.

[c] R-factor/R-free = $_h|F_{h(o)} - F_{h(c)}|/_h|F_{h(o)}|$, where R-free was calculated with 5% of the data excluded from refinement.

[d] Includes atoms in alternate conformations.

Table 4. Protein cross-linking of the aMCL1·Mcl-1 complex. Cross-links above the 25 Å limit for cross-linking reagents are shaded dark gray. Note that in this instance, the sequences for crystallized aMCL1 and the Mcl-1-targeting design model M-CDP04 are identical, as no optimization was required beyond computational design.

Protein 1 (Residue No.)	Protein 2 (Residue No.)	Distance (Crystal), Å	Distance (Design Model), Å	Cross-linking Experiment
aMCL1 (73)	aMCL1 (76)	5.2	4.9	DSS, BS3, DSG
aMCL1 (30)	aMCL1 (34)	7.3	6.6	DSS, BS3, DSG
aMCL1 (102)	aMCL1 (97)	8.8	8.7	DSS, BS3, DSG
aMCL1 (102)	aMCL1 (22)	9.2	9.5	DSS, BS3, DSG
aMCL1 (11)	aMCL1 (5)	9.6	9.5	DSS, BS3, DSG
Mcl-1 (194)	Mcl-1 (197)	9.7	Not Modeled	BS3
aMCL1 (11)	aMCL1 (4)	10.3	10.3	DSS, BS3, DSG
Mcl-1 (234)	aMCL1 (113)	11.8	12.8	DSG
aMCL1 (11)	aMCL1 (97)	12	11.3	DSS, BS3
Mcl-1 (244)	aMCL1 (43)	12.6	12	DSS, BS3, DSG
aMCL1 (68)	aMCL1 (76)	12.8	12.3	DSS, BS3, DSG
Mcl-1 (244)	aMCL1 (44)	12.9	12.3	DSS, BS3, DSG
aMCL1 (113)	aMCL1 (34)	13.4	13.4	DSS, BS3, DSG
aMCL1 (102)	aMCL1 (11)	13.5	12.2	DSS, BS3, DSG
aMCL1 (5)	aMCL1 (73)	13.6	12.8	DSS, BS3, DSG
aMCL1 (113)	aMCL1 (22)	13.6	12.5	DSS, BS3, DSG
Mcl-1 (276)	Mcl-1 (194)	13.9	14.1	DSS, BS3, DSG
Mcl-1 (238)	aMCL1 (43)	14.1	14.1	BS3
aMCL1 (34)	aMCL1 (44)	14.2	13.6	DSS, BS3, DSG
Mcl-1 (194)	Mcl-1 (208)	14.3	14.1	DSS, BS3, DSG
aMCL1 (30)	aMCL1 (44)	14.7	13.6	DSS, BS3
aMCL1 (34)	aMCL1 (43)	14.8	14.2	BS3
aMCL1 (68)	aMCL1 (97)	14.8	14.3	DSS, BS3, DSG
Mcl-1 (234)	Mcl-1 (244)	15	14.5	DSS
Mcl-1 (197)	Mcl-1 (208)	15.3	Not Modeled	DSS, BS3, DSG
Mcl-1 (279)	Mcl-1 (194)	15.3	15.7	DSG
aMCL1 (9)	aMCL1 (73)	15.3	14.7	BS3
aMCL1 (102)	aMCL1 (113)	16.5	16.7	DSS, BS3
aMCL1 (11)	aMCL1 (22)	16.7	16.3	DSS, BS3
Mcl-1 (238)	aMCL1 (44)	17	16.9	DSS
aMCL1 (5)	aMCL1 (76)	17.2	16.5	DSS
Mcl-1 (234)	aMCL1 (22)	18.5	17.8	DSS
Mcl-1 (208)	aMCL1 (68)	18.6	20.5	DSS, BS3
Mcl-1 (308)	Mcl-1 (208)	19.1	18.9	DSS, BS3
Mcl-1 (234)	aMCL1 (34)	19.2	19	DSS, BS3
Mcl-1 (279)	Mcl-1 (197)	20.8	Not Modeled	DSS, BS3, DSG
Mcl-1 (308)	aMCL1 (73)	20.8	24	DSS, BS3
Mcl-1 (208)	aMCL1 (73)	21.1	24.4	DSS, BS3
Mcl-1 (208)	aMCL1 (76)	22.5	25.1	DSS, BS3, DSG
Mcl-1 (308)	aMCL1 (76)	24.2	26.5	BS3
Mcl-1 (308)	aMCL1 (9)	24.7	27.5	DSS, BS3
Mcl-1 (208)	Mcl-1 (238)	32.8	32.8	DSS
Mcl-1 (308)	aMCL1 (44)	32.8	31.7	BS3
Mcl-1 (208)	Mcl-1 (234)	33.9	33.7	DSS
Mcl-1 (308)	Mcl-1 (234)	35.9	35.1	DSS
Mcl-1 (208)	aMCL1 (44)	36.8	36.3	BS3
Mcl-1 (197)	aMCL1 (76)	37.6	Not Modeled	BS3
Mcl-1 (197)	aMCL1 (44)	39.3	Not Modeled	BS3
Mcl-1 (308)	aMCL1 (34)	43.9	42.3	BS3, DSG

Table 5. Sort conditions for pro-survival-targeting *in vitro* evolution experiments.

Library	Sort	Incubation conditions		Specificity [competitor]/[target]
		Target conc. (nM)	Competitor conc. (nM)	
2-CDP06 SSM	1	0.5	40	80
2-CDP06 SSM	2	0.25	40	160
X-CDP07 SSM	1	2	4	2
X-CDP07 SSM	2	2	4	2
X-CDP07 combinatorial	1	1	8	8
X-CDP07 combinatorial	2	0.5	32	64
X-CDP07 combinatorial	3	0.35	64	183
X-CDP07 combinatorial	4	0.2	100	500
X-CDP07 combinatorial	5	0.1	200	2000
W-CDP03 SSM	1	2	8	4
W-CDP03 SSM	2	0.5	2	4
W-CDP03 combinatorial	1	0.5	2	4
W-CDP03 combinatorial	2	0.15	3	20
W-CDP03 combinatorial	3	0.05	20	400
W-CDP03 combinatorial	4	0.05	40	800
W-CDP03 combinatorial	5	0.05	80	1600
M-CDP02 SSM (Mcl-1)	1	4	12	3
M-CDP02 SSM (Bfl-1)	1	20	2	0.1
M-CDP02 SSM (Bcl-B)	1	20	4	0.2
M-CDP02 SSM (Bcl-2)	1	8	4	0.5
M-CDP02 SSM (Bcl-XL)	1	20	2	0.1
M-CDP02 SSM (Bcl-W)	1	100	2	0.02
F-CDP01 SSM	1	4	4	1
F-CDP01 SSM	2	4	4	1
F-CDP01 combinatorial	1	4	8	2
F-CDP01 combinatorial	2	2	8	4
F-CDP01 combinatorial	3	2	16	8
F-CDP01 combinatorial	4	2	16	8
F-ECM04 error-prone PCR	1	0.75	40	53
F-ECM04 error-prone PCR	2	0.5	40	80
F-ECM04 error-prone PCR	3	0.5	40	80
F-ECM04 error-prone PCR	4	0.5	40	80
F-ECM04 error-prone PCR	5	0.5	40	80
B-CDP01 SSM	1	4	8	2
B-CDP01 SSM	2	4	8	2
B-CDP01 combinatorial	1	4	8	2
B-CDP01 combinatorial	2	2	8	4
B-CDP01 combinatorial	3	2	16	8
B-CDP01 combinatorial	4	2	16	8
B-ECM01 error-prone PCR	1	0.5	40	80
B-ECM01 error-prone PCR	2	0.2	40	200
B-ECM01 error-prone PCR	3	0.2	40	200
B-ECM01 error-prone PCR	4	0.1	40	400
B-ECM01 error-prone PCR	5	0.1	40	400

Table 6. Mutation summary of evolved pro-survival-targeting variants.

			Combinatorial library		No combinatorial library		
Final Variant	**Target**	**Computational Design**	**SSM mutations included in combinatorial library**	**Mutations in best clone from combinatorial library**	**SSM-guided point mutants considered**	**Point mutants combined for final design**	**Additional mutations from error prone-PCR library**
αBCL2	Bcl-2	2-CDP06	N/A	N/A	E20N, K24R, V46E, V46R, D47F, D47W, R50D, R50L, R50M, S53D, S53K, S53R, S57H, S57N, L68R, R100F, R100K, R100N, G107M, G107R	K24R, S57N, G107R	N/A
αBCLXL	Bcl-xL	X-CDP07	E24R, L28K, D43R, L47R, A48E, A48K A48Q, A48T, I54F, A55Q, F57H, M65H, M65K, M65R, E66H, E66K, E66R, L68K, L68N, L68R, E69R, E70R, E93K, E93R, D96T, A100E, A100K, A100Q, E111R	L47R, A48T, I54F, A55Q, F57H, M65K, E66H, L68K, E93R, A100E, E111R	N/A	N/A	N/A
αBCLW	Bcl-w	W-CDP11	A9L, R19N, R19Q, E46D, E46T, A53E, A53H, A53Q, A54I, A54L, A54M, A54S, A54T, A54V, A59I, A59M, A59T, A59V, I60E, A63F, A63I, A63L, A63M, F64I, F64L, F64M, N76R, E85R, Q92M, Q92T, E93V, E97D, F99E, E110K	A9L, E46T, A53Q, A54L, I60E, A63I, F64M, Q92M, E110K	N/A	N/A	N/A
αMCL1	Mcl-1	M-CDP04	N/A	N/A	N/A	N/A	N/A
αBFL1	Bfl-1	F-CDP01	Q46S, Q46E, Y47I, Y47V, I50K, I50L, I50M, M53C, M53I, M53V, L54N, I57F, I57H, I57L, I57N, I57S, I57T, Q69E, H104E, H104R, H104S, H104T, S108K, S108N, Y111H, Y111K, Y111W, L114R, E115G, E115Q, E115R	Q46E, Y47V, I50L, M53V, I57H, Q69E, H104S, S108K, L114R, E115R	N/A	N/A	M41K, A49T, K108N
αBCLB	Bcl-B	B-CDP01	I6V, A14V, N16K, E20F, L21V, E46H, E46Q, E46Y, W47F, W47I, W47L, W47V, Y49F, I50L, A51E, A51I, A51K, A51R, L54I, G58A, G58S, D59A, D59K, D59N, D59S, D59T, A63L, A63V, E93K, A96T, K97E, R101Q	V6I, A14V, E46H, W47V, G58A, D59A, A96T, K97E, R101Q	N/A	N/A	A51E, L61M, F110L

Table 7. Initial YSD screening data and computational metrics for Bak- and Bax-targeting designs.

									YSD screen		
Design name	Total free energy (REU)	Binding energy (ddG)	Shape complementarity	Buried polar atoms	Solvent-accessible surface area (SASA)	ddG per 1000 sasa	Intended target	Starting model or variant of	Expression	Binds Bak	Binds Bax
Bak-CDP01	-534.8	-57.3	0.66	3	2917	-19.7	Bak	2M5B	+++	++	++
Bak-CDP02	-524.0	-42.5	0.56	3	2888	-14.7	Bak	2M5B	+++	++	+
Bak-CDP03	-519.7	-59.4	0.62	3	2459	-24.2	Bak	2M5B	+++	-	-
Bak-CDP04	-526.9	-53.6	0.56	4	2452	-21.9	Bak	2M5B	+++	-	-
Bak-CDP05	-547.5	-53.2	0.66	2	2471	-21.5	Bak	4OYD*	+++	-	-
Bak-CDP06	-520.7	-41.1	0.61	0	2192	-18.7	Bak	4OYD*	+++	-	-
Bak-CDP07	-526.6	-46.0	0.62	3	2272	-20.3	Bak	4OYD*	+++	-	-
Bak-CDP08	-532.3	-37.3	0.66	1	2286	-16.3	Bak	4OYD*	+++	-	-
Bak-CDP09	-501.2	-32.5	0.63	3	2321	-14.0	Bak	4OYD*	+++	-	-
Bak-CDP10	-533.2	-70.9	0.72	5	2627	-27.0	Bak	4OYD**	+++	-	+
Bak-CDP11	-514.3	-44.2	0.68	3	2349	-18.8	Bak	4OYD**	+++	-	+
Bak-EC1M01	-526.9	-29.2	0.64	5	2449	-11.9	Bak	Bak-CDP02			
Bak-EC1M02	-552.8	-35.5	0.59	3	2433	-14.6	Bak	Bak-CDP02			
Bak-EC1M03	-532.3	-38.6	0.64	3	1671	-23.1	Bak	Bak-CDP02			
Bak-EC1M04	-534.7	-35.8	0.58	3	2214	-16.2	Bak	Bak-CDP02			
Bak-EC1M05	-539.2	-36.4	0.57	7	2642	-13.8	Bak	Bak-CDP02			
Bak-EC1M06	-525.4	-24.0	0.65	3	2453	-9.8	Bak	Bak-CDP02			
Bak-EC2M01	-511.3	-26.6	0.49	4	2359	-11.3	Bak	Bak-EC1M06			
Bak-EC2M02	-505.1	-20.3	0.53	5	2416	-8.4	Bak	Bak-EC1M06			
Bak-EC2M03	-498.9	-38.5	0.50	6	2528	-15.2	Bak	Bak-EC1M06			
Bak-EC2M04	-505.8	-35.5	0.50	3	2330	-15.2	Bak	Bak-EC1M06		NA	
Bak-EC2M05	-501.4	-31.9	0.54	5	2325	-13.7	Bak	Bak-EC1M06			
Bak-EC2M06	-511.4	-39.6	0.55	5	2588	-15.3	Bak	Bak-EC1M06			
Bak-EC2M07	-492.6	-47.1	0.56	7	2562	-18.4	Bak	Bak-EC1M06			
Bak-EC2M08	-503.3	-29.5	0.54	3	2562	-11.5	Bak	Bak-EC1M06			
Bak-EC2M09	-511.7	-36.2	0.47	4	2483	-14.6	Bak	Bak-EC1M06			
Bak-EC2M10	-500.5	-30.8	0.50	3	2347	-13.1	Bak	Bak-EC1M06			
Bak-EC2M11	-503.3	-29.6	0.52	3	2349	-12.6	Bak	Bak-EC1M06			
Bak-EC2M12	-496.5	-25.9	0.48	3	2415	-10.7	Bak	Bak-EC1M06			
Bak-EC2M13	-510.5	-30.0	0.55	4	2335	-12.9	Bak	Bak-EC1M06			
Bax-CDP01	-475.9	-48.0	0.67	2	2187	-21.9	Bax	1F16	+++	-	+++
Bax-CDP02	-502.4	-61.2	0.58	0	2099	-29.2	Bax	1F16	+++	-	-
Bax-CDP03	-521.7	-66.9	0.72	5	2014	-33.2	Bax	1F16	+++	-	-
Bax-CDP04	-508.0	-60.3	0.65	1	2196	-27.5	Bax	1F16	+++	++	+++
Bax-CDP05	-450.9	-49.2	0.64	5	2148	-22.9	Bax	4BD2	+++	-	-
Bax-CDP06	-474.6	-67.3	0.73	3	2062	-32.6	Bax	4BD2	+	-	-
Bax-CDP07	-486.0	-62.3	0.68	4	2325	-26.8	Bax	4BD2	+++	-	++
Bax-CDP08	-460.9	-57.0	0.70	2	2182	-26.1	Bax	4BD2	++	-	+
Bax-CDP09	-466.0	-57.5	0.65	5	1973	-29.1	Bax	4BD2	-	NA	NA
Bax-CDP10	-451.8	-61.2	0.72	5	2092	-29.2	Bax	4BD2	+	-	-
Bax-CDP11	-497.1	-49.1	0.61	4	2297	-21.4	Bax	4BD6	++	-	++
Bax-CDP12	-476.5	-42.5	0.65	7	2131	-19.9	Bax	4BD6	+++	-	-
Bax-CDP13	-500.8	-52.9	0.66	4	2190	-24.2	Bax	4BD6	+	+	+
Bax-CDP14	-475.5	-45.8	0.70	6	2187	-21.0	Bax	4BD6	+++	-	-
Bax-CDP15	-497.2	-39.6	0.63	5	2415	-16.4	Bax	4BD6	++	-	++
Bax-CDP16	-493.3	-66.0	0.73	4	2647	-24.9	Bax	4OYD*	-	NA	NA
Bax-CDP17	-471.3	-54.5	0.59	3	2384	-22.9	Bax	4OYD*	+++	-	-
Bax-CDP18	-481.2	-46.4	0.68	2	2211	-21.0	Bax	4OYD*	-	NA	NA
Bax-CDP19	-478.8	-61.8	0.66	3	2248	-27.5	Bax	4OYD*	+++	-	-
Bax-CDP20	-485.8	-59.8	0.64	6	2581	-23.2	Bax	4OYD*	+++	-	-
Bax-CDP21	-478.8	-52.6	0.68	3	2668	-19.7	Bax	4OYD*	+++	-	+
Bax-CDP22	-463.8	-48.6	0.62	5	2462	-19.7	Bax	4OYD*	++	-	-
Bax-CDP23	-493.4	-67.7	0.65	7	2640	-25.6	Bax	4OYD*	+	-	-
Bax-CDP24	-484.8	-50.1	0.56	6	2259	-22.2	Bax	4OYD**	+++	-	++
Bax-CDP25	-469.4	-52.8	0.62	4	2270	-23.3	Bax	4OYD**	+++	-	-
Bax-CDP26	-472.5	-54.9	0.63	4	2321	-23.7	Bax	4OYD**	+++	-	+
Bax-CDP27	-463.4	-55.6	0.61	3	2177	-25.5	Bax	4OYD**	+++	+	-
Bax-CDP28	-456.1	-54.1	0.62	2	2068	-26.2	Bax	4OYD**	++	-	+
Bax-CDP29	-459.2	-50.5	0.60	5	2343	-21.6	Bax	4OYD**	+++	-	-
Bax-CDP30	-477.9	-61.1	0.69	3	2214	-27.6	Bax	4OYD**	+++	+	++
Bax-CDP31	-476.3	-61.1	0.66	2	2206	-27.7	Bax	4OYD**	+++	-	++
Bax-EC1M01	-507.3	-57.4	0.62	1	2557	-22.5	Bax	Bax-CDP01			
Bax-EC1M02	-472.9	-33.6	0.47	3	1952	-17.2	Bax	Bax-CDP01			
Bax-EC1M03	-488.2	-38.5	0.62	1	2350	-16.4	Bax	Bax-CDP01			
Bax-EC1M04	-487.2	-60.5	0.67	2	2380	-25.4	Bax	Bax-CDP01			
Bax-EC1M05	-495.4	-54.9	0.66	1	2294	-23.9	Bax	Bax-CDP01		NA	
Bax-EC1M06	-487.1	-55.6	0.64	2	2470	-22.5	Bax	Bax-CDP01			
Bax-EC2M01	-489.0	-49.5	0.61	2	2608	-19.0	Bax	Bax-EC1M01			
Bax-EC2M02	-498.6	-60.0	0.65	4	2826	-21.2	Bax	Bax-EC1M01			
Bax-EC2M03	-487.4	-54.4	0.60	2	2812	-19.4	Bax	Bax-EC1M01			
Bax-EC2M04	-495.4	-51.7	0.59	7	2587	-20.0	Bax	Bax-EC1M01			

* homology model, diversified backbone scaffold set

** homology model, original BINDI scaffold backbone

Table 8. Design sequences targeting pro-apoptotic BCL2 members Bak and Bax.

>Bak–CDP01
GADPKKVLDKAKDQAENVVRKLKQKLEELYKEARKLDLTQDEKIELILKYIAAMLAAIGDILQAIMDAKLEADKLKKAGLVNSQQLDELKRRLEELREKAARKAEKYAREFAKKLKYG
>Bak–CDP02
GADPKKVLDKAKDQAENVVRKLKQILEELYKEARKLDLTQDEKIELILRYIAAMLAAIGDILEAIRQAKEEADKLKKAGLVNSQQLDELKRRLEELRKEAARKARDYAEEFRNKLEYG
>Bak–CDP03
GADPKKVLDKAKDQAENRVRELEQKLRELYKEARKLDLTQEQKDKLQKRYLQALREALKDIENAIRQAKQEADKLKKAGLVNSQQLDELKRRLEKLRQEAVIKAIALALAFIGDLEQG
>Bak–CDP04
GADPKKVLDKAKDQAENRVRELEQKLRELYKEARKLDLTQEEKRKLKKRYEQALREAHKDIRNAIRQAKQEADKLKKAGLVNSQQLDELKRRLEKLRKEAAIKAIALALAFIGDLEQG
>Bak–CDP05
GADPKKVLDKAKDQAENRVQELRQKLEELYKEARKLDLTQEERRKLEERYRAALEEARRDIENAIRQAKQEADKLKKAGLVNSRQLKKLKQLLNVLAIAANLQAIGDAIEFEYRLEYG
>Bak–CDP06
GADPKKVLDKAKDQAENRVRELKQKLEELYKEARKLDLTQEQKDKLRERYREAAEQAARDIYNAIRQAKQEADKLKKAGLVNSQQLDELKRRLEKLRAEAEVKAIAYALQFIGDLEAG
>Bak–CDP07
GADPKKVLDKAKDQAENRVRELKQKLEELYKEARKLDLTQEQRRKLEERYRAALEEARKDIENAIRQAKQEADKLKKAGLVNSRQLKKLKQELNRLAIAANLQAIGDAIEFEYRLEYG
>Bak–CDP08
GADPATVLIAAALQAIGDVEALREILEELYKEARKLDLTQEERRKLEERYKKAEEKARRDIYEAIKRAKERADELKKAGLVNSQQLDELKRRLERLKEQASREARELAREFQQKLEYG
>Bak–CDP09
GADPKKVLDKAKDQAENRVRELAQKLEELYKEARKLDLTQEERRKLEERYRAALEEALKDIDNAIRQAKQEADKLKKAGLVNSRQLKKLKQELNRLAIAAKLQAIGDAIEFEYRLEYG
>Bax–CDP01
GADPKKVLDKARDQAENRVRELAQKLEELYKEARKLDLTQEERRKLEKRYKAAMEEAIKDIREAIRQAKQEADKLKKAGLVNSQQLKELKQRLNELAIAAALRAIGDAIEFRRKLQYG
>Bax–CDP02
GADPAEVLIAAALRAIGDVIELREILKELYKEARKLDLTQEQRRKLEERYRAAMEKAQANIYKAIKQAKEEADKLKKAGLVNSQQLDELKKRLEKLRQEASRKARDDAREFQQKLEYG
>Bax–CDP03
GADPAEVLIAAALRAIGDVIELRKILEELYKEARKLDLTQEERRKLEERYRAAMEKAQANIYNAIKQAKEEADKLKKAGLVNSQQLDELKKRLEKLRKQASKKARDDAREFQQKLEYG
>Bax–CDP04
GADPKKVLDKARDQAENRVRELAQKLEELYKEARKLDLTQEERRKLEERYRAAMEEAIEDIKKAIKQAKQEADKLKKAGLVNSQQLEELKRELNILAIAAALRAIGDAYEFRRRLQYG
>Bax–CDP05
GANPLEVLIAAMLAAIGDVEALRQILNELYKEARKLDLTQEQRRKLEERYEAAMRKAQEAIRQAIEAAKREADKLKKAGLVNSQQLDELKRRLEKLKENASRQARDYAREFQQKLEYG
>Bax–CDP06
GANPLEVLIAAMLAAIGDVIALREILKELYKEARKLDLTQEERRKLEERYKAAREKARENIRAAIEEAKKEADKLKKAGLVNSQQLDELKRRLERLKKEASRQARDYAREFQQKLEYG
>Bax–CDP07
GADPKKVLDKARKQAIEVVARLAKKLKELEKEARKLDLTQEERRKLEKRYQAAMQEARDDIKNAIRQAKQEADKLKKAGLVNSDQLRELKNRLIALAIAALLAAIGDAYEFERRLEYG
>Bax–CDP08
GANPLEVLIAATLAAIGDVHALRAILQELYKEARKLDLTQEQRRKLEERYKQAREEARERIRAAIEAAKREADKLKKAGLVNSQQLDELKRRLEKLKEKASRQARDYAREFQQKLEYG
>Bax–CDP09
GANPLEVLIAAMLAAIGDVIALREILRELYKEARKLDLTQEERRKLEKRYEAAMKKAQKNIEAAIREAKKEADKLKKAGLVNSQQLDELKRRLEKLKKEASRQARDYAREFQQKLEYG
>Bax–CDP10
GANPLEVLIAAMLAAIGDVYALKAILDELYKEARKLDLTQEQRRKLEKRYKAAMDKARKAIRDAIKAAKEEADKLKKAGLVNSQQLDELKRRLERLKKEASRQARDYAREFQQKLEYG
>Bax–CDP11
GADPKKVLDKARKQADQRVQELRKKLEELYKEARKLDLTQEQRRKLEERYRAAMEEAIKDIRNAIRQAKQEADKLKKAGLVNSQQLRRLKTLLNILAIAAALRAIGDAEAFRQKLEYG
>Bax–CDP12
GANPAEVLIAAALMAIGDVEALRQELNELYKEARKLDLTQEERRKLEERYRAAMEKAQEAIKRAIKAAKEEADKLKKAGLVNSQQLDKLKRELEKLRQEASRLARDYAREFQQKLEYG
>Bax–CDP13
GADPKKVLDKARKQAEQRVRELAKKLKELKKEARKLDLTQEQRRKLEERYRAAMEEAIKDIRNAIRQAKQEADKLKKAGLVNSQQLRRLKTLLNILAIAAALMAIGDAFQFEQDLEYG
>Bax–CDP14
GANPAEVLIAAALMAIGDVHALREELQELYKEARKLDLTQEERRKLEERYRAAMEKAQQAIEDAIKAAKEEADKLKKAGLVNSQQLDKLKRELEKLKREASRQARDYAREFQQKLEYG
>Bax–CDP15
GADPKKVLDKARKQALQRVQELRKKLEELEKEARKLDLTQEQRRKLEERYRAAMEEAIKDIENAIRQAKQEADKLKKAGLVNSQQLRRLKTLLNILAIAAALMAIGDAQEFRDRLEYG
>Bax–CDP16
GADPKKVLDKAKDQAENVVRELKQRLEELYKEARKLDLTDEEKERLKIRFIAAALLAIGDIIRAIAEAKREADKLKKAGLVNSQQLDELKRRLEELKKEAQRKAAEYAEEFYRKLQYG
>Bax–CDP17
GADPKKVLDKARDQAENRVQELRQKLEELYKEARKLDLTQEQRRKLEERYEAAMKEAEKDIYNAIRQAKQEADKLKKAGLVNSDQLKELKIRLAELAIAAALLAIGDAEAFRYLLEYG
>Bax–CDP18
GADPKKVLDKAKDQAENRVRELKQKLEELYKEARKLDLTQEQKNKLKERARAAAEEAAKDIENAIRQAKQEADKLKKAGLVNSQQLDELKKRLEKLKIKAAEKAIAYALLFIGDLEAG
>Bax–CDP19
GADPKKVLDKARDQAENRVQELRQKLEELYKEARKLDLTQEQRRKLEERYRAAMEEAERDIKNAIRQAKQEADKLKKAGLVNSDQLKELKLRLAELAIAAALLAIGDAEAFRDLLEYG
>Bax–CDP20
GADPKKVLDKAKDQAENRVRELKQELEELYKEARKLDLTDEQKEQLKIRFIAAALLAIGDIIEAIDRAKQEADKLKKAGLVNSQQLDELKRRLEELEREAARKAAEYAREFYEKLQYG
>Bax–CDP21
GADPKKVLDKAKDQAENVVRELKQRLEELYKEARKLDLTDEEKRRLKIRFIAAALLAIGDIEKAIHDAKREADKLKKAGLVNSQQLDELKRRLDELRKKAQKKAAEYAREFYEKLQYG
>Bax–CDP22
GADPKKVLDKAKDQAENVVRELKQILEELYKEARKLDLTDEEKRQLKIRFIAAALLAIGDIIKAIYDAKAEADKLKKAGLVNSQQLDELKRRLEELERKAAEKAARLAREFYKKLQYG
>Bax–CDP23
GADPKKVLDKAKDQAENRVRELKQILEELYKEARKLDLTDEEKRRLKIRFIAAALLAIGDIIVAIAEAKREADKLKKAGLVNSQQLDELKRRLEELEREAARKAAELAREFYEKLQYG
>Bak–CDP10
GADPKKVLDKAKDQAENRVRELKQKLEELYKEARKLDLTEEMRKKLELRFIAAMLQAIGDIINAIYKAKQEADKLKKAGLVNSQQLDELKRRLEELANEAARKARDLAQEFQEKLQYG
>Bak–CDP11
GADPKKVLDKAKDQAENRVRELKQKLEELYKEARKLDLTDEMKKKLELRFIAAMLQAIGDIINAIYKAKQEADKLKKAGLVNSQQLDELKRRLEELAKEAARKAEELAKEFQKKLQYG
>Bax–CDP24
GADPKKVLDKAKDQAENRVRELKQKLEELYKEARKLDLTSDMEKKLRLRFIAALLAAIGDIAHAIYQAKQEADKLKKAGLVNSQQLDELKRRLEELKKEALRKAEDAAREFQEKLEYG
>Bax–CDP25
GADPKKVLDKAKDQAENRVRELKQKLEELYKEARKLDLTEDMRKKLELRFIAALLAAIGDIAQAIYQAKQEADKLKKAGLVNSQQLDELKRRLEELKKEALRKAYEAAREFQEKLEYG
>Bax–CDP26
GADPKKVLDKAKDQAENRVRELKQKLEELYKEARKLDLTEDMRKDLELRFIAALLAAIGDIAHAIYQAKQEADKLKKAGLVNSQQLDELKRRLEELRKEALRKAEDAAREFQEKLEYG
>Bax–CDP27
GADPKKVLDKAKDQAENRVRELKQKLEELYKEARKLDLTERMKEELLLRFIAAALMAIGDIRAAIYQAKQEADKLKKAGLVNSQQLDELKRRLEELRKEALRKARDAAEEFQRKLEYG
>Bax–CDP28
GADPKKVLDKAKDQAENRVRELKQKLEELYKEARKLDLTEEMKRELLLRFIAALLMAVGDILAAIYQAKQEADKLKKAGLVNSQQLDELKRRLEELRKEALRKARDAAREFQEKLEYG
>Bax–CDP29
GADPKKVLDKAKDQAENRVRELKQKLEELYKEARKLDLTRDMEKELRLRFIAALLMAQGDIDQAIYQAKQEADKLKKAGLVNSQQLDELKRRLEELKKEARRKARDAAKEFQDKLEYG
>Bax–CDP30
GADPKKVLDKAKDQAENRVRELKQILEELYKEARKLDLTDEMKKKLKLRFIAAMLLAIGDILNAIYQAKQEADKLKKAGLVNSQQLDELKRRLEELKKEAQRKASEAAREFLEKLEYG
>Bax–CDP31
GADPKKVLDKAKDQAENRVRELKQILEELYKEARKLDLTEEMRKKLELRFIAAMLLAIGDILNAIYQAKQEADKLKKAGLVNSQQLDELKRRLEELKKEAQRKASEAAEEFRRKLEYG
>Bak–EC1M01
GADPKKVLDKAKDQMENVVRKLKQILEELYKEARKLDLTQHEKIELILRYIVAHLAAIGDIEEAIREAKEEAQKLKKAGLVNSQQLREFKRRLEELHKEADRKRRDYAEEFRNKLEYG
>Bak–EC1M02
GADPKKVLDKFKDQAENVVRKLKQILEELIKEARKLDLTQHEKIELIIRYIVAHLAAIGDIEEAIREAKEEADKLKKAGLVNSQQLDEFKRRLEELHKEADRKRRDYAEEFRNKLEYG
>Bak–EC1M03

GADPKKVLDKAKDQMENVVRKLKQILEELAKEARKLDLTQHEKIELILRYIVAHLAAIGDIEEAIREAKEEADKLKKAGLVNSQQLREFKRRLEELHKEADRKRRDYAEEFRNKLEYG
>Bak-EC1M04
GADPKKVLDKFKDQAENVVRKLKQILEELAKEARKLDLTQHEKIELILRYIVAHLAAIGDIEEAIREAREEADKLKKAGLVNSQQLRELKRRLEELHKEADRKRRDYAEEFRNKLEYG
>Bak-EC1M05
GADPKKVLDKAKDQAENVVRKLKQILEELAKEARKLDLTQHEKIELILRYIVAHLAAIGDIEEAIREAREEAQKLKKAGLVNSQQLDEFKRRLEELHKEADRKRRDYAEEFRNKLEYG
>Bak-EC1M06
GADPKKVLDKAKDQMENVVRKLKQILEELAKEARKLDLTQDEKIELILRYIVAHLAAIGDIEEAIREAKEEADKLKKAGLVNSQQLDEFKRRLEELHKEADRKRRDYAEEFRNKLEYG
>Bax-EC1M01
GADPKKVLDKARDQAENRVRELAQKLEELYKEARKLDLTQEERRKLEKRYKAAMEEAIKDIHEAIEQAKEEADKLKDAGLVNEQQLKELKQRLNELAIAAAFRASGDTIEFRRKLQYG
>Bax-EC1M02
GADPKKVLDKARDQAENRVRELAQKLEELYKEARKLDLTQEERRKLESRYKAEMEEAIKDIHEAIEQAKEEADKLQDAGLVNSQQLKELTQRLNELAIAAAFRASGDAIEFRRKLQYG
>Bax-EC1M03
GADPKKVLDKARDQAENRVRELAQKLEELYKEARKLDLTQEERRKLEKRYKAAMEEAIKDIHEEISQAKEEADKLHKAGLVNSQQLKELKQRLNELAIAAAFRASGDAIEFRRKLQYG
>Bax-EC1M04
GADPKKVLDKARDQAENRVRELAQKLEELYKEARKLDLTQEERRKLEKRSKAAMEEAIKDIREEISQAKEEADKLKDAGLVNEQQLKELTQRLNELAIAAAFRASGDTIEFRRKLQYG
>Bax-EC1M05
GADPKKVLDKARDQAENRVRELAQKLEELYKEARKLDLTQEERRKLEKRYKAAMEEAIKDIHEEIHQAKQEADKLQDAGLVNSQQLKELKQRLNELAIAAAFRASGDTIEFRRKLQYG
>Bax-EC1M06
GADPKKVLDKARDQAENRVRELAQKLEELYKEARKLDLTQEERRKLEKRYKAAMEEAIKDIREAISQAKEEADKLQKAGLVNEQQLKELKQRLNELAIAAAFRASGDTIEFRRKLQYG
>Bak-EC2M01
GADPKKVLDKADDQMENVVVTLKQELEELAKERRKLDLTQSEKIELKLRYIVAHLAAIGDIEEAIREAKEEADKLKKAGLVNSQQFAEFKRRLEELHKEADRKRRDYAEEFRNKLEYG
>Bak-EC2M02
GADPKKVLDQAKDQMENVVLTLKFELEELAKEARKLDLTQSEKIELKLRYIVAHLAAIGDIEEAIREAKEEADKLKKAGLVNSQQFSEFKRRLEELHKEADRKRQDYAEEFRNKLEYG
>Bak-EC2M03
GADPKFVLDKADDQMENVVRTLKFELEELAKERRKLDLTQSEKIELKLRYIVAHLAAIGDIEEAIREAKEEADKLKKAGLVNSQQFAEFKRRLEELHKEADRKRQDYAEEFRNKLEYG
>Bak-EC2M04
GADPKKVLDQAKDQMENVVVTLKQELEELAKERRKLDLTQSEKIELKLRYIVAHLAAIGDIEEAIREAKEEADKLKKAGLVNSQQLSEFKRRLEELHKEADRKRQDYAEEFRNKLEYG
>Bak-EC2M05
GADPKKVLDQAKDQMENVVVTLKFELEELAKERRKLDLTQSAKIELKLRYIVAHLAAIGDIEEAIREAKEEADKLKRAGLVNSQQFDEFKRRLEELHKEADRKRQDYAEEFRNKLEYG
>Bak-EC2M06
GADPKFVLDQAKDQMENVVVTLKQELEELAKERRKLDLTQSAKIELKLRYIVAHLAAIGDIEEAIREAKEEADKLKKAGLVNSQQLSEFKRRLEELHKEADRKRADYAEEFRNKLEYG
>Bak-EC2M07
GADPKKVLDQANDQMENVVRTLKQELEELAKERRKLDLTQSAKIELKLRYIVAHLAAIGDIEEAIREAKEEADKLKKAGLVNSQQFSEFKRRLEELHKEADRKRVDYAEEFRNKLEYG
>Bak-EC2M08
GADPKFVLDQAKDQMENVVLTLKQELEELAKEARKLDLTQSAKIELKLRYIVAHLAAIGDIEEAIREAKEEADKLKRAGLVNSQQFSEFKRRLEELHKEADRKRRDYAEEFRNKLEYG
>Bak-EC2M09
GADPKFVLDKADDQMENVVLTLKQELEELAKEARKLDLTQSEKIELKLRYIVAHLAAIGDIEEAIREAKEEADKLKKAGLVNSQQFAEFKRRLEELHKEADRKRVDYAEEFRNKLEYG
>Bak-EC2M10
GADPKKVLDQANDQMENVVRTLKFELEELAKERRKLDLTQSEKIELKLRYIVAHLAAIGDIEEAIREAKEEADKLKRAGLVNSQQFAEFKRRLEELHKEADRKRADYAEEFRNKLEYG
>Bak-EC2M11
GADPKKVLDKANDQMENVVLTLKFELEELAKERRKLDLTQSEKIELKLRYIVAHLAAIGDIEEAIREAKEEADKLKKAGLVNSQQFSEFKRRLEELHKEADRKRVDYAEEFRNKLEYG
>Bak-EC2M12
GADPKKVLDQAKDQMENVVVTLKQDLEELAKERRKLDLTQSEKIELKLRYIVAHLAAIGDIEEAIREAKEEADKLKKAGLVNSQQFAEFKRRLEELHKEADRKRQDYAEEFRNKLEYG
>Bak-EC2M13
GADPKKVLDKAKDQMENHVLTLKQELEELAKERRKLDLTQSAKIELKLRYIVAHLAAIGDIEEAIREAKEEADKLKKAGLVNSQQFAEFKRRLEELHKEADRKRQDYAEEFRNKLEYG
>Bax-EC2M01
GADPKKVLDKARDQAENRVRELRQKLTELYKEARKLDLTQEERRKLIKRYKAAMNEAIKDIHEAIEQAKEEADKLKDAGLVNEQQLKELKQRLNEKALAAAFRASGDTWHARRKLQYG
>Bax-EC2M02
GADPKKVLDKARYQAENRVRELRQKLTELYKEARKLDLTQEERRKLSKRYKAAMNEAIKDIHEAIEQAKEEADKLKDAGLVNEQQLKELKQRLNEKALAAAFRASGDTWHFRRKLQYG
>Bax-EC2M03
GADPKKVLDKARYQAENRVRELRQKLEEYYKEARKLDLTQEERRKLIKRYKAAMNEAIKDIHEAIEQAKEEADKLKDAGLVNEQQLKELKQRLNEKALAAAFRASGDTWHARRKLQYG
>Bax-EC2M04
GADPKKVLDKARDQAENRVRELRQKLEEYYKEARKLDLTQEERRKLSKRYKAAMEEAIKDIHEAIEQAKEEADKLKDAGLVNEQQLKELKQRLNEKALAAAFRASGDTWHARRKLQYG

Table 9. Dissociation constants (KDs) for native interactions with the BH3-binding cleft of Bak and Bax. All values are in nanomolar. Binding affinities for Bcl-2 and Bcl-xL were determined in order to compare values to existing literature.

	Bak	Bax	Bcl-2	Bcl-xL
MBP-BimBH3	4,000 ± 2,000	500 ± 100	0.9 ± 0.2	1.6 ± 0.1
MBP-BidBH3	> 4 μM	464 ± 4	47 ± 5	2.3 ± 0.4

Table 10. Sort conditions for Bak- and Bax-targeting *in vitro* evolution experiments.

Library	Target	Sort	Incubation conditions		Specificity [competitor]/[target]
			Target conc. (nM)	Competitor conc. (nM)	
Bak-CDP02 SSM	Bak	1 (affinity)	40	NA	NA
		1 (specificity)	100	2	0.02
		2 (affinity)	10	NA	NA
		2 (specificity)	50	4	0.08
Bak-CDP02 combinatorial	Bak	1	25	4	0.16
		2	10	16	1.6
		3	10	16	1.6
		4	5	25	5
		5	5	32	6.4
		6	2	32	16
Bak-EC1M06 SSM	Bak	1 (affinity)	1	NA	NA
		1 (specificity)	2	64 nM Bcl-2, 32 nM all others	32 for Bcl-2, 16 for all others
		2 (affinity)	0.5	NA	NA
		2 (specificity)	1	80 nM Bcl-2, 40 nM all others	80 for Bcl-2, 40 for all others
Bak-EC1M06 combinatorial	Bak	1	1	80 nM Bcl-2, 40 nM all others	80 for Bcl-2, 40 for all others
		2	1	120 nM Bcl-2, 40 nM all others	120 for Bcl-2, 40 for all others
		3	1	240 nM Bcl-2, 40 nM all others	240 for Bcl-2, 40 for all others
		4	1	240 nM Bcl-2, 40 nM all others	240 for Bcl-2, 40 for all others
		5	1	240 nM Bcl-2, 40 nM all others	240 for Bcl-2, 40 for all others
Bax-CDP01 SSM	Bax	1 (affinity)	10	NA	NA
		1 (specificity)	25	8	0.32
		2 (affinity)	4	NA	NA
		2 (specificity)	16	16	1
Bax-CDP01 combinatorial	Bax	1	16	8	0.5
		2	8	25	3.125
		3	4	25	6.25
		4	2	50	25
		5	1	50	50
		6	1	50	50
Bax-EC1M01 SSM	Bax	1 (affinity)	5	NA	NA
		1 (specificity)	6	100 nM Bfl-1, 50 nM all others	16.7 Bfl-1, 8.3 all others
		2 (affinity)	0.5	NA	NA
		2 (specificity)	1	80 nM Bfl-1, 40 nM all others	80 for Bfl-1, 40 for all others
Bax-EC1M01 combinatorial	Bax	1	1	120 nM Bfl-1, 40 nM all others	120 Bfl-1, 40 all others
		2	0.5	160 nM Bfl-1, 40 nM all others	320 Bfl-1, 80 all others
		3	0.5	280 nM Bfl-1, 40 nM all others	560 Bfl-1, 80 all others
		4	0.5	280 nM Bfl-1, 40 nM all others	560 Bfl-1, 80 all others
		5	0.5	280 nM Bfl-1, 40 nM all others	560 Bfl-1, 80 all others

Table 11. Mutation summary of evolved Bak- and Bax-targeting variants.

Library	Target	Theoretical Diversity	Mutations (if applicable)	Mutations in best selected variant
Bak-CDP02 SSM	Bak	2,321	all single mutants	NA
Bak-CDP02 combinatorial	Bak	35,831,808	A10F, A14F, A14M, Y29A, Y29I, D40H, L47I, A51V, M53H, A56N, A56Y, I60T, L61E, Q66E, K68R, D72Q, D72R, D72Y, D86R, L88F, R96D, R96H, A100D, A100E, A103R, A103S, R111H, R111T	**Bak-EC1M01**: A14M, Y29A, A51V, M53H, L61E, Q66E, L88F, R96H, A100D, A103R
Bak-EC1M06 SSM	Bak	2,321	all single mutants	NA
Bak-EC1M06 combinatorial	Bak	13,934,592	K5F, K5V, V6E, K9Q, K11D, K11N, V17H, R19L, R19V, K20T, Q23F, I24D, I24E, I24H, I24Q, I24S, I24T, A32N, A32R, D40S, E41A, E41R, I43K, I46K, K76R, L85F, D86A, D86S, R104A, R104Q, R104V	**Bak-EC2M01**: K9Q, K11N, K20T, Q23F, I24E, A32R, D40S, I46K, K76R, L85F, D86A, R104A
Bax-CDP01 SSM	Bax	2,321	all single mutants	NA
Bax-CDP01 combinatorial	Bax	11,943,936	V18A, K44N, K47S, A52E, K58E, R61H, A63E, R65E, R65H, R65S, K68M, K68T, Q69E, K75H, K75Q, K76D, S82E, K86N, K89E, K89T, N93D, N93E, I97F, L101F, L101M, I104Q, I104S, A107T, I108D	**Bax-EC1M01**: R61H, R65E, Q69E, K76D, S82E, L101F, I104S, A107T
Bax-EC1M01 SSM	Bax	2,321	all single mutants	NA
Bax-EC1M01 combinatorial	Bax	65,536	D8S, D12Y, A22R, E26T, L28Y, E46I, E46N, E46S, E54H, E54N, E54S, L95A, L95K, L95V, I97L, I108W, E109D, E109H, E109S, F110A	**Bax-EC2M03**: D12Y, A22R, L28Y, E46I, E54N, L95K, I97L, I108W, E109H, F110A